Title
Chemoproteomic tools for studying kinase signaling

Permalink
https://escholarship.org/uc/item/36s7z46m

Author
Levin, Rebecca

Publication Date
2016

Peer reviewed|Thesis/dissertation

Chemoproteomic tools for studying kinase signaling

by

Rebecca Levin

DISSERTATION

Submitted in partial satisfaction of the requirements for the degree of

DOCTOR OF PHILOSOPHY

in

Chemistry and Chemical Biology

in the

GRADUATE DIVISION

of the

UNIVERSITY OF CALIFORNIA, SAN FRANCISCO

Acknowledgements

Part of this thesis is a reproduction of material previously published, and contains contributions from collaborators listed therein.

Chapter 2 is reproduced in part from:

Sanso, M. Levin, R.S**.**, Lipp, J., Bosken, C., Larochelle, S., Rana, T.M., Tong, L., Geyer, M., Shokat, K.M., Fisher, R.P. "A chemical-genetic substrate screen identifies RNA processing factors directly regulated by cyclin dependent kinase 9", *Genes Dev,* 2016, 30(1):117-31

And

Schaffer, B.E., Levin, R.S., Hertz, N.T., Schoof, M.L., Banko, M.R., Shaw, R.J., Maures, T.J., Shokat, K.M, Brunet, A. "Discovery of in vivo AMPK substrates and phosphorylation sites by a peptide-capture approach reveals a role for AMPK in cell motility and invasion", *Cell Metabolism*, 2015, 22(5):907-21.

Chapter 3 is reproduced in part from:

Levin, R.S., Hertz, N.T., Burlingame, A.L., Shokat, K.M., Mukherjee, S. "The innate immunity kinase TAK1 phosphorylated Rab1 on a hotspot for post-translational modifications by host and pathogen" In press, *Proceedings of the National Academy of Science*.

Chapter 4 is reproduced in part from:

Sos, M.L., Levin, R.S.*, Gordan, J.D.*, Oses-Prieto, J.A., Webber, J.T., Salt, M., Lipp, J., Hann, B., Burlingame, A.L., McCormick, F., Bandyopadhyay, S., and Shokat, K.M. "Oncogene mimicry as a mechanism of primary resistance to BRAF inhibitor" *Cell Reports,* 2014, 8(4):1037-48.

Chapter 5 is reproduced in part from:

Chemoproteomic tools for studying kinase signaling

by

Rebecca Levin

Abstract

Protein kinases are key signaling proteins responsible for maintaining cellular homeostasis. These enzymes catalyze the transfer of the γ-phosphate of adenosine triphosphate (ATP) to a serine, threonine or tyrosine residue of a substrate protein. The introduction of this additional negative charge may control the function of the substrate, by altering conformation or altering sites of protein binding. Over 500 kinases serve diverse roles in integrating signals from extracellular stimuli, regulating the cell cycle, and regulating gene expression. The field of mass spectrometry based proteomics has made identifying and quantifying sites of phosphorylation on a proteome-wide basis relatively facile, with hundreds of thousands of sites of phosphorylation identified to date. However, there remains a disconnect between the few known substrates, and thus function, of any given kinase, and the hundreds of thousands of known sites of phosphorylation across the proteome. In this thesis, we describe efforts to close this gap through the engineering of a kinase to accept a bio-orthogonal analog of ATP as a substrate, and thus trace its substrates via mass spectrometry. We apply the technique to Cdk9, identifying a novel regulatory function in transcript termination, and AMPK, identifying evidence for the involvement of AMPK in mediating cell motility and adhesion. Furthermore, we demonstrate that GTPase Rab1 is a substrate of innate immunity kinase TAK1, and show phosphorylation of the dynamic switch region of Rab1, and perhaps Rab GTPases as a family, can regulate its function. In the second half of this thesis, we address efforts to further understand the interconnectivity of the kinome, as many kinases function in tightly orchestrated signaling cascades, with kinases phosphorylating substrate kinases. Through the use of the Multiplexed Kinase Inhibitor Bead (MIB) methodology, we investigate the how mis-regulation of

these cascades drives oncogenesis. Through the use of the MIBs approach, which enriches for

activated kinases and is coupled to quantitative proteomics, we identify mechanisms of

resistance to targeted kinase therapeutics as well as identify non-mutated kinase drivers of

tumorgenesis. Lastly, we describe increased MIBs sensitivity through the use of parallel reaction

monitoring (PRM), a targeted proteomic approach.

Table of Contents

List of Figures

Chapter 1

Introduction: Proteomics methods for studying kinase signaling

Proteins drive the biochemical reactions necessary for producing life and provide the structure to support it. Regulation of protein function occurs in many forms, from the complex regulation of gene expression to interference in translation by non-coding RNA. Post-translational modifications (PTMs) of proteins offer a unique means of protein regulation. PTMs are the covalent addition of chemical moieties spanning in size from a few atoms to entire small proteins to residues of existing proteins. Through the addition of moieties as small as a single phosphate or methyl group, the function of a modified protein can be completely shifted. The addition of a PTM can drive the localization, activation, interactions or degradation of the substrate protein through only a small change in charge or mass. Unlike the regulation of gene expression, PTM mediated protein control is rapid, as the transfer of a PTM requires only a single chemical reaction. PTM are also regulatable, with classes of enzymes responsible for placing and removing modifications. Unbiased mass spectrometry based methods have been instrumental in uncovering both the breadth and complexity of PTMs across the entire proteome, with hundreds of thousands of sites of modification identified across the proteome(1). Thus, post-translational modifications are a powerful and ubiquitous means of regulating protein function within the cell. However, one of the largest challenges in biology is to understand the architecture of signaling networks comprised of these thousands of post-translational modifications and how they serve to relay signals.

Phosphorylation is the widest studied post-translational modification, in part because of the importance of protein kinases, the enzymes responsible for phosphorylation, in cancer. The

earliest identified oncogene was v-Src, a tyrosine kinase(2). Many of the most commonly observed and widest studied oncogenes are kinases, such as EGFR, BRAF, the HER family and Abl, or key mediators of kinase signaling, such as RAS(3).The discovery that abnormal kinase activity, i.e. abnormal phosphorylation, is transforming, along with the discovery that growth factor and hormone receptors were kinases, provided insight into the regulation of normal cellular processes. These insights spurred the development of a wide range of mass spectrometry based proteomic techniques for enriching, identifying and quantifying peptides (4), allowing large scale phosphoproteomics experiments to become fairly routine. While these experiments can produce broad outlines of kinase signaling networks, the exact connectivity of these networks remains to be determined.

In order to study kinase signaling networks, we can think of kinase signaling networks as comprised of three levels. First is the core function of a kinase, directly phosphorylating a set of protein targets, called substrates, which may include other kinases. Second is the broader set of downstream targets regulated by the kinase. Many kinases function in signaling cascades, so the initiating kinase regulates the activity of a number of substrate kinases and, in turn, their direct targets. Lastly, kinase signaling cascades, and the kinome as a whole, are integrated, with the activity of individual signaling arms influencing others, and providing high-level coordination of many individual signaling pathways and cellular responses to stimuli. Significant gaps in knowledge exist for each level of kinase signaling. To that end, this thesis focuses on the application and continued development of three chemical biology driven proteomics methods for deepening our understanding of kinase signaling network architecture on each of these three levels (Figure 1). Described within are projects utilizing an engineered kinase system to identify direct substrates of kinases, standard quantitative proteomics to understand resistance to targeted therapeutics in cancer, and a method to capture a snapshot of kinome activity, called multiplexed kinase inhibitor beads (MIBs).
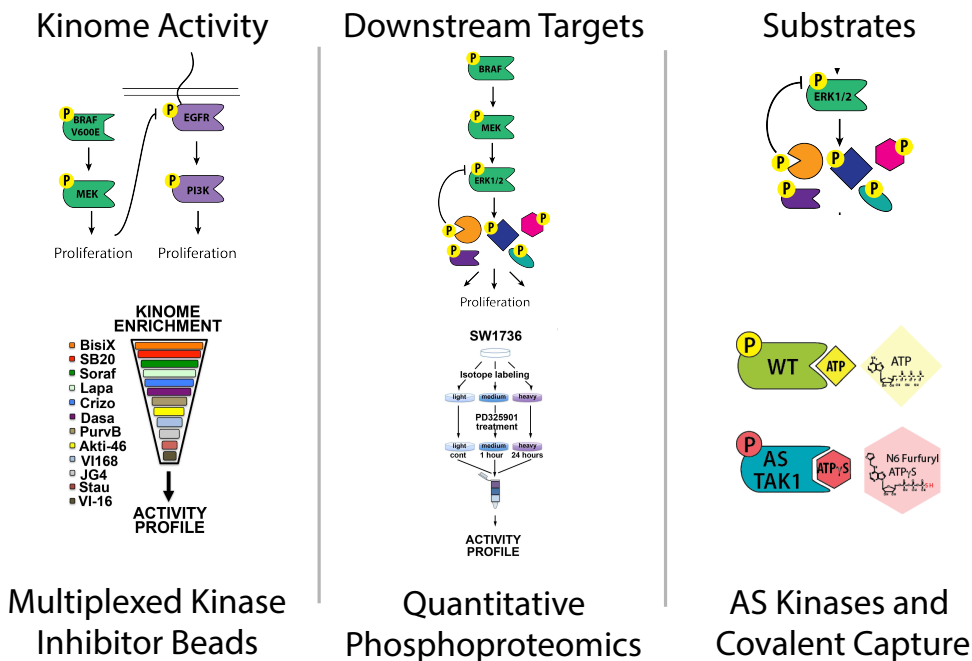
Figure 1. Three approaches for mapping kinase signaling networks

The core catalytic function of a protein kinase is to phosphorylate a protein substrate. 518

kinases and hundreds of thousands of phosphosites have been identified(1, 5). However, there

are few precise connections known between kinases and specific substrate sites, which would

inform the function and role of the substrate phosphorylation and regulatory role of the kinase of

interest (6). Thus, a variety of methods have been developed to link kinases to their direct

substrates. In vitro kinase assays, in the form of individual assays, peptide arrays or protein

arrays, demonstrate the ability of a kinase to directly phosphorylate a substrate, but are far

removed from the context of a cellular environment(7, 8). Searching for kinase interacting

proteins and confirming phosphorylation of these proteins has also served to identify substrates,

but these approaches will miss transient kinase-substrate interactions, which is important as

transient interactions are thought to be common for kinases and substrates(9). Large scale

phosphoproteomic approaches, where kinase activity is disrupted by genetic or chemical means

and changes in resulting phosphorylation are quantified by mass spectrometry after

phosphopeptide enrichment, are useful in identifying kinase – downstream target relationships, but do not establish direct kinase-substrate relationships(6).

To address this challenge, multiple techniques have been developed that allow for the direct detection of kinase substrate relationships. In an approach called KALIP, cell lysates are dephosphorylated, labeled by the addition of a kinase of interest and ATP and analyzed by quantitative phosphoproteomics. Thus any changes in phosphopeptide abundance can be directly attributed to the activity of the added kinase and substrates assigned to that kinase, however this method is experimentally intensive(10). Previous scientists in the Shokat lab developed an elegant approach to identify kinase substrates by mutating a kinase of interest to accept bulky ATPγS analogs, termed an analog specific kinase (AS-kinase). The direct interaction of the AS-kinase and substrate thereby results in a thiophosphorylation of the substrate, providing a reactive chemical handle for enriching and identifying the substrate and exact phosphosite(11). In this approach, a purified mutated kinase is added to a cell lysate with a bulky ATPγS analog and allowed to thiophosphorylate its substrates, followed by enrichment and LC-MS/MS based detection. Outside groups have taken steps to optimize this technique by using in cell labeling coupled with microscale enrichment of phosphopeptides, which yields impressive results but requires specialized equipment and significant technical skill(12). We find that the updated Shokat approach(13) is more than adequate for making significant strides to close the gap between kinase and known substrates, and has the added benefit of being an technique that can be performed in any lab without specialized equipment. Chapters 2 and 3 detail this use of the protocol for 3 different kinases of interest and highlight important biological findings from these results.

Quantitative phosphoproteomics has been a workhorse of kinase biology for the last 15 years. Identification and assignment of phosphorylation sites is made difficult by the low relative

stoichiometry of phosphorylation, so only a small fraction of a given protein in the cell will be phosphorylated at any time(14). Thus, enrichment methods such as immobilized metal affinity chromatography (IMAC) or immunoaffinity enrichment are used to isolate phosphorylated peptides from a digested cell lysate prior to LC-MS/MS identification of peptides(4, 15). These standard approaches are useful for identifying sites of phosphorylation, but do not provide any information about dynamics or relative abundance. Non-quantitative phosphoproteomics provides only nodes in, not connectivity of, kinase signaling networks. For many years, instability and variability between LC-MS/MS runs was relatively high, making direct comparisons of peptide abundance between samples difficult. The introduction of methods to provide relative quantitation of peptide abundance between samples, including stable isotope labeling in cell culture (SILAC)(16) and isotope tagging reagents like TMT and iTRAQ(17, 18), made a significant impact on the field. Quantitation allows for monitoring of changes in the abundance of phosphorylation driven by manipulation of kinase activity by treatment with kinase inhibitors or genetic means(19, 20). Broad sets of kinase targets can be determined from these experiments, which have become semi-ubiquitous in the study of kinases. The downside of quantitative proteomics is the vast quantity of data generated often far exceeds the ability of an experimentalist to confirm relationships and delve deeper into the biology of the signaling network. Bioinformatic methods to integrate data from multiple studies strive to make this abundance of data more interpretable and accessible(21). Quantitative phosphoproteomics will continue to be key to mapping kinase signaling networks, and be more informative when complemented with bioinformatics and new advances in studying kinome activity as a whole.

From the development of targeted kinase inhibitors for use in treating diseases such as cancer has emerged a number of new kinase signaling phenomena. The use of these drucs in the clinical setting has revealed both initial, primary resistance to targeted therapeutics and resistance developed over long exposure to drug. Although mutation of the target kinase to

escape inhibition is perhaps the most common means to develop resistance, bypass of inhibition through activation of alternate kinase pathways has also been observed(22). The outstanding question of how, why and which cancers may activate bypass pathways to evade an inhibitor has highlighted the importance of understanding the interconnectivity of kinases with themselves, or the "kinome". To that end, the same compounds that are designed with the hope of treating patients may be used to probe the activity of the kinome. Kinase inhibitors of broad specificity can be coupled to resin and used to enrich protein kinases from cell lysates, which can then be identified and quantified by LC-MS/MS(23–27). The original use of this technique was to identify off targets of kinase inhibitors. Cells treated with compound or DMSO were subject to kinase enrichment, with reduced enrichment of any kinase attributed to off target binding of the compound blocking the ability of the kinase to bind the resin(26). The technique was also used to identify changes in kinase abundance during the cell cycle(25). These early approaches required significant amounts of protein input, kinase inhibitor resins, and fractionation of purified kinases, making these methods both costly and time consuming. Recent approaches have reduced the input needed by utilizing newer, more sensitive instruments and broader classes of inhibitors as bait(28). Importantly for the mapping of kinase signaling networks, inhibitors for use on the resin may be specifically selected in order to enrich for active kinases(23, 29). Thus, the activity of the whole kinome can be monitored in different contexts. This is especially useful in the case of studying the kinome response to kinase targeted therapeutics, as kinase pathways activated to bypass inhibitors will be enriched on this activity-biased resin. The use of an activity-biased resin is one of the only ways to study the activation of kinases on a kinome wide scale in an unbiased fashion. We have used this technique to identify activation of bypass mechanisms in the case of resistance, and we continue the use of this approach to identify non-mutant kinase drivers of cancers.

By considering kinase signaling networks at the three levels of substrate, pathway and kinome, we can map kinase signaling networks with detailed connectivity. This thesis describes projects utilizing all three of these approaches to uncover novel, core functions of kinases and probe complex signaling networks dictating response to therapy in the context of cancer. The overlap of these three tools allows us an unparalleled ability to delve into the study of kinase signaling.

References

1.	Hornbeck P V, et al. (2012) PhosphoSitePlus: a comprehensive resource for investigating the structure and function of experimentally determined post-translational modifications in man and mouse. *Nucleic Acids Res* 40(Database issue):D261–70.
2.	Smart JE, et al. (1981) Characterization of sites for tyrosine phosphorylation in the transforming protein of Rous sarcoma virus (pp60v-src) and its normal cellular homologue (pp60c-src). *Proc Natl Acad Sci U S A* 78(10):6013–7.
3.	Blume-Jensen P, Hunter T (2001) Oncogenic kinase signalling. *Nature* 411(6835):355–65.
4.	Dephoure N, Gould KL, Gygi SP, Kellogg DR (2013) Mapping and analysis of phosphorylation sites: a quick guide for cell biologists. *Mol Biol Cell* 24(5):535–42.
5.	Manning G, et al. (2002) The protein kinase complement of the human genome. *Science* 298(5600):1912–34.
6.	Xue L, Tao WA (2013) Current technologies to identify protein kinase substrates in high throughput. *Front Biol (Beijing)* 8(2):216–227.
7.	Mok J, Im H, Snyder M (2009) Global identification of protein kinase substrates by protein microarray analysis. *Nat Protoc* 4(12):1820–7.
8.	Houseman BT, Huh JH, Kron SJ, Mrksich M (2002) Peptide chips for the quantitative evaluation of protein kinase activity. *Nat Biotechnol* 20(3):270–4.
9.	Amano M, et al. (2015) Kinase-interacting substrate screening is a novel method to identify kinase substrates. *J Cell Biol* 209(6):895–912.
10.	Xue L, Arrington J V., Andy Tao W (2016) Identification of direct kinase substrates via kinase assay-linked phosphoproteomics. *Methods in Molecular Biology*, pp 263–273.
11.	Blethrow JD, Glavy JS, Morgan DO, Shokat KM (2008) Covalent capture of kinase-specific phosphopeptides reveals Cdk1-cyclin B substrates. *Proc Natl Acad Sci U S A* 105(5):1442–7.
12.	Carlson SM, White FM (2012) Labeling and identification of direct kinase substrates. *Sci Signal* 5(227):pl3.
13.	Hertz NT, et al. (2010) Chemical genetic approach for kinase-substrate mapping by covalent capture of thiophosphopeptides and analysis by mass spectrometry. *Curr Protoc Chem Biol* 2(1):15–36.
14.	Olsen J V, et al. (2010) Quantitative Phosphoproteomics Reveals Widespread Full Phosphorylation Site Occupancy During Mitosis -- Olsen et al. 3 (104): ra3 -- Science Signaling. *Sci Signal* 3(104):ra3.
15.	Ficarro SB, et al. (2002) Phosphoproteome analysis by mass spectrometry and its application to Saccharomyces cerevisiae. *Nat Biotechnol* 20(3):301–305.
16.	Ong S-E (2002) Stable Isotope Labeling by Amino Acids in Cell Culture, SILAC, as a Simple and Accurate Approach to Expression Proteomics. *Mol Cell Proteomics* 1(5):376–

386.

17. Li Z, et al. (2012) Systematic comparison of label-free, metabolic labeling, and isobaric chemical labeling for quantitative proteomics on LTQ Orbitrap Velos. *J Proteome Res* 11(3):1582–90.

18. Wiese S, Reidegeld KA, Meyer HE, Warscheid B (2007) Protein labeling by iTRAQ: A new tool for quantitative mass spectrometry in proteome research. *Proteomics* 7(3):340–350.

19. Blagoev B, Ong S-E, Kratchmarova I, Mann M (2004) Temporal analysis of phosphotyrosine-dependent signaling networks by quantitative proteomics. *Nat Biotechnol* 22(9):1139–1145.

20. White FM (2008) Quantitative phosphoproteomic analysis of signaling network dynamics. *Curr Opin Biotechnol* 19(4):404–409.

21. Narushima Y, Kozuka-Hata H, Tsumoto K, Inoue J, Oyama M (2016) Quantitative phosphoproteomics-based molecular network description for high-resolution kinase-substrate interactome analysis. *Bioinformatics*:btw164–.

22. Niederst MJ, Engelman JA (2013) Bypass mechanisms of resistance to receptor tyrosine kinase inhibition in lung cancer. *Sci Signal* 6(294):re6.

23. Duncan JS, et al. (2012) Dynamic reprogramming of the kinome in response to targeted MEK inhibition in triple-negative breast cancer. *Cell* 149(2):307–21.

24. Oppermann FS, et al. (2009) Large-scale proteomics analysis of the human kinome. *Mol Cell Proteomics* 8(7):1751–64.

25. Daub H, et al. (2008) Kinase-selective enrichment enables quantitative phosphoproteomics of the kinome across the cell cycle. *Mol Cell* 31(3):438–48.

26. Bantscheff M, et al. (2007) Quantitative chemical proteomics reveals mechanisms of action of clinical ABL kinase inhibitors. *Nat Biotechnol* 25(9):1035–44.

27. Knight JDR, Pawson T, Gingras A-C (2012) Profiling the kinome: Current capabilities and future challenges. *J Proteomics*:1–13.

28. Daub H (2015) Quantitative Proteomics of Kinase Inhibitor Targets and Mechanisms.

29. Stuhlmiller TJ, et al. (2015) Inhibition of Lapatinib-Induced Kinome Reprogramming in ERBB2-Positive Breast Cancer by Targeting BET Family Bromodomains Article Inhibition of Lapatinib-Induced Kinome Reprogramming in ERBB2-Positive Breast Cancer by Targeting BET Family Bromodomains. *CellReports*:1–15.

Chapter 2

Identifying kinase substrates using the analog specific kinase and covalent capture approach: use on tyrosine kinases and collaborative projects

Introduction

Through the course of my PhD, I have worked on many projects using the analog-specific kinase approach for identification of kinase substrates. This chapter describes a number of successful collaborations with other labs using the technique, for which I did experimental work and provided technical expertise. The text is adapted from these collaborations, with appropriate reference to the published papers in the text and acknowledgements. In addition, a brief project applying the covalent capture approach to tyrosine kinases is described, as well as recommendations for improving the technique. Lastly, a number of false positive substrates commonly observed in the many substrate identification projects the lab has worked on are listed and discussed.

Identifying substrates of Tyrosine kinases

Engineering of the kinase ATP binding site has proven a useful tool for studying kinase biology. Mutation of a single residue at the entrance to the ATP binding site, termed the gatekeeper residue, to a smaller, less bulky residue expands the binding pocket, creating a synthetic hole. This expanded binding site will than accept non-native substrates, including bulky analogs of ATP which wild type kinases are unable to bind. These mutated kinases are referred to as Analog Specific (AS) (1, 2). Prior generations of students in the Shokat lab adapted this technique for use in identifying kinase substrates. A radiolabeled ATPγ^{32}P analog was originally used to trace AS kinase activity (1, 3). Later, a biorthogonal affinity purification approach was

developed, using bulky ATPγS analogs, a thiophosphate esterification reaction to tag sites of

thiophosphorylation and an immunoaffinity purification of tagged substrates(4, 5). However, the

use of a iodoacetyl resin to covalently capture thiophosphorylated peptides produced by

incubation of a AS kinase, an ATPγS analog and protein lysate has proved most efficient at

identifying substrates and specific sites of phosphorylation derived from the kinase of

interest(6).

While initial experiments demonstrating the concept of gatekeeper mutation for the generation

of an AS kinase were done in a tyrosine kinase(1, 2), no tyrosine kinase substrate identification

projects had been undertaken with the modern, covalent capture approach. Serine/threonine

kinases had been well studied with the approach, and continue to be well studied as described

in this chapter and Chapter 3. Upon entering the lab, I sought to identify substrates of the Src

tyrosine kinase using this approach as a proof of concept. We focused our initial efforts on

identifying Src substrates in brain lysates using exogenously expressed kinase. The kinase

domain of AS (T338A) and wild type (WT) Src was expressed and purified from bacteria. Src

was then incubated with brain lysate to label substrates by kinase reaction in the presence of N^6

modified ATPγS analogs. While the vast majority of kinases cannot use these ATPγS analogs,

some highly active and abundant kinases will use the ATPγS analogs to phosphorylate

substrates. Therefore we utilized several important controls to help us identify true substrates.

We used Src WT, which cannot utilize the ATPγS, Kinase Dead AS-Src (KD-AS) and lysate

alone as negative controls and the T338A Src as our experimental group to label the substrates.

We optimized the labeling of lysates using AS-Src, with a distinct increase in

thiophosphorylation in only samples labeled with AS kinase (Figure 1A). In addition we have

shown that AS-Src selectively thiophosphorylates a known substrate, FAK, by

immunoprecipitation and western blot (data not shown). By covalent capture and mass

spectrometry, we have successfully identified the autophosphorylation of AS-Src (Figure 1B).

However, by LC-MS/MS we were only able to identify a few sites of pTyr phosphorylation

unique to AS-Src labeled samples (data not shown). We feel these numbers can be significantly

improved, epically in comparison compared to the number of putative substrates normally

identified for a serine/threonine kinase.
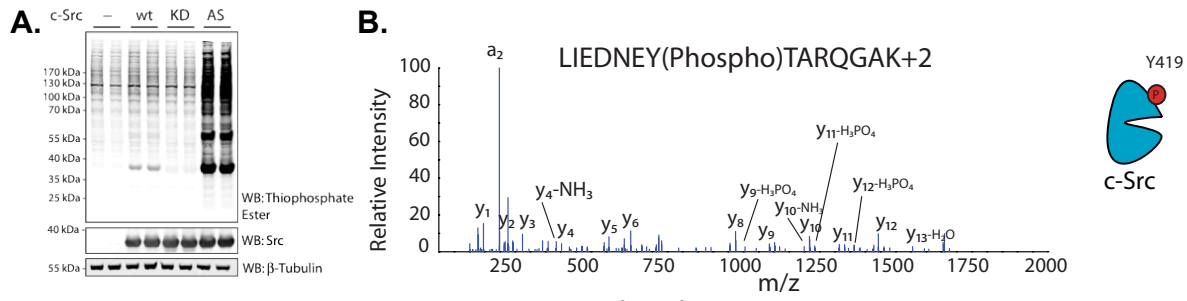
Figure 1. AS-Src can label substrates and autophosphorylate **A**. Labeling of mouse brain
lysates with no, wild type, kinase dead and AS Src. **B.** Spetrum of peptide containing Src
autophosphorylation identified by covalent capture

Identification of substrates of Tyr kinases may face challenges due to the unique nature of

tyrosine phosphorylation. While phosphorylation occurs ubiquitously across the proteome, it is

thought that tyrosine phosphorylation accounts for a minority of total phosphorylations and is

significantly more dynamic than S/T phosphorylation. These traits have necessitated the

development of specific pTyr enrichment protocols(7), as the abundance of pTyr is too low to be

identified normal phosphopeptide enrichment protocols in the context of normal, significantly

more abundant S/T phosphorylation. Given these known difficulties in identifying pTyr, we

anticipated adjustments to the covalent capture technique would be needed to identify pTyr

peptides. In order to apply the covalent capture approach to Tyr kinases, it may be necessary to

incorporate additional steps of pTyr enrichment into the workflow. One option would be to

incorporate a pTyr or phosphopeptide enrichment following release of phosphopepties from the

iodoacetyl resin, to increase signal from pTyr peptides over background peptides. Alternatively,

a thiophosphorylated tyrosine specific antibody could be developed and used to identify sites of

thiophosphorylated tyrosine, which pTyr antibodies do not recognize. Given the success of immunoprecipitation for identifying pTyr sites, this approach may indeed be worth the effort.

Identification of AMPK phosphorylation sites reveals a network of proteins involved in cell invasion and facilitates large-scale substrate prediction

In general, AS kinase substrate identification is performed by purifying the kinase domain of the protein of interest and then labeling a cell lysate by adding the purified kinase and appropriate ATP analog. This approach has several drawbacks. The use of a truncated kinase increases the ease of purification, however domains which may dictate substrate interaction are removed. Secondly, by performing the labeling in a lysate environment removes localization of substrates or off targets to specific organelles or membrane surfaces, perhaps preventing interactions between the kinase and substrate proteins which are driven by co-localization within the cell. To address these concerns our collaborators in the Brunet lab at Stanford drove the development of an *in vivo* system for identifying AMPK substrates(8) by stably overexpressing full length WT and AS AMPKa2 in HEK 293Ts. In the original publication, the authors utilized the thiophosphate ester immunoprecipitation approach and only 28 candidate substrates were identified. Given the limited number of substrates identified, together we embarked on improving the *in vivo* identification technique. The following descriptions of this work are adapted from a recent publication describing the project(9).

The Brunet lab optimized an inducible over-expression system of AMPKα1 and α2 WT and AS in U2OS cells (Figure 2A). Our collaborators identified the optimal stable over expression constructs, as well as conditions to stimulate AMPK activity by treatment with 2-deoxy-D-glucose or the specific AMPK activator A769662. One major challenge in utilizing the covalent capture system in cells is the impermeability of ATPγS analogs across the cell membrane. Thus, significant time was invested in optimizing permeabilization of the U2OS cells with

digitonin to allow ATPγS to enter the cells. By western blot, thiophosphorylation of cell lysates was observed at a much higher abundance in cells overexpressing AS AMPK, with an increase in labeling in the presence of activators (Figure 2B, C). Once these conditions were optimized, we performed covalent capture on labeled cell lysates for a variety of conditions (Figure 2D) totaling over 20 datasets collected, the largest dataset for substrate identification collected by this lab to date. This represents months of troubleshooting, bench work and weeks of instrument time invested by our lab, in addition to the extensive work by our collaborators in establishing the system. A number of known substrates were identified in this screen (Figure 2E) proving the validity of the approach.

A

A769662

2DG

WT-kinase

WT-kinase Substrate

AS-AMPKα2

AS-AMPKα1

A*TPγS

AMPK Substrate

AMPK Substrate

WT-kinase Substrate

AMPK activation and thiophosphorylation of substrates in whole cells

PNBM

Validation: substrate alkylation for western blot analysis

thioP antibody

AMPK Substrate

Screen: peptide capture

Cell lysis and protein digest

Covalent capture of thiophosphorylated peptides on iodoacetyl resin

H_2O +

Oxone-mediated elution and hydrolysis of thiophosphate group

LC-MS/MS

Output

| Protein | Phosphosite | Phosphopeptide |

B

Cell type: 293T / U2OS
AMPKα isoform: α2 / α1 / α2
HA-AMPKα: - WT AS / - WT AS / WT AS

150 —
50 —
37 —
thioP

75 —
50 —
α
γ1
β1
HA (AMPK subunits)

C

100 mM 2DG (-) serum — HA-AMPKα subunits
50 mM 2DG — HA-AMPKα subunits
300 µM A769662 — HA-AMPKα subunits

Empty, α1WT, α1AS, α2WT, α2AS

150 —
50 —
37 —
thioP

75 — HA (AMPKα)
75 — AMPKα1
75 — AMPKα2
37 — β-actin

D

Summary of mass spectrometry datasets

Cell type	AMPK stimuli	AS datasets	Control datasets	# AS datasets generated
293T	100 mM 2DG (-) serum	AS-AMPKα2 + β1 + γ1	β1 + γ1 only; WT-AMPKα2 + β1 + γ1	2
U2OS	100 mM 2DG (-) serum	AS-AMPKα1 AS-AMPKα2	Empty WT-AMPKα1 WT-AMPKα2	12
	50 mM 2DG	AS-AMPKα1 AS-AMPKα2	Empty WT-AMPKα1 WT-AMPKα2	2
	300 µM A769662	AS-AMPKα1 AS-AMPKα2	Empty WT-AMPKα1 WT-AMPKα2	6

E

Known AMPK substrates identified in screen

Protein	Phosphosite	Phosphopeptide	Identified in "x" datasets
ACC1	S80	SSM**S**GLHLVK	4
RAPTOR	S721IS722	**S**V**SS**YGNIR	4
TBC1D1	S325IS237	**S**F**S**QPGLR	5
BAIAP2	S364IS365IS366	**SSS**MAAGLER	5
KLC2	S545	SG**S**FGKLR	4

14

Figure 2.Identification of AS-AMPK substrates (A) Schematic of the peptide-capture technique used to identify analog-specific (AS) AMPKα1 and α2 substrates and phosphorylation sites in whole cells. 2DG, 2-deoxy-D-glucose. (B) HA-tagged AS-AMPKα1 and α2 thiophosphorylate endogenous substrates in U2OS cells without overexpression of the β and γ subunits. Cells were serum-starved for 2 hr and stimulated for 5 min with 100 mM 2DG, then incubated with ATPγS. Whole-cell lysates were analyzed for the presence of thiophosphorylation (thioP) and exogenous AMPK subunits (HA tag). (C) HA-tagged AS-AMPKα1 and α2 thiophosphorylate endogenous substrates under different AMPK-activating conditions. Whole-cell lysates were analyzed for the presence of thiophosphorylation (thioP) and AMPKα (HA tag, AMPKα1, AMPKα2). First panel: 2 hr of serum starvation with 5 min of 100 mM 2DG; second panel: 15 min of 50 mM 2DG; third panel: 30 min of 300 µM A769662. Representative of 6, 1, and 3 independent experiments for 2DG (−) serum, 2DG, and A769662, respectively. Empty, empty vector; α1WT, WT-AMPKα1; α1AS, AS-AMPKα1; α2WT, WT-AMPKα2; α2AS, AS-AMPKα2. (D) Summary of mass spectrometry datasets. AMPK-activating conditions as in Figure 2C. (E) Known AMPK substrates identified in multiple AS-AMPK datasets.

A vast quantity of data was identified in these substrate identification LC-MS/MS runs. As with the previously published attempts at in vivo substrate identification, few substrates were identified in any individual sample. However, the size of the dataset collected allowed for unique analysis by a stringent pipeline developed by our collaborators after discussion of the best way to sort the data. Phosphopeptides that were found in experimental datasets, but never in control datasets, were considered candidate substrates according to the logic outlined in Figure 3. In order to categorize substrates, the number of identifications of a particular phosphosite was used to categorize the strength of any candidate substrate, with identification in multiple samples representing high confidence. The motifs surrounding phosphorylation sites on phosphopeptides seen in 3 or more of the 22 experimental datasets (Group A) strongly adhered to the known AMPK motif(10) (Figure 3B), while those seen less frequently adhered less well to the AMPK motif (Figure 3C, D). In addition, many known AMPK substrates were identified in Group A. Thus, there is high confidence that the 21 previously unknown substrates identified in Group A are AMPK targets. While the general filtering approach used by this lab is appropriate for most datasets, the approach generated by Schaffer et al may be of particular use to those interested in using the AS kinase technique with large datasets.
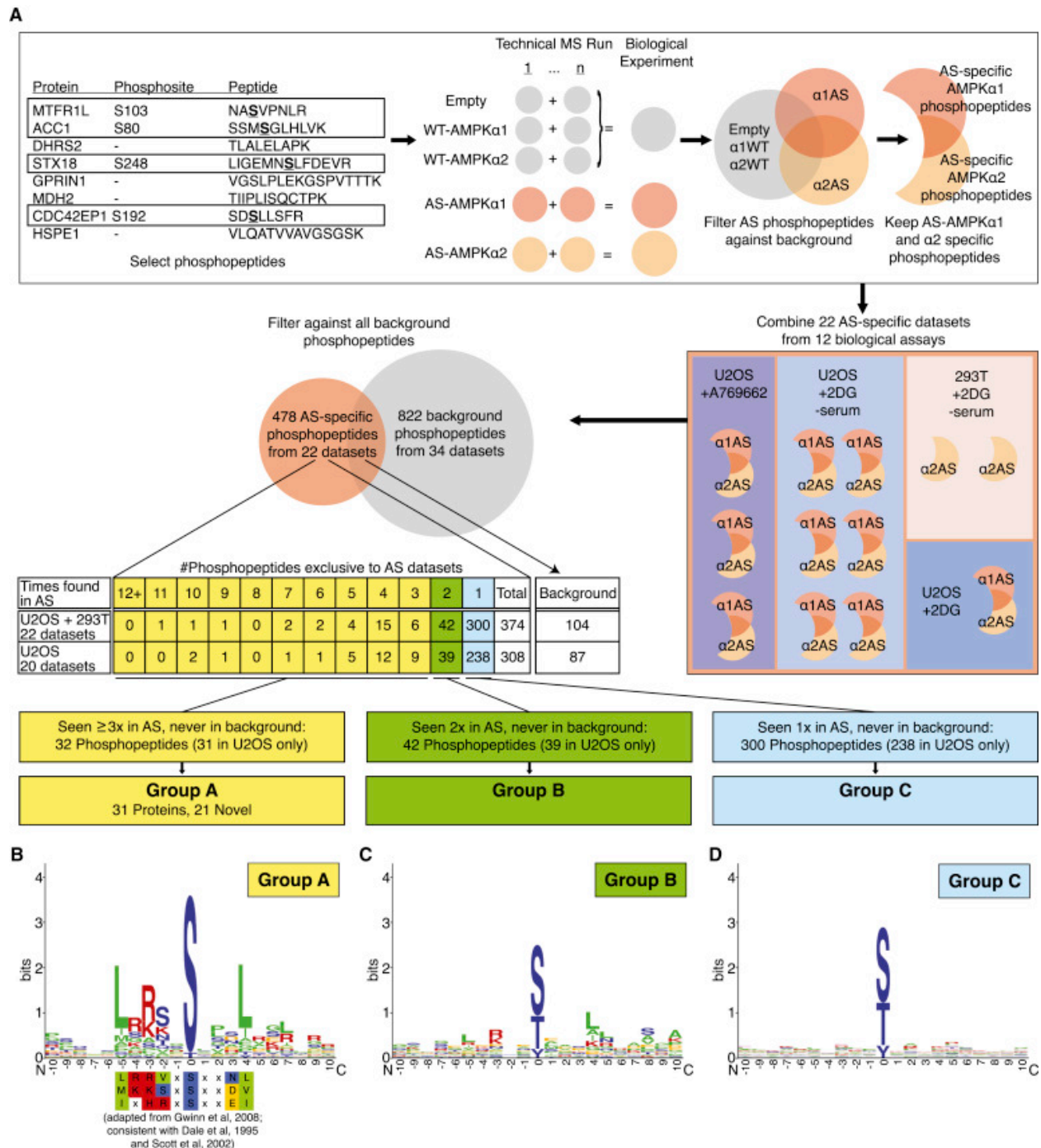
Figure 3 Grouping of AMPK substrates by relative strength (A) Schematic of the pipeline used to identify AS-AMPK substrates in LC-MS/MS datasets. Phosphopeptides only found in AS-AMPK datasets were classified as Group A, B, or C based on the number of biological samples in which they were identified. α1WT, α2WT, α1AS, α2AS: WT or AS-AMPKα1 or α2.(B–D) Logo motif of the most common phosphorylation sites on each phosphopeptide from Group A (B), Group B (C), and Group C (D). The established in vitro AMPK phosphorylation motif displayed below Group A generated in that study using a positional scanning peptide library (10). Green, hydrophobic residues; red, basic; yellow, acidic; blue, neutral polar.

16

Substrates identified by LC-MS/MS were extensively validated by further thiophosphorylation experiments. Through the use of GO term enrichment, AMPK substrates were shown to be enriched for roles in cell motility, adhesion and invasion. These conclusions were further supported by experiments demonstrating the role of AMPK driven phosphorylation of novel substrate NET1a in inhibiting extracellular matrix degradation. Furthermore, the identification of substrates enabled a large scale prediction of AMPK substrates, when combined with existing quantitative phosphoproteomic datasets, a novel use of substrate lists generated by the AS kinase covalent capture approach.

P-TEFb regulation of transcription termination factor Xrn2 revealed by a chemical genetic screen for Cdk9 substrates

Cyclin dependent kinases (CDKs) regulate gene expression through phosphorylation of the C-terminal domain of Rbp1, the largest subunit of RNA polymerase II (Pol II). Phosphorylation of heptad repeats of the sequence YSPTSPS drives the recruitment of factors and enzymes involved in RNA processing and maturation(11). Cdk7 and Cdk9 are the primary CDKs associated with regulation of gene transcription, unlike the many CDKs involved in cell cycle regulation. Cdk9, the catalytic subunit of positive transcription elongation factor b (P-TEFb), is thought to aid in overcoming promoter proximal Pol II pausing through phosphorylation of Pol II, DSIF and NELF, but the precise mechanism and staging remain undetermined(12). Thus, the exact targets and mechanisms through which P-TEFb regulated gene expression are largely undefined. In collaboration with the Fisher lab at the Icahn School of Medicine at Mount Sinai, we undertook a systematic identification of human Cdk9 substrates using the AS kinase system(13).

Cdk9 was co-purified with cyclin T1 to ensure constitutive activity in vitro. Mutation of Phe103 to

Gly allowed for the selective use of N6-modified ATPγS in vitro, unlike the wild type protein. This AS-Cdk9 construct was then used to label lysates from HCT116 cells, yielding clear labeling above background by AS-Cdk9 but not WT-Cdk9 or no kinase conditions, indicating thiophosphorylation of substrate proteins (Figure 4B). The remainder of these labeled lysates were digested, captured on iodoacetyl resin, released and analyzed by LC-MS/MS according to the normal laboratory protocol (described extensively in Chapter 3 and reference (13)) This data was analyzed by an in house R-script which filtered phosphopeptides exclusive to AS labeled samples and to exclude common contaminants based on a combined set of available experimental data from multiple AS kinase substrates (described in the next section). This yielded a total of 295 peptides phosphorylated by AS-Cdk9, derived from 172 proteins. Similar to the previously derived phosphorylation motifs for Cdk9, we observed the majority of phosphorylations to occur on S/T residues with P in the +1 position (Figure 4C). For high confidence substrates which fit the S/T-P motif, we grouped targets on the basis of function (Figure 4D). Transcription and RNA metabolism and splicing accounted for ~50% of the substrates, including known targets Spt5, BRD4 and AFF1. Certain known targets like Rpb1 were not identified in the dataset, possibly due to the lack of tryptic cleavage sites within the C-terminal domain that Cdk9 phosphorylates.

A

PNBM

N6-phenethyl-ATPγS

Cdk9as

Protein Mixture

Immunoblot

Trypsin

affinity purification

covalent capture and release

LC MS/MS

B

no kinase | Cdk9^WT cycT1 | Cdk9^as cycT1
1 2 | 1 2 | 1 2

250 –
150 –
110 –
75 –

ThioP

50 –

Cdk9

C

probability

1.0

0.5

0.0

-5   0   5

Position

WebLogo 3.4

D

CYTOSKELETON
ABI2
CALD1
CAMSAP2
CAMSAP3
CCDC6
DNMBP
KIF5B
LMNA
LIMA1
MAP7
PALLD

METABOLIC PROCESS
PDXDC1

PROTEIN FOLDING
TUBB2A

CELL CYCLE
CLASP1
HAUS6
SEPTIN 9
MCMBP
PPP1R35
PPP1CC
PPP1CB

UNKNOWN
C9ORF129
KIAA1430
XKR5

DNA DAMAGE
TRIP12

TRANSLATION
EEF2K
EIF4EN1F1
EIF4G1

SIGNAL TRANSDUCTION
AJUBA   IRS1
CANX   MLF2
DCBLD2   PXN
IK   RANBP9
ITSN2   SH3GL1
TJP1   TRAFD1

TRANSPORT
GULP1
LMAN1
SEC61B
SEC16A

MITOCHONDRIA
COQ9

UBIQUITYLATION
OS9
UBAP1

CELL DIFFERENTIATION & DEVELOPMENT
OSBPL8
PDLIM5
SPEG
STMN1
USH1G
SSFA2

BIOSYNTHESIS
DPH2
DPM1
PIKFYVE
PYCR1

TRANSCRIPTION

RNA METABOLISM & SPLICING

AFF1   HIVEP2   POLR3D   ZBTB7B
BRD4   HNRPUL1   SUPTH5   ZNF318
CRTC2   IRF2BP1   TCF3   ZNF648
ERF   NFATC1   TCOF1   ZNF763
FOXK1   NPM1   TRIM28   PPP1R13L
FOXK2   ONECUT1   YAP1

CDC5L   DCP1a   LARP1   RPL18
PRRC2A   XRN2   MEPCE   RPS20
RBMX   EDC4   NOB1   RPS17
SF3B1   IWS1   PPP4R2   RPS11
SRRM2   RAVER1   PUM1   SMG7
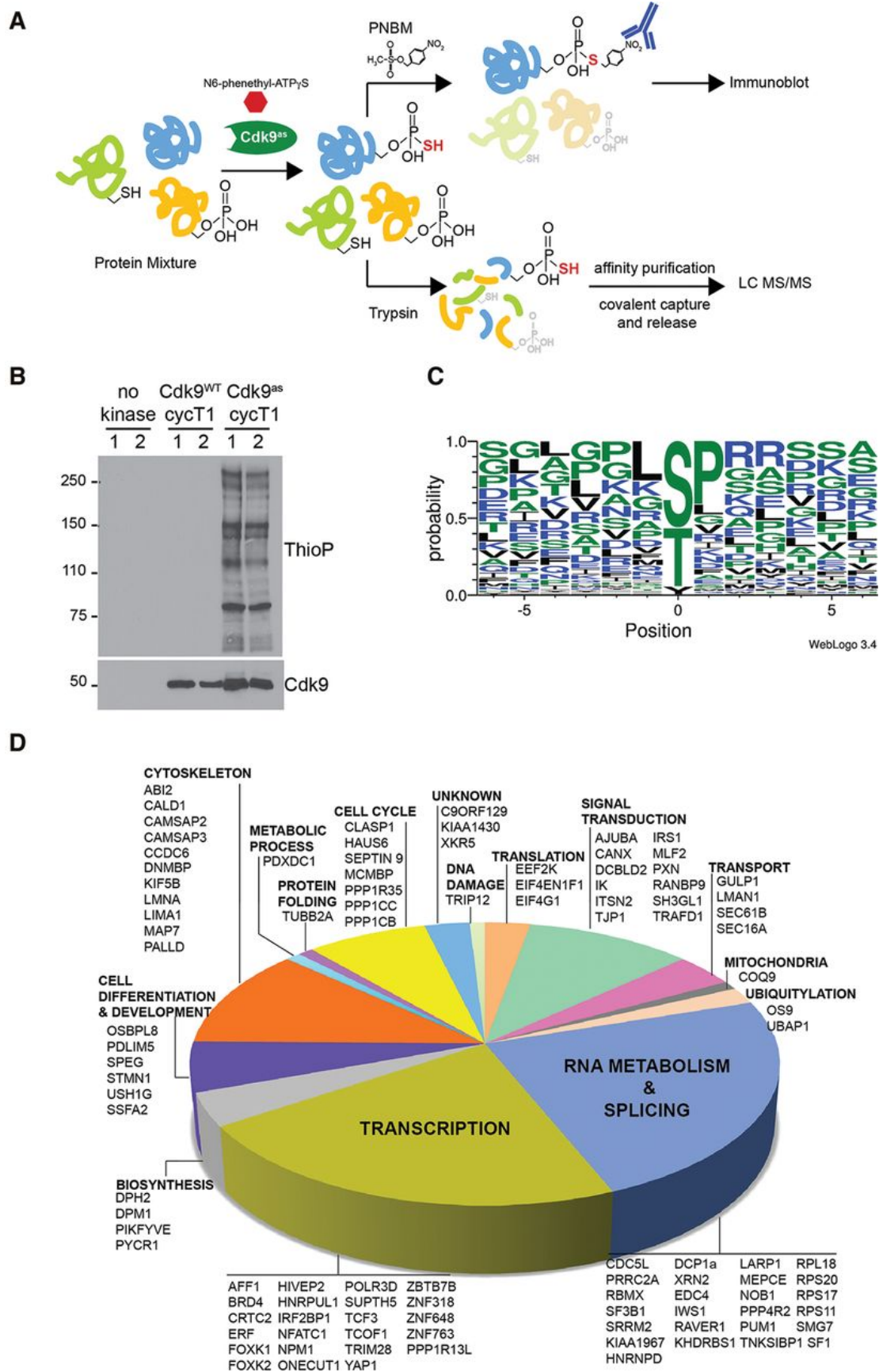KIAA1967 KHDRBS1   TNKSIBP1 SF1
HNRNPD

19

Figure 4. Identification of P-TEFb substrates. (A) Schematic diagram of AS labeling and substrate identification protocol. (B) Detection of substrates thiophosphorylated by Cdk9. (Lanes 1,2) Lysates of HCT116 cells were incubated in duplicate with Cdk9WT/cyclin T1, Cdk9as/cyclin T1, or no added kinase, as indicated, in the presence of N6-(phenethyl)-ATPγS. After alkylation with PNBM, samples were analyzed by immunoblotting for thiophosphate esters (ThioP) and Cdk9, as indicated. (C) Cdk9 consensus recognition sequence derived from phosphopeptides recovered at least twice in samples incubated with Cdk9as. (D) Selected gene ontology (GO) terms for Cdk9 substrates. Proteins phosphorylated at S/T-P sites were grouped on the basis of function.

Cdk9 modified proteins implicated in RNA 5' end processing splicing and transcription. Among these was Xrn2, the nuclear 5′-to-3′ exoribonuclease required for Pol II termination(14). Using an antibody generated for the phosphorylated residue Thr439, Cdk9 phosphorylation of Xrn2 was validated in vivo. Phosphorylation of Xrn2 was observed mainly when Xrn2 is bound to chromatin, suggesting a co-transcriptional function and possible regulation of that function by Cdk9. Phosphorylation of Thr439 enhanced the exoribonuclease activity of Xrn2 toward synthetic substrates in vitro. Inhibition or depletion of Cdk9 resulted in phenotypes consistent with inefficient termination in human cells, such as impaired Xrn2 chromatin localization and increased read through transcription of endogenous genes. Thus, in addition to the elongation promoting function of P-TEFb by phosphorylation of Pol II, P-TEFb can directly regulate co-transcriptional events such as termination by phosphorylating components of the relevant RNA processing machineries, including Xrn2. Discovery of this new role of P-TEFb was driven by the unbiased and systematic identification of Cdk9 substrates.

Common contaminants in covalent capture experiments and thoughts on the continued development of the covalent capture approach

During my time in the Shokat lab, the lab used the AS kinase and covalent capture methodology on at least 7 kinases, likely more, with only a small portion of that data reaching publication at the time this thesis was written. From these experiences, the lab has a significant, empirical knowledge about the quality of data produced from any experiment. In some experiments, very high numbers of phosphopeptides are identified. Thus, it is useful to develop means of ranking

substrates of interest, as discussed above for AMPK(9), Cdk9(13) and in Lipp et al(15). Over all of these experiments and despite extensive negative controls, we have noticed there are a number of phosphoproteins that are observed frequently in many datasets. Postdoc Dr. Jesse Lipp devised and in-house R script to cull common contaminants from a database of substrate identification experiments for at least 5 kinases for both human and mouse. These common contaminants or false positives are listed in Figure 5 for human and mouse. We can only theorize on why these proteins occur, perhaps we can consider them "promiscuous substrates". In general, we recommend against investing significant time and energy in following up substrates on this list, and focusing on phosphoproteins unique to one's own dataset. Should an AS kinase substrate identification experiment yield candidate substrate lists of very few phosphoproteins or predominantly phosphoproteins from these lists, we strongly suggest repeating the experiment. To that extent, previously published work(16), as well as work we have done with collaborators (unpublished), indicates that coupling a phosphopeptide enrichment step following elution from the iodoacetyl resin greatly increases identifications. I recommend the next generations of students establish protocols for phosphopeptide enrichment following covalent capture. During my tenure, I made multiple attempts to couple TiOx tip-based phosphopeptide enrichment with limited success. Recent and significant advancements in tip-based phosphopeptide enrichment will likely be better suited for coupling to covalent capture.

Human				Mouse			
Gene	**Accesion**	**Gene**	**Accesion**	**Gene**	**Accesion**	**Gene**	**Accesion**
AHNAK	Q09666	MOBKL1A	Q7L9L4	Apc	Q61315	Map2	P20357
ALS2CR8	Q8N187	MUC5AC	P98088	Arhgef2	Q60875	Mapt	P10637
ARHGEF16	Q5VV41	NADKD1	Q4G0N4	Bcas1	Q80YN3	Marcks	P26645
BAIAP2L2	Q6UXY1	NAGK	Q9UJ70	Camk2a	P11798	Marcksl1	P28667
BANF1	O75531	NUCKS1	Q9H1E3	Camk2b	P28652	Mbp	P04370
C20orf4	Q9Y312	PDHA1	P08559	Caskin1	Q6P9K8	Mtm1	Q9Z2C5
C2orf16	Q68DN1	PDHA1	P08559	Cep170	Q6A065	Mtss1l	Q6P9S0
CANX	P27824	PDIA6	Q15084	Ctnnd2	O35927	Nagk	Q9QZ08
CCDC94	Q9BW85	PFN1	P07737	Dbnl	Q62418	Nav1	Q8CH77
CTNNA1	P35221	PKM2	P14618	Dclk1	Q9JLM8	Nelf	Q99NF2
EEF1A1	P68104	PLIN4	Q96Q06	Dclk2	Q6PGN3	Nucks1	Q80XU3
EEF1B2	P24534	PPP1R12A	O14974	Ddx3x	Q62167	Pclo	Q9QYX7
EEF2	P13639	RAPH1	Q70E73	Dlgap2	Q8BJ42	Pdap1	Q3UHX2
ENSA	O43768	RBM14	Q96PK6	Dmxl2	Q8BPN8	Pde4a	O89084
ERC1	Q8IUD2	RPL23A	P62750	Dos	Q66L44	Pgrmc1	O55022
FBXO24	O75426	RPLP2	P05387	Dpysl2	O08553	Pkm2	P52480
GLT6D1	Q7Z4J2	RRM2	P31350	Elfn2	Q68FM6	Ppp2r5c	Q60996
HIST1H2BK	O60814	SAMHD1	Q9Y3Z3	Exoc8	Q6PGF7	Psd2	Q6P1I6
HSP90AB1	P08238	SCAF11	Q99590	Fam160a2	Q3U2I3	Purb	O35295
HSP90B1	P14625	SRRM1	Q8IYB3	Frmd4a	Q8BIE6	Rapgef2	Q8CHG7
HSPB1	P04792	SSB	P05455	Gap43	P06837	Rbm14	Q8C2Q3
KIAA0802	Q9Y4B5	SURF2	Q15527	Grin2b	Q01097	Reep1	Q8BGH4
KIAA2012	Q0VF49	TNRC6A	Q8NDV7	H1foo	Q8VIK3	Reep2	Q8VCD6
LMNA	P02545	TXN	P10599	Hsp90ab1	P11499	Shank2	Q80Z38
LMNB1	P20700	UPF3B	Q9BZI7	Hsp90b1	P08113	Shisa6	Q3UH99
LMNB2	Q03252	VSTM2L	Q96N03	Hspa8	P63017	Slc12a5	Q91V14
LRIG1	Q96JA1	WDR43	Q15061	Htatsf1	Q8BGC0	Sncb	Q91ZZ3
MAPKAPK2	P49137	ZFHX4	Q86UP3	Iqsec1	Q8R0S2	Srcin1	Q9QWI6
MARCKS	P29966	ZNF763	Q0D2J5	Kiaa0100	Q5SYL3	Stx1a	O35526
MARCKSL1	P49006			Kiaa0196	Q8C2E7	Stx1b	P61264
				Kiaa0284	Q80U49	Syn1	O88935
				Klc2	O88448	Tceal3	Q8R0A5
				Ksr1	Q61097	Ttn	A2ASS6
				Macf1	Q9QXZ0	Tuba1a	P68369
				Map1b	P14873	Wdr60	Q8C761

Figure 5. Common contaminant phosphoproteins found in Human and Mouse datasets. Observed sites of phosphorylation vary from experiment to experiment, but the protein in some phosphorylated form is found across many samples.

References

1. Liu Y, Shah K, Yang F, Witucki L, Shokat KM (1998) Engineering Src family protein kinases with unnatural nucleotide specificity. *Chem Biol* 5(2):91–101.
2. Liu Y, Shah K, Yang F, Witucki L, Shokat KM (1998) A molecular gate which controls unnatural ATP analogue recognition by the tyrosine kinase v-Src. *Bioorg Med Chem* 6(8):1219–26.
3. Shah K, Liu Y, Deirmengian C, Shokat KM (1997) Engineering unnatural nucleotide specificity for Rous sarcoma virus tyrosine kinase to uniquely label its direct substrates. *Proc Natl Acad Sci U S A* 94(8):3565–70.
4. Allen JJ, et al. (2007) A semisynthetic epitope for kinase substrates. *Nat Methods* 4(6):511–516.

5.   Allen JJ, Lazerwith SE, Shokat KM (2005) Bio-orthogonal affinity purification of direct kinase substrates. *J Am Chem Soc* 127(15):5288–9.

6.   Blethrow JD, Glavy JS, Morgan DO, Shokat KM (2008) Covalent capture of kinase-specific phosphopeptides reveals Cdk1-cyclin B substrates. *Proc Natl Acad Sci U S A* 105(5):1442–7.

7.   Rush J, et al. (2005) Immunoaffinity profiling of tyrosine phosphorylation in cancer cells. *Nat Biotechnol* 23(1):94–101.

8.   Banko MR, et al. (2011) Chemical genetic screen for AMPKα2 substrates uncovers a network of proteins involved in mitosis. *Mol Cell* 44(6):878–92.

9.   Schaffer BE, et al. (2015) Identification of AMPK Phosphorylation Sites Reveals a Network of Proteins Involved in Cell Invasion and Facilitates Large-Scale Substrate Resource Identification of AMPK Phosphorylation Sites Reveals a Network of Proteins Involved in Cell Invasion and Fa. 907–921.

10.   Gwinn DM, et al. (2008) AMPK Phosphorylation of Raptor Mediates a Metabolic Checkpoint. *Mol Cell* 30(2):214–226.

11.   Hsin J-P, Manley JL (2012) The RNA polymerase II CTD coordinates transcription and RNA processing. *Genes Dev* 26(19):2119–2137.

12.   Nechaev S, Adelman K (2011) Pol II waiting in the starting gates: Regulating the transition from transcription initiation into productive elongation. *Biochim Biophys Acta - Gene Regul Mech* 1809(1):34–45.

13.   Sansó M, et al. (2016) P-TEFb regulation of transcription termination factor Xrn2 revealed by a chemical genetic screen for Cdk9 substrates. *Genes Dev*:117–131.

14.   Kim M, et al. (2004) The yeast Rat1 exonuclease promotes transcription termination by RNA polymerase II. *Nature* 432(7016):517–22.

15.   Lipp JJ, Marvin MC, Shokat KM, Guthrie C (2015) SR protein kinases promote splicing of nonconsensus introns. *Nat Struct Mol Biol* 22(8):611–617.

16.   Carlson SM, et al. (2011) Large-scale discovery of ERK2 substrates identifies ERK-mediated transcriptional regulation by ETV3. *Sci Signal* 4(196):rs11.

Chapter 3

The innate immunity kinase TAK1 phosphorylates Rab1 on a hotspot for post-translational modifications by host and pathogen

Rebecca S. Levin[a], Nicholas T. Hertz[a,1], Alma L. Burlingame[b], Kevan M. Shokat[a,2], Shaeri Mukherjee[c,2]

[a]Department of Cellular and Molecular Pharmacology and Howard Hughes Medical Institute, University of California, San Francisco, San Francisco, CA 94158, USA
[b]Department of Pharmaceutical Chemistry, University of California, San Francisco, San Francisco, CA 94158, USA
[c]Department of Microbiology and Immunology, University of California, San Francisco, San Francisco, CA 94143, USA

Abstract

TGF-β Activated Kinase 1 (TAK1) is a critical signaling hub responsible for translating antigen binding signals to immune receptors for the activation of the AP-1 and NF-κB master transcriptional programs. Despite its importance, known substrates of TAK1 are limited to kinases of the MAPK and IKK families and include no direct effectors of biochemical processes. Here, we identify over 200 novel substrates of TAK1 using a chemical genetic kinase strategy. We validate phosphorylation of the dynamic switch II region of GTPase Rab1 at T75 to be regulated by TAK1 in vivo. TAK1 preferentially phosphorylates the inactive (GDP-bound) state of Rab1. Phosphorylation of Rab1 disrupts interaction with GDP Dissociation Inhibitor 1 (GDI1), but not GEF or GAP enzymes, and is exclusive to membrane localized Rab1, suggesting phosphorylation may stimulate Rab1 activation and membrane association. We found phosphorylation of Rab1 at T75 to be necessary for normal Rab1 mediated ER to Golgi vesicular transport. Previous studies established that the pathogen *Legionella pneumophila* is capable of hijacking Rab1 function through post-translational modifications of the switch II region. Here, we present the first evidence that Rab1 is regulated by the host in a similar

fashion; and that the innate immunity kinase TAK1 and *Legionella* effectors compete directly to regulate Rab1 by switch II modifications during infection.

Significance Statement

Rab GTPases regulate vesicle traffic within the cell by switching between active (GTP-bound) and inactive (GDP-bound) states. The switch II region of Rab proteins undergoes a significant conformational change in order to switch between states. Rab1 is hijacked during intracellular *Legionella pneumophila* infection by bacterial effector mediated post-translational modifications of the switch II region, a unique mechanism for regulation of Rab function. We present new evidence that Rab1 is endogenously modified within switch II by TAK1, a kinase crucial for responding to infection. Phosphorylation of Rab1 is necessary for normal Rab1 function in ER to Golgi vesicle transport. Interestingly, phosphorylation of Rab1 is competed during *Legionella* infection, adding to evidence that *Legionella* target substrates of the innate immunity kinase TAK1.

Introduction

Cellular response to microbial infection is a complex, coordinated process that is initiated by innate immune receptors at the cell surface in response to cytokines or pathogen associated molecular patterns (PAMPs). Pattern recognition receptors (PRRs) trigger cellular response cascades culminating in activation of two master transcriptional programs, AP-1 and NF-κB, which drive cytokine production and recruitment of immune cells. In particular, Toll like receptor (TLR) signaling cascades require the intricate orchestration of activation of downstream pathway components through formation of diverse complexes and intensive reliance on post-translational modifications for regulation. Ultimately, these pathways converge on the activation of an essential kinase, TGF-β activated kinase 1 (TAK1), which is responsible for translating receptor activation for the activation of these master transcriptional programs(1).

In the early phase following activation of receptors such as TLR2 or 4, an unusual non-degradative ubiquitin scaffold is assembled, leading to the activation of TAK1, also known as MAP3K7. Once activated, TAK1 serves two roles. First, TAK1 acts as a canonical MAPKKK by phosphorylating the MAPKKs MKK4/7 and MKK3/6. These MKKs phosphorylate and activate p38 and JNK, respectively, initiating AP-1-mediated transcription. Second, TAK1 provides a priming phosphorylation to IKKβ, which co-localizes with TAK1 to M1-poly-Ub chains generated by TRAF6 upon TLR activation(2, 3). Activation of IKKβ leads to the activation IKKα, degradation of IκBα, and lastly activation of NF-κB driven transcription. The known direct substrates of TAK1 are limited to these protein kinases, TAB1 and an additional protein kinase AMPK(4, 5). TAK1 is primarily viewed as an initiator of kinase signaling cascades that lead to transcription factor activation.

Kinases often serve as signaling relays, transferring phosphorylation down a cascade of kinases, but also commonly function as direct effectors of biochemical processes via phosphorylation of enzymes from many classes. Given the importance of TAK1 as the terminal output of PRR activation, we wondered if TAK1 might possess direct substrates beyond the three characterized classes of downstream kinases. Only one study has characterized a small number of downstream targets of TAK1 using quantitative phosphoproteomics. While no direct TAK1-substrate relationships were established, GO term enrichment of TAK1-regulated phosphoproteins suggested involvement in GTPase regulation and membrane organization(6). Other studies have suggested a role for TAK1 in directly regulating protein degradation to prevent accumulation of reactive oxygen species(7). Thus, we turned to the analog specific kinase covalent capture methodology(8, 9) to identify direct TAK1 substrates *in vitro*. Through this method, we identified hundreds of candidate substrates.

We decided to focus, in particular, on a novel phosphorylation site within a dynamic region of small Ras-like GTPase Rab1. Rab proteins are the largest family of small Ras-like GTPases and serve to regulate many steps of membrane trafficking. They act as molecular switches, cycling through active, GTP-bound and inactive, GDP-bound states. Two regions of the GTPases, termed switch I and switch II, undergo significant conformational shifts between these states, altering the ability of the protein to bind interactors. Rab nucleotide state, and therefore signaling, is tightly regulated by Guanine Exchange Factors (GEFs) and GTPase-Activating Proteins (GAPs). By binding Rab proteins in the cytoplasm, GDP Dissociation Inhibitors (GDIs) sequester inactive Rab proteins to further control Rab activation. While the C-terminal tails of Rab proteins are geranylgeranylated to mediate insertion into membranes, there are few examples of regulation of Rab proteins, or small GTPases in general, by post-translational modification of the core GTPase domain. Although phosphorylation of Rab proteins, and other Ras-like GTPases, has been previously observed on the C-terminal tail and other outlying regions, there is little consensus on the regulatory effect of these phosphorylations (10–13). The strongest examples of small GTPase regulation by post-translational modification are when the core GTPase domain is modified, rather than tails. Such modifications are almost exclusively the result of infection by pathogens, such as phosphorylation of switch I of immunity-related GTPases (IRGs) by a secreted *Toxoplasma gondii* kinase in mice (14) or AMPylation and phosphocholination of the switch region of Rab1 by *Legionella pneumophila* (15, 16).

Here, we demonstrate that TAK1 phosphorylation of Rab1 within the dynamic switch II region is key to Rab1 signaling. Phosphorylation of Rab1 is necessary for normal Rab1-mediated ER to Golgi vesicle transport, and disrupts interaction with GDP Dissociation Inhibitor 1 (GDI1), allowing for activation of Rab1. More interestingly, TAK1 mediated phosphorylation of Rab1 is competed by *Legionella pneumophila* during intracellular infection. We believe Rab1 is a newly

recognized hotspot for regulation via post-translational modifications, both by a bacterial

pathogen, and now by TAK1, a host kinase responsible for responding to infection.

Results

Identification and Validation of Novel TAK1 substrates

We first sought to identify direct substrates of TAK1 using a chemical genetic, analog specific

kinase approach (Figure 1A)(8, 9). Mutation of a single bulky residue within the active site of a

kinase, termed the active site gatekeeper residue, to alanine or glycine expands the native ATP

binding pocket. This mutation allows the kinase to accept a N^6 substituted ATPγS analogs,

bulky variants of ATP which fit in the newly expanded active site but not the active sites of wild-

type kinases, creating an Analog-Specific (AS) kinase. The AS-kinase transfers the γ-

thiophosphate of the ATP analog to its substrates. This thiophosphorylation acts as a uniquely

reactive chemical handle that can be alkylated for detection of substrates by western blotting or

used to affinity purify and identify substrate proteins by LC-MS/MS. We generated a

constitutively active form of TAK1 by expressing and purifying from insect cells a fused TAK1

construct containing the kinase domain of TAK1 fused to the TAK1-activating domain of binding

partner TAB1 (Figure 2A)(17).   We will refer to this fusion construct as TAK1^f, with WT

indicating no mutations to the gatekeeper residue. Analog-specific TAK1^f (AS-TAK1^f) was

generated by mutation of gatekeeper methionine 81 to alanine. We tested the specificity and

preference of AS-TAK1^f for N^6 substituted ATPγS analogs through an *in vitro* kinase assay

using myelin basic protein (MBP) as a generic substrate (Figure 2B). AS-TAK1^f utilized both

ATPγS and N^6-furfuryl-ATPγS efficiently for autophosphorylation and transphosphorylation of

MBP. In contrast, WT- TAK1^f was largely incapable of using any bulky ATP analogs. N^6-furfuryl-

ATPγS was used for lysate labeling experiments to ensure any detected thiophosphorylation

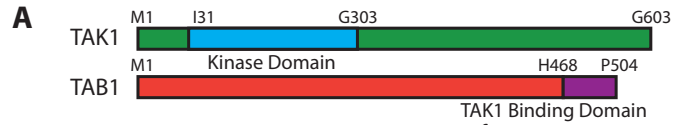was the result of AS- TAK1^f activity.

A

Labeling With AS Kinase:

Detecting/Identifying Substrates:

React PNBM

Western Blot a-thiophosphate ester

OR:

ID Substrate Phosphopeptide by LC-MS/MS

Trypsin Digest

Selective Capture

Release
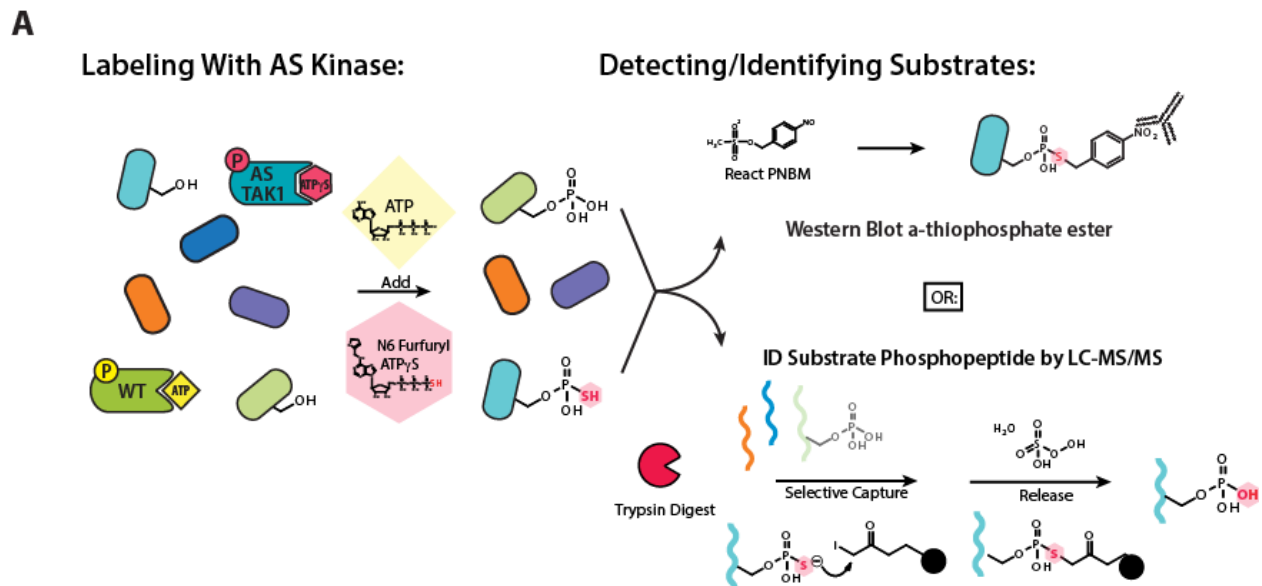
B

Cell Line	Phosphoproteins	Phosphopeptides	phosphosites ID'ed in ≥2 samples
CaCo2	131	195	69
SW620	97	142	60
DU145	98	163	61
PC3	86	130	45
Total Unique	269	424	169

Figure 1. Schematic of analog specific substrate capture and identification of TAK1 substrates. (**A**) Schematic of lysate labeling with AS-TAK1 versus WT-TAK1. Kinase is spiked into cell lysates with a bulky ATP analog, here N^6 furfuryl ATPγS, which selectively thiophosphorylates substrates. Thiophosphorylated proteins can be detected two ways: by western after alkylation to form a thiophosphate ester, or by digestion and capture on a thiol-reactive iodoacetyl resin, release and analysis by LC-MS/MS. (**B**) Numbers of unique phosphoproteins and phosphopeptides identified in each cell line and in total.

We next sought to identify proteins selectively thiophosphorylated by AS TAK1[f] in lysates from 4 cell lines from 2 cancer types, colorectal (CaCo2, SW620) and pancreatic (PC3, DU145). These cell lines were selected because TAK1 has been shown to be particularly important in colorectal and prostate cancers(18, 19). Lysates were individually labeled by spiking in N^6-furfuryl-ATPγS and purified AS-TAK1[f], WT-TAK1[f] or with no added kinase. A portion of each sample was analyzed by western blot, where an obvious increase in thiophosphorylation is observed

exclusively in the AS labeled colorectal cell line samples, the contrast between AS and WT or

no kinase conditions is less obvious in the pancreatic cell lines, as these cell lines displayed

much higher background thiophosphorylation (Figure 2C, Figure 1B). We attribute this

difference, in part, to variability between cell lines in the background proteome activity toward

the ATPγS analog. The remainder of the thiophosphorylated lysates were digested,

thiophosphorylated peptides covalently captured, converted to phosphorylated peptides upon

elution from resin and analyzed by mass spectrometry. Despite differences in levels of

thiophosphorylation by western blot, many more phosphopeptides were identified in all AS-

TAK1[f] labeled samples versus controls. (data not shown). Thus, although western detection of

thiophosphorylation is a useful tool, it is limited in comparison to mass spectrometry results as

observed in this study and others (20).

A

TAK1

M1   I31   G303   G603
            Kinase Domain

TAB1

M1   H468 P504
                            TAK1 Binding Domain

Constituenly Active TAK1-TAB1 Fusion (TAK1^f) Expression Constructs

WT-TAK1^f 5x His   I31   G303 H468 P504

AS-TAK1^f 5x His   I31 M81A   G303 H468 P504

B

	WT-TAK1^f				AS-TAK1^f			
N^6-ATPγS	A	FF	Bn	PE	A	FF	Bn	PE

α-Thiophosphate Ester — p-TAK1^f

— p-Mbp

Ponceau — Mbp

C

TAK1^f	SW620			CaCo2			PC3			Du145		
	–	WT	AS	–	WT	AS	–	WT	AS	–	WT	AS

α–Thiophosphate Ester

His-TAK1^f

β-Tubulin

D

DU145   PC3

CaCo2   SW620

40   34
   3   16   2
68   6   0   42
   5   4
   3   9
      17
      20
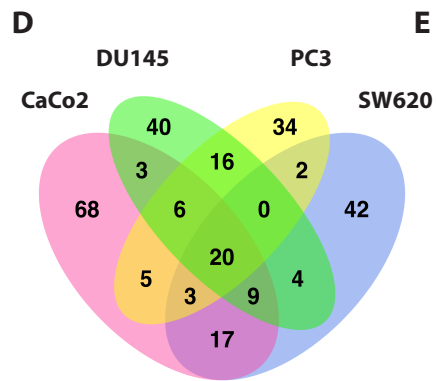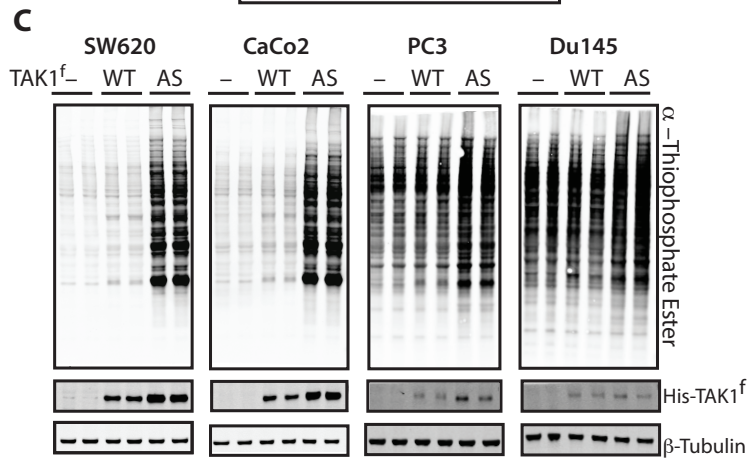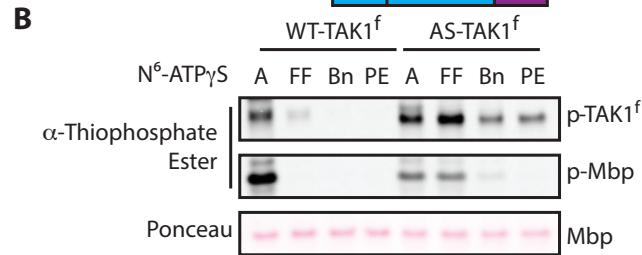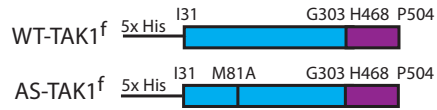
E

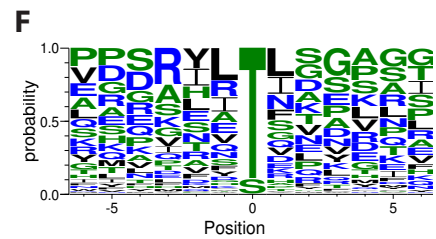| Gene	Site
EEF1A1	T261
EIF4B	S230
FLNA	T1286
GAPVD1	S1012|T1013
HNRNPA2B1	T176
HSP90B1	S674|T675
HSP90B1	T669
HSP90B1	T675
LDHA	T3
POLD2	T33
RAB1A	T75
RBMX	T216
TUBA1B	T334
TUBB	T166

F

31

Figure 2. Characterization of AS-TAK1[f] and identification of TAK1 substrates. (**A**) Schematic of full length TAK1, TAB1 and constituently active fusion constructs of WT-TAK1[f] and AS-TAK1[f] used for protein purification. (**B**) *In vitro* kinase assay with TAK1[f], MBP and bulky N^6 substituted ATPγS analogs (A – ATPγS, FF – N^6 furfuryl, Bn – N^6 benzyl, PE – N^6 phenethyl). Thiophosporylation was evaluated by western blot. (**C**) Lysate from SW620, CaCo2, PC3 and Du145 cells were labeled with no kinase (-), His-tagged WT-TAK1[f] (WT), or His-tagged AS-TAK1[f] (AS) in biological duplicate. (**D**) Venn diagrams of phosphoproteins identified in 4 cell cancer lines, colorectal (SW620, CaCo2), pancreatic (DU145, PC3) (**E**) Phosphosites exclusive to and identified in all 8 individual AS-TAK1[f] labeled samples. (**F**) TAK1 consensus motif derived from all phosphopeptides identified in ≥ 2 samples

The data were filtered by cell type to exclude background phosphopeptides from the WT-TAK1[f]

and no kinase conditions(21), leaving phosphopeptides exclusive to AS-TAK1[f]. In total, 269

phosphoproteins yielding 424 phosphopeptides were identified as candidate TAK1 substrates

(Figure 1B). A list of all candidate substrate phosphopeptides identified is available in Appendix

1. The difference in peptide versus protein number is a result of the identification of multiple

phosphopeptides per protein and, in some cases, a single peptide identified multiple times with

differing sites of phosphorylation. While all cell lines shared a set of 20 substrate proteins,

generally substrates were shared more frequently between cell lines of the same origin, with

many substrates uniquely identified in a single cell line (Figure 2D). Although the stochastic

nature of shotgun LC-MS/MS identification may explain some of the lack of overlap, we believe

the method of capture utilized is able to identify cell-type specific substrates. Conservation of a

substrate across cell types may be indicative of a central, conserved function, and therefore a

useful means to triage substrates for further study. Fourteen phosphopeptides were identified in

all AS-TAK1[f] samples analyzed (Figure 2E). To further analyze the substrate preferences of

TAK1, we generated a TAK1 consensus sequence from phosphopeptides identified in at least 2

samples (Figure 2F)(22). We observed a strong preference for phosphorylation of threonine,

with some preference for aliphatic -1 and +1 residues.

To corroborate our MS results, a subset of substrates identified by mass spectrometry were

selected for further validation. We assessed the ability of TAK1 to phosphorylate substrates

overexpressed with N-terminal Flag or GST tags and immunoprecipitated from HEK-293Ts by *in vitro* radioactive kinase assay with WT-TAK1[f]. As a positive control, we sought to confirm that our WT-TAK1[f] would strongly phosphorylate a known substrate, MKK6. MKK6 was not identified by MS due to the presence of cysteine in tryptic MKK6 peptides containing TAK1 phosphorylation sites, as Cys-containing peptides are permanently retained on the capture resin(9). TAK1 strongly phosphorylated kinase-dead MKK6 as shown by the incorporation of ^{32}P in the WT-TAK1[f] labeled sample (Figure 3A). Of the 8 candidate substrates tested, only PSMC4 was not strongly phosphorylated by WT-TAK1[f]. The remaining 7 substrates were strongly phosphorylated by TAK1 (Figure 3A, B, C). Interestingly, WT-TAK1[f] was clearly able to phosphorylate more than the single identified site on three substrates, Vinexin, EIF4B, EIF3I, as shown by incorporation of ^{32}P into the non-phosphorylatable T to A mutants (Figure 3B). It is possible additional phosphosites in these proteins are within regions not amenable for detection by trypsin-based LC-MS/MS and were therefore not detected. Given the high rate of substrate validation, we have high confidence in the validity of the candidate substrates identified by mass spectrometry.
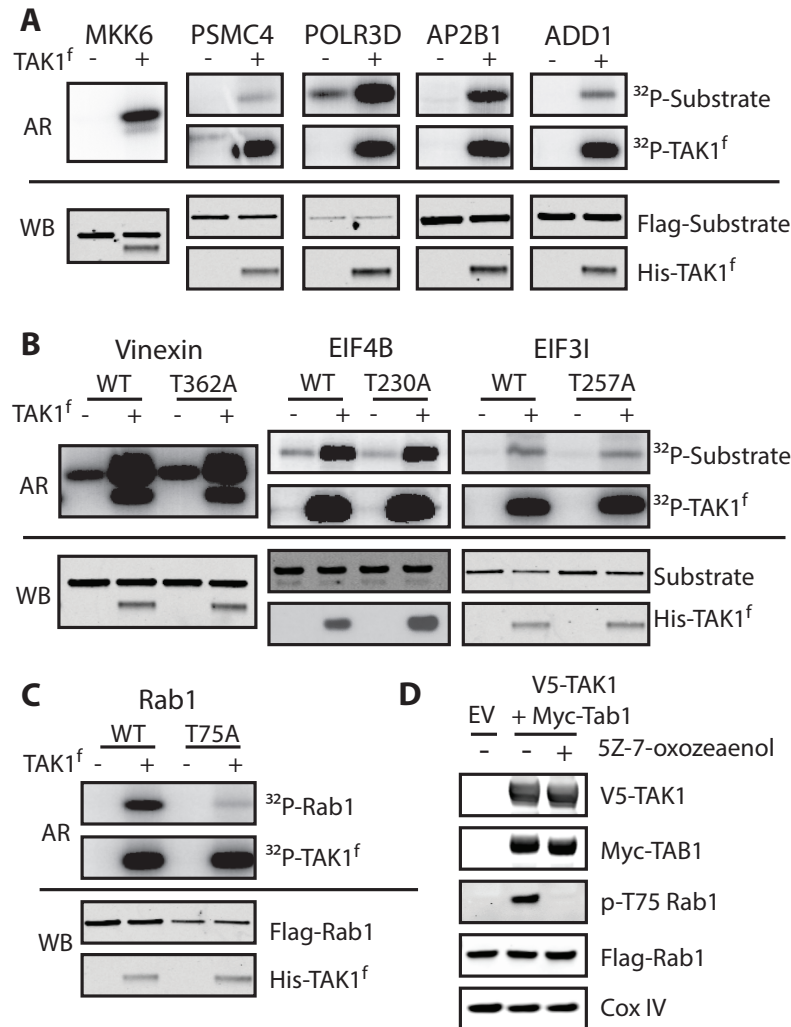
Figure 3. Validation of TAK1 substrates *in vitro* and *in vivo*. (**A, B, C**) In vitro radioactive kinase assays with GST- or Flag-tagged TAK1 substrates. Substrates immunoprecipitated from HEK-293Ts were incubated with purified WT-TAK1[f] (300nM) and γ^{32}P-ATP, run on a gel and imaged by autoradiography (AR). Aliquots removed prior to γ^{32}P-ATP addition were used to assess loading by western blot (WB). MKK6 (kinase dead) is a known substrate and positive control. (**D**) HEK-293s stably expressing Flag-Rab1 were transfected with either empty vector(EV) or full length V5-TAK1 and Myc-TAB1 were analyzed by western for pT75 Rab1. One condition was dosed with 2.5µM TAK1 inhibitor 5z-7-oxozeaenol for 1 hour.

TAK1 selectively phosphorylated GDP-bound Rab1

Rab1 was the sole protein tested that was phosphorylated by WT-TAK1[f] at a single site, T75, within its switch II region, in all 4 cell lines (Figure 3C). Switch II is a conserved region within the catalytic domain of GTPases that undergoes a conformational shift between the active (GTP-

bound) and inactive (GDP-bound) states(23) and is not a common site of post-translational modification. This selective phosphorylation motivated us to carry out *in vivo* validation with a polyclonal antibody raised against pT75 Rab1. In HEK-293 cells stably expressing Flag-Rab1, overexpression of full length V5-TAK1 and activating partner Myc-TAB1(24) led to increased phosphorylation of Rab1 T75. Addition of a TAK1-selective inhibitor, 5z-7-oxozeaenol(25), eliminated phosphorylation of Rab1 (Figure 3D). The increased abundance of pT75 Rab1 following TAK1 overexpression and loss of phosphorylation upon inhibition of TAK1 was also observed by LC-MS/MS analysis of immunoprecipitated Rab1 (data not shown). A similar increase in phosphorylation of endogenous Rab1 is observed upon TAK1 overexpression in normal HEK-293T, as is a decrease in phosphorylation after TAK1 inhibition. The modulation of pT75 Rab1 levels upon manipulation of TAK1 catalytic activity by overexpression and inhibition suggests Rab1 is a direct substrate of TAK1 *in vivo*.

Because switch II occupies two distinct conformations, we hypothesized that the nucleotide state of Rab1 may influence the ability of TAK1 to phosphorylate T75. Radiometric *in vitro* kinase assays with GST-Rab1 purified from a bacterial expression system and WT-TAK1^f showed preferential phosphorylation of the inactive, GDP-locked Rab1S25N(26) and reduced phosphorylation of active state mimetic Rab1Q70L(27) (Figure 4A). Correspondingly, TAK1 preferentially phosphorylated Rab1 loaded with GDP by nucleotide exchange versus non-hydrolyzable GTPγS (Figure 4B). The preference of TAK1 for GDP-Rab1 may be explained by available structural data of the yeast homolog of Rab1, Ypt1. Alignment of the structure of GDP [PDB: 2BCG] and GTP mimetic GppNHp [PDB: 1YZN] bound Ypt1 shows the switch II region to be flipped outward from the body of the protein, exposing T75-equivalent residue T72 (Figure 4C). Our findings suggest that T75 is only accessible for phosphorylation by TAK1 when GDP binding to Rab1 causes the switch II region to become disordered(23). Interestingly, the intracellular pathogen *Legionella pneumophila* is well documented to hijack the function of Rab1

in infected cells by post-translational modification of nearby switch II residues including adenylylation, also known as AMPylation, of Y80 and phosphocholination of S79 (Figure 4D)(15, 16, 28).
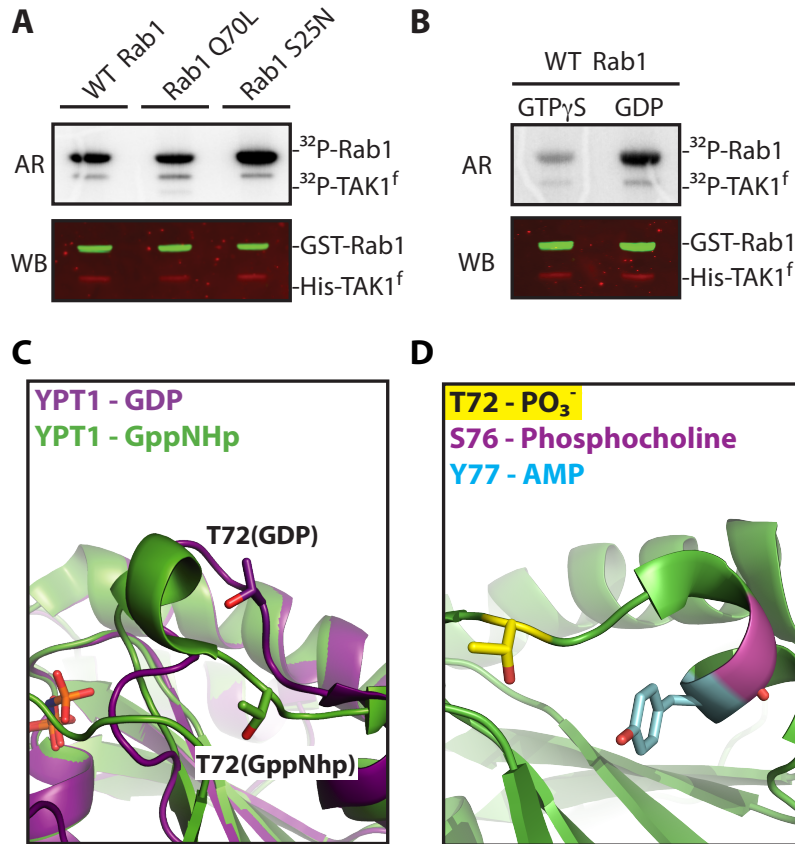
Figure 4. TAK1 preferentially phosphorylates GDP-bound Rab1. (**A**) *In vitro* kinase assay of purified GST-Rab1 mutants (10μM) and WT-TAK1^f (100nM) imaged by autoradiography (AR) and western blot (WB) as loading control. (**B**) *In vitro* kinase assay of WT- TAK1^f (100nM) and purified GST-WT Rab1 (10μM) loaded with the indicated nucleotide. (**C**) Alignment of Rab1-homolog Ypt1 structures bound to GDP [PDB: 2BCG] or GTP analog GppNHp [PDB: 1YZN]. Ypt1 T72 aligns to Rab1 T75. (**D**) Mapping of post-transnationally modified Rab1 residues within switch II where S76 and Y77 (Rab1 S79 and Y80 as aligned to YPT1 structure PDB:1YZN) are sites of *Legionella* derived modifications.

Phosphorylation of Rab1 disrupts GDI but not GAP, GEF interactions

During activation, switch II becomes more ordered and T75 is flipped inward towards the core of Rab1 (Figure 4C). It is possible that phosphorylation may block Rab1 from binding GTP and localizing to the membrane by sterically hindering the conformational shift of switch II. In order to determine whether phosphorylation may disrupt GTP binding, we assayed the nucleotide

36

affinities of Rab1 mutants using 2′-deoxy-3′-O-(*N*-methylanthraniloyl) (mant)-dGDP (mant-GDP)

loaded Rab1, which forms a fluorescent complex. EDTA was used to catalyze nucleotide

exchange while titrating unlabeled GDP or GTP(29), with a reduction in fluorescence due to

mant-GDP displacement corresponding to affinity for the titrated nucleotide. All constructs

tested, including WT-Rab1 phosphorylated by pre-incubation with TAK1 and ATP, maintained a

similar affinity for GDP (Figure 5A). A slight increase in affinity for GTP was observed for

Rab1Q70L, phosphomimetic Rab1T75E, and WT-Rab1 pre-incubated with TAK1 and ATP

(Figure 5B, C). The catalysis of nucleotide exchange by ETDA suggests that phosphorylation

does not prevent activation of Rab1, and may in fact enhance GTP affinity.

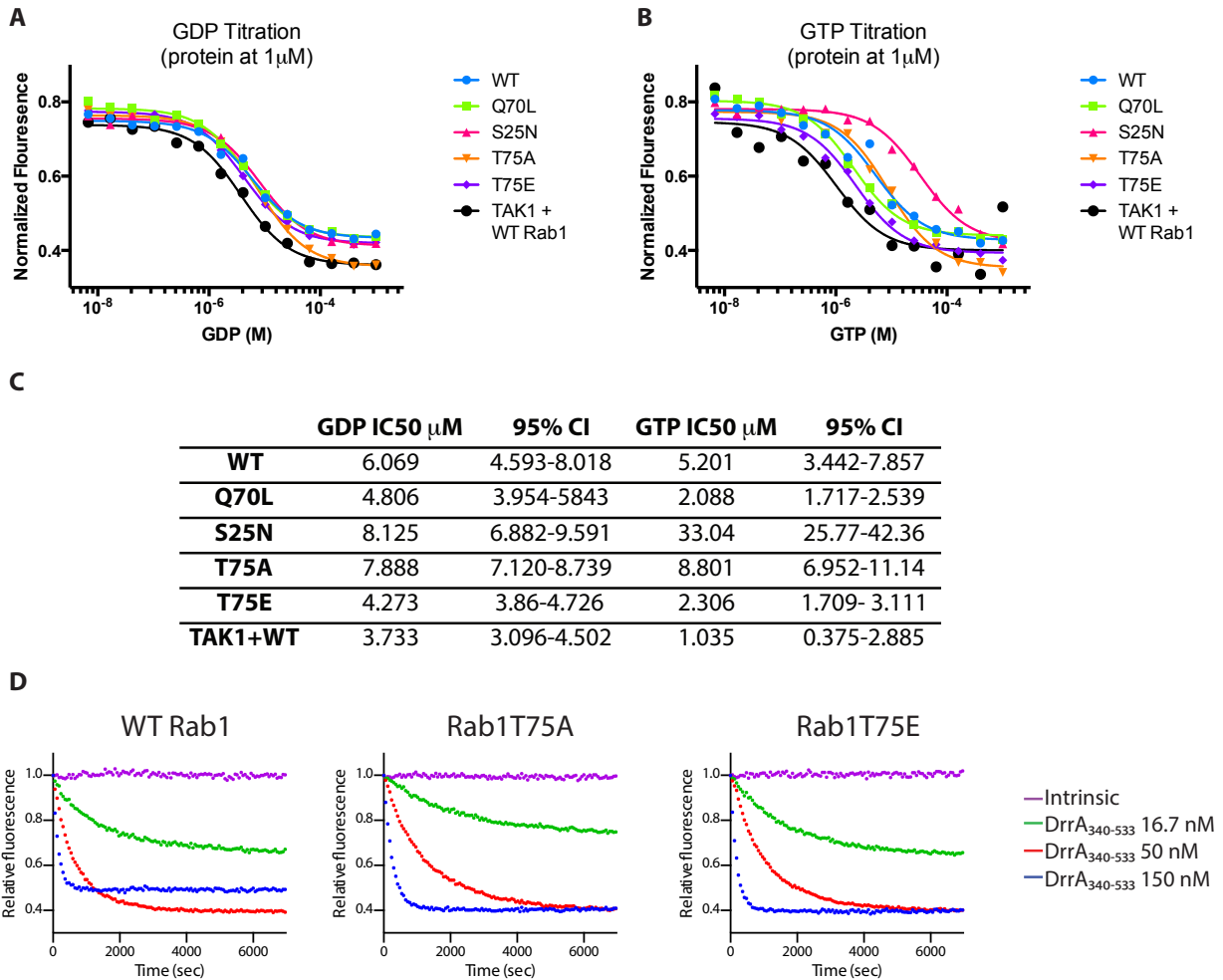|	GDP IC50 μM	95% CI	GTP IC50 μM	95% CI
WT	6.069	4.593-8.018	5.201	3.442-7.857
Q70L	4.806	3.954-5843	2.088	1.717-2.539
S25N	8.125	6.882-9.591	33.04	25.77-42.36
T75A	7.888	7.120-8.739	8.801	6.952-11.14
T75E	4.273	3.86-4.726	2.306	1.709- 3.111
TAK1+WT	3.733	3.096-4.502	1.035	0.375-2.885

Figure 5. GDP and GTP affinities for GST-Rab1 mutants and GEF catalyzed GDP exchange. (A) mant-GDP is first loaded on GST-Rab1 mutants and excess mant-GDP removed. A single concentration of mant-GDP bound Rab1 (1µM) is subject to EDTA (5mM) catalyzed nucleotide exchange in the presence of varying conditions of free GDP (x-axis). The reaction is allowed to proceed for 1 hour, and remaining mant-GDP-Rab1 complex is quantified by fluorescence and normalized to an EDTA free condition (y-axis). (n=1) (**B**) Similar to **A**, except with varying concentrations of free GTP(n=1). (**C**) Quantification of GDP and GTP titrations in A and B, where IC_{50} values were obtained from sigmoidal fits (CI: confidence interval). (**D**) Representative single experiment data for DrrA340-533 catalyzed nucleotide exchange from all mant-GDP bound Rab1 mutants in the presence of excess GTP (see Figure 6A, B).

Multiple studies have shown that phosphocholination and AMPylation of Rab1 switch II manipulate Rab1 function by blocking the ability of Rab1 to interact with Guanine Exchange Factors (GEF) and GTPase Activating Proteins (GAP)(16, 28, 30), as switch II serves as the primary interface for these binding events. In order to investigate whether phosphorylation of Rab1T75 may have a similar effect, we assayed the ability of the *Legionella* Rab1 GEF DrrA (GEF domain only, residues 340-533) to catalyze the displacement of mant-GDP from WT and mutant Rab1 *in vitro* (Figure 6A, B, 5D). $DrrA_{340-533}$ was selected for these assays due to numerous publications(30–32) describing similar experiments with this enzyme. We found no significant difference in the k_{cat}/K_m of $DrrA_{340-533}$ toward WT Rab1 and Rab1T75E, and only a slight difference with Rab1T75A, thus we infer that it is unlikely phosphorylation of T75 prevents Rab1 interaction with GEFs or interferes with activation. Phosphomimetic mutant Rab1T75E yields similarly insignificant effects on the ability of a *Legionella* GAP, LepB (33), to stimulate Rab1 hydrolysis of GTP, as measured with the Promega GTPase-Glo system(34). Briefly, increasing concentrations of LepB with excess GTP held at a constant concentration are added to wells containing a constant concentration of Rab1 and allowed to react for 1 hour. The amount of remaining, unhydrolyzed GTP in each condition is detected by luminescence-coupled assay, plotted against GAP concentration and a LepB EC_{50} is determined. We found no difference in LepB activity towards WT, T75E or T75A (Figure 7A, B), which suggests phosphorylation does not interfere with inactivation of Rab1 by GAPs. Considering the GTP/GDP affinity, GEF assay and GAP assay together, we conclude phosphorylation of Rab1

does not impact the ability of Rab1 to cycle between GDP and GTP bound states or interact

with GAP and GEFs.
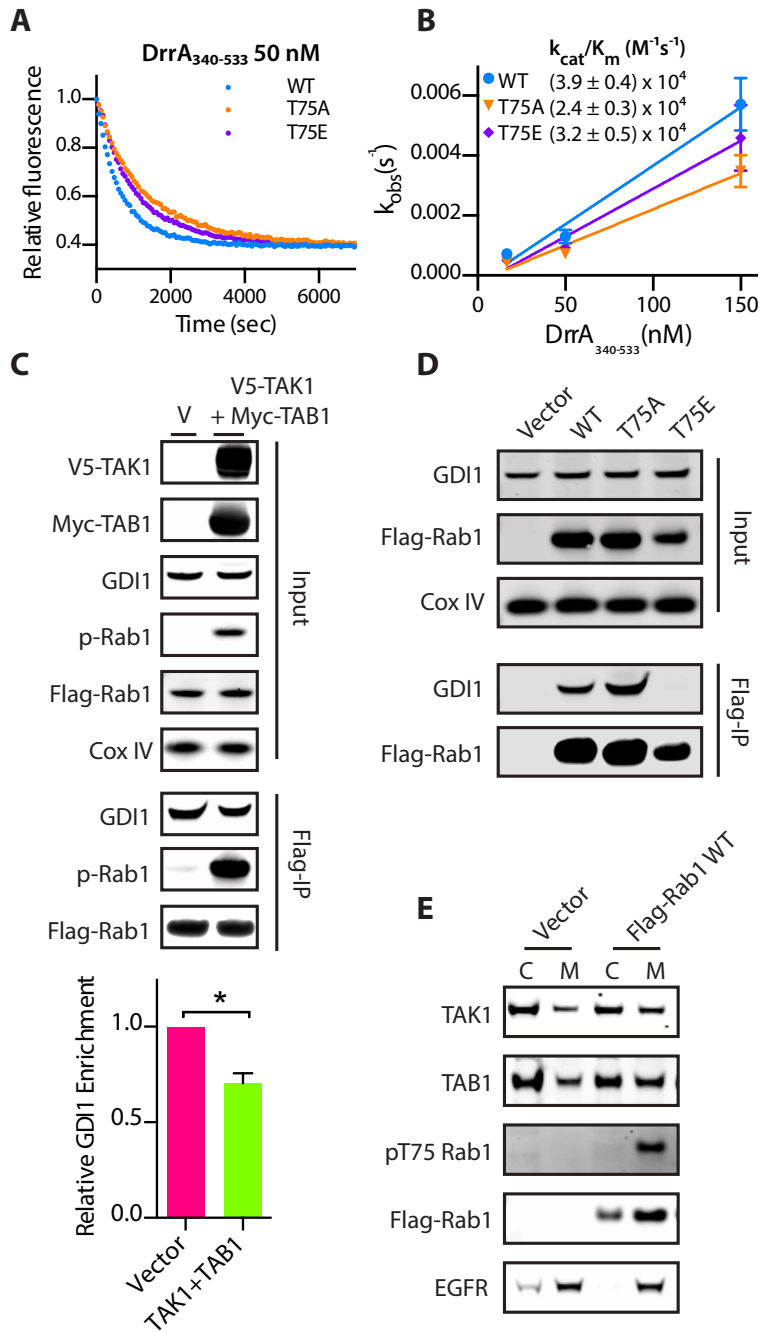
Figure 6. Phosphorylation of Rab1 disrupts interaction with GDI but not GEFs. (**A**) Measurement of mant-GDP dissociation from GST-Rab1 mutants by $DrrA_{340-533}$ from a single representative experiment where each data point represents the mean of technical replicates (n=3). (**B**) Observed rate constants (k_{obs}) for DrrA catalyzed mant-GDP dissociation with error bars for mean ± SD (n=2) and extrapolated catalytic efficiencies (k_{cat}/K_m). (**C**) HEK-293s stably expressing Flag-Rab1 were transiently transfected with either empty vector(V) or full length V5-

TAK1 and Myc-TAB1. Lysates were subject to immunoprecipitation of Flag-Rab1 using α-Flag antibody coupled magnetic beads and analyzed by western for co-immunoprecipitation of GDI1. The bar graph represents the ratio of precipitated GDI:Flag-Rab1 (n=2). (**D**) HEK-293Ts were transiently transfected with vector, Flag-Rab1 WT, T75A or T75E and subject to immunoprecipitation of Flag-Rab1. Quantitation is in Supplemental Figure S4B. (**E**) Cell fractionation of HEK-293Ts transiently transfected with empty vector or Flag-Rab1 with cytoplasmic (C) or membrane (M) fractions.

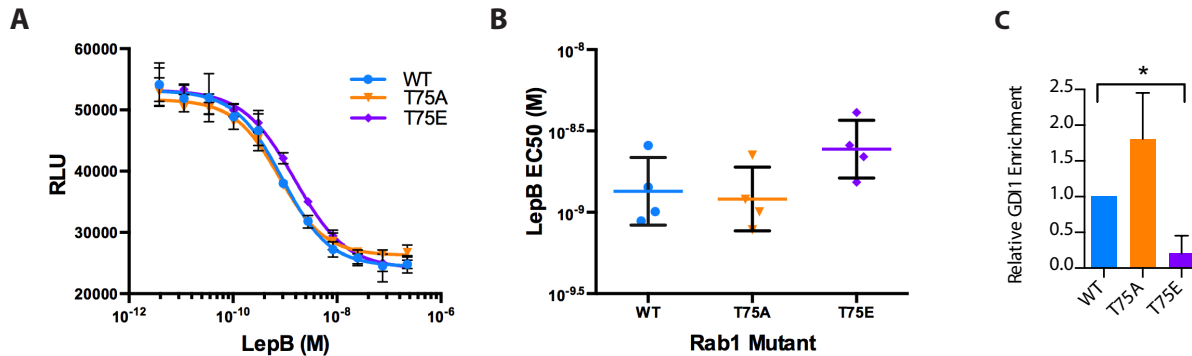**Figure 7.** GAP catalyzed hydrolysis of GTP by Rab1 is not disrupted by phosphomemetic mutation T75E, but interaction with GDI1 is. (**A**) Representative data from a single experiment of a GAP assay using Promega GTPase-Glo. Error bars are mean ± SD for 3 wells per condition. Purified GST-Rab1 mutants (30 μM) were incubated with excess GTP and varying concentrations of Legionella Rab1 GAP LepB for 1 hour. Remaining GTP concentrations were assayed by a luminescence coupled assay and plotted versus LepB concentration. (**B**) LepB EC50 values calculated from the LepB curves in A for 4 independent experiments (black lines: mean EC50 ± SD for n=4). (**C**) Quantitation related to Figure 4D where relative GDI enrichment represents the normalized ratio of immunoprecipitated GDI:Flag-Rab1 (n=2).

The subcellular location of Rab1 is also generally dictated by its nucleotide association, as recruitment of Rab1 to the membrane of the ER from the cytoplasm is concurrent with displacement of GDP and activation of Rab1 upon binding of GTP(35). Until this displacement occurs, inactive GDP-Rab1 is sequestered in the cytoplasm in complex with a GDI. Similar to their effect on GAPs and GEFs, *Legionella* derived post-translational modifications of Rab1 disrupt association with the GDI(31). We immunoprecipitated Flag-Rab1 from HEK-293 cells stably expressing Flag-Rab1 transfected with either vector or the combination of TAK1 and TAB1. The relative amount of GDI1 co-precipitating with Rab1 (GDI:Flag-Rab1) decreased in

cells with highly phosphorylated Rab1 resulting from TAK1 and TAB1 overexpression (Figure 6C). More strikingly, little to no GDI1 co-immunoprecipitates with Flag-Rab1T75E transiently over expressed in HEK 293Ts, whereas Flag-Rab1T75A increases association with GDI1 (Figure 6D, 5C). Disruption of the GDI:Rab1 complex by phosphorylation suggests pT75-Rab1 is be available for activation and recruitment to the ER membrane. Thus, we examined the localization of pT75 Rab1 by cellular fractionation of HEK 293Ts transiently expressing Flag-Rab1 (Figure 6E). While total Flag-Rab1 is distributed between cytoplasmic and membrane fractions, pT75 Rab1 is exclusively detected in the membrane fraction, where Rab1 activation occurs. Taken together, these results suggest that phosphorylation of Rab1 by TAK1 may be an important precursor to GTP binding and activation by driving dissociation from the GDI.

Rab1 phosphorylation is required to maintain Golgi structure

Rab1 is responsible for transporting vesicles from the ER to the Golgi. Disruption of Rab1 activity, by knockdown or overexpression of the dominant negative Rab1S25N, results in fragmentation of the Golgi apparatus(36, 37). We tested the effect of overexpression of non-phosphorylatable T75A and phosphomimetic T75E Rab1 on Golgi structure to determine if the T75 site was critical for Rab1 function. Immunofluorescence was performed in HeLa cells transiently overexpressing GFP-Rab1 mutants (Figure 8A,B) and the Golgi was stained with a cis-Golgi marker, GM130. As previously shown, overexpression of Rab1S25N acts in a dominant negative fashion, disrupting Golgi structure whereas Rab1Q70L, the active state mimic, has no effect on Golgi structure. Similarly, Rab1T75E has no effect on the Golgi. However, Rab1T75A acts in a dominant negative fashion similar to Rab1S25N to cause extensive Golgi fragmentation.
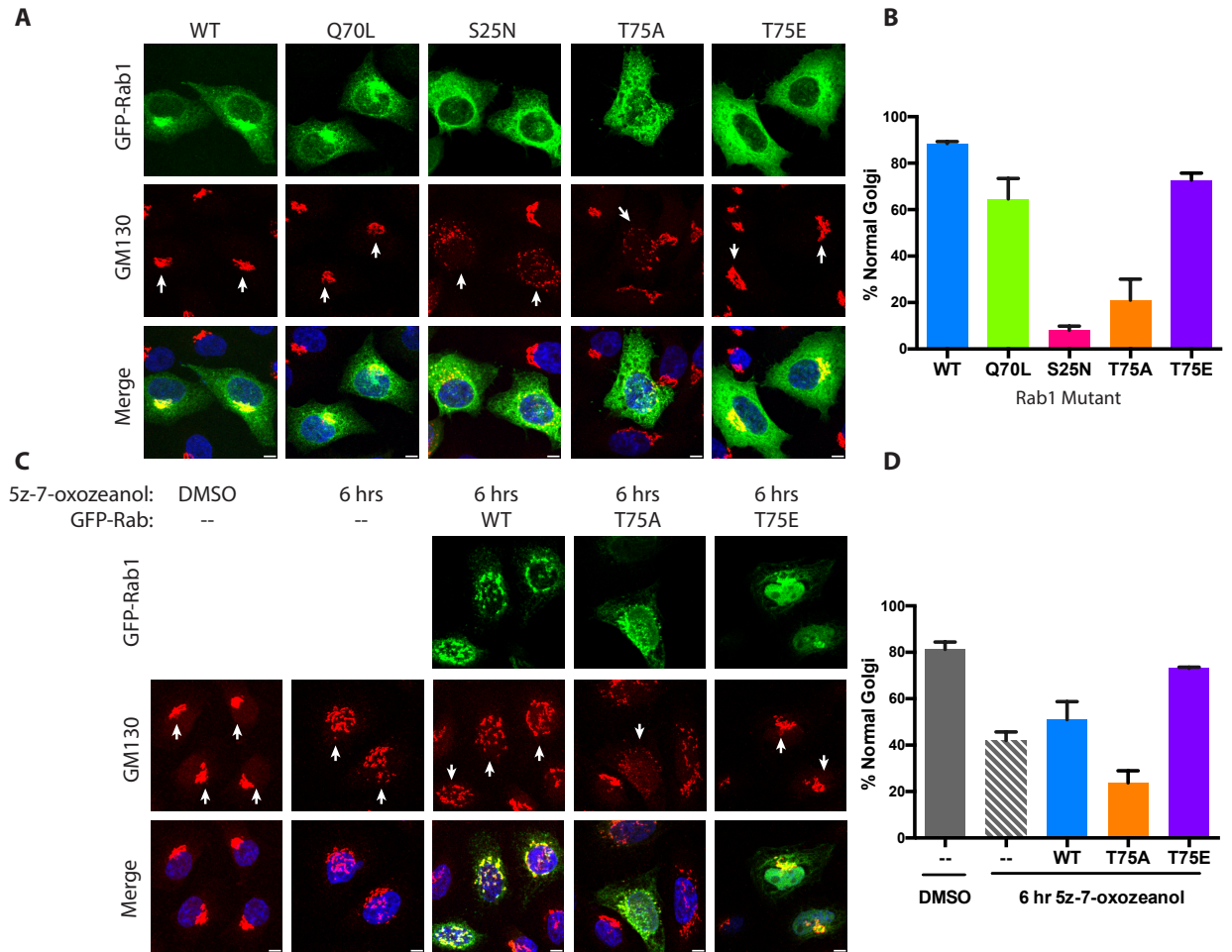
Figure 8. Fragmentation of the Golgi is a result of overexpression of Rab1T75A or inhibition of TAK1. (**A**) Representative images of HeLa cells transfected with GFP-Rab1 in green and stained for GM130, a cis-Golgi marker in red, and DAPI, in blue. (**B**) Quantitation of immunofluorescence experiment (n=3 replicates, 33 cells/replicate). (**C**) Representative images of HeLa cells stained for GM130 after dosing with 2.5µM TAK1 inhibitor 5z-7-oxozeaenol for 6 hours and preceding transfection with GFP-Rab1 where indicated (**D**) Quantitation of immunofluorescence experiment (n=3 replicates, 33 cells/replicate).

To complement these results, we assayed the effect of inhibiting TAK1 with 5z-7-oxozeaenol(25) on Golgi structure by immunofluorescence. Inhibition of TAK1 for 6 hours leads to a marked disruption of normal Golgi structure versus DMSO (Figure 8C,D). This effect is largely rescued by over expression of GFP-Rab1T75E, but not WT or T75A in the presence of inhibitor. We conclude from this data that the phosphorylation of Rab1, or ability of Rab1 to be

phosphorylated, plays an important role in ER to Golgi vesicle transport, and in maintaining proper Golgi structure.

Innate immunity kinase TAK1 and pathogen *Legionella* compete to post-transnationally modify Rab1

There is a well-established precedent for regulation of Rab1 function by post-translational modification during microbial infection. The intracellular bacterial pathogen *Legionella pneumophila* utilizes post-translational modifications of Rab1 in order the to establish the *Legionella* Containing Vacuole (LCV). *Legionella* effectors DrrA and AnkX are secreted into the host cell cytoplasm during infection and catalyze the AMPylation at Y80 and phosphocholination at S79 of Rab1, respectively (Figure 4F)(15, 16, 38, 39). As discussed earlier, these modifications serve as locks on the Rab1 nucleotide state and block interactions with the host enzymes normally responsible for regulating Rab1. Two additional *Legionella* enzymes, SidD and Lem3, have cognate Rab1 demodifying activities(28, 40). *Legionella* maintains exquisite and tightly regulated control of Rab1 in order to mature its replication vacuole by carefully timing the sequential secretion of these effectors and subsequent recruitment of Rab1 to the LCV.

As TAK1 is a kinase activated by pathogens, such as *Legionella*, and *Legionella* extensively modifies the Rab1 switch II region, we examined the interplay between TAK1 mediated phosphorylation of Rab1 and *Legionella* infection. HEK-293 cells stably expressing FCγIII receptor (to allow for opsonization and endocytosis of *Legionella* in HEK-293 cells) and Flag-Rab1 were infected with *Legionella* (WT), an isogenic strain lacking the Dot/Icm Type IV secretion system (Δ*dotA*), an isogenic strain lacking the two known Rab1 post-translational modifying enzymes DrrA and AnkX (Δ*ankX,drrA*)*,* or left mock infected (Figure 9A). Some basal phosphorylation of Rab1 was detected in the mock infected (0 hrs) sample. Phosphorylation of Rab1 increased slightly at 1hr in WT condition, then tapered to below basal levels at 4 and 6

hours. Infection with both ΔdotA and ΔankX,drrA strains lead to increased levels of pT75-Rab1 at 1 and 4 hours, with levels remaining high at 6 hours in ΔdotA. Deletion of AnkX and DrrA provided a moderate restoration of pT75-Rab1 levels versus WT infection, suggesting these enzymes may be responsible for outcompeting TAK1 for control of Rab1 during wild type infection. We next considered the contribution of the AMPylation versus GEF activity of DrrA toward reducing pT75-Rab1 levels during WT infection. GST-Rab1 was incubated for 15 minutes with ATP and either WT-TAK1[f] or full length DrrA in the presence of excess GTP or GDP, then incubated for an additional 15 minutes after addition of the remaining enzyme. Aliquots were removed and quenched at 0, 15 and 30 minutes and analyzed by western blot (Figure 9B). AMPylation of Rab1 is not affected by pre-existing phosphorylation in the presence of either nucleotide. However, phosphorylation of Rab1 by TAK1 is significantly hindered only when excess GTP is present, suggesting that it is the DrrA catalyzed Rab1-GTP binding which reduces phosphorylation levels, not the presence of AMPylation disrupting the TAK1 phosphorylation site. While the contribution of phosphocholination and other factors to outcompeting Rab1 phosphorylation remain to be determined, these results suggest that TAK1 may be outcompeted in part by *Legionella* for modification and control of Rab1 during infection by the GEF activity of DrrA.
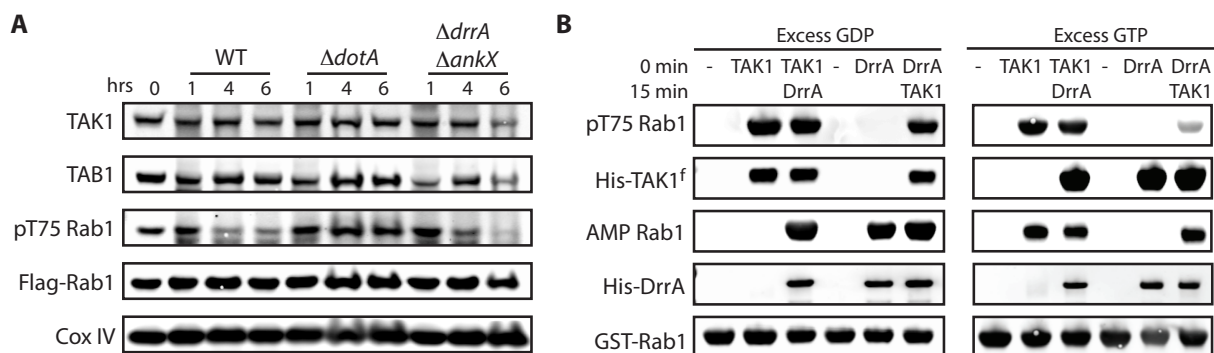
Figure 9. pT75 Rab1 levels decrease during *Legionella* infection due to the GEF activity of DrrA. (**A**) HEK-293 cells stably expressing FCγIII receptor and Flag-Rab1 were mock infected (0 hrs), infected with wild type (WT), secretion deficient (ΔdotA) or AnkX and DrrA deficient (ΔankX,drrA) *Legionella* for 1, 4 or 6 hours and analyzed by western blot. (**B**) Sequential modification of Rab1 by TAK1 and DrrA. Enzymes were added at 0 and 15 minutes, with

aliquots of sample removed at 0(just prior to enzyme addition), 15 and 30 minutes for analysis in the presence of excess GDP or GTP (30μM).

Discussion

Here, we present the first effort to identify a broad set of substrates of TAK1, a S/T kinase with crucial function in the innate immune system. We generated an ATP analog specific mutant of TAK1, termed AS-TAK1[f] to selectively label, isolate and identify novel substrates. We identified over 200 novel substrate proteins of TAK1, with a subset validated by in vitro kinase assays. TAK1 demonstrated striking preference for threonine in the identified phosphosites. A recent study demonstrated that kinases with a β-branched residue in the conserved DFG loop drives specificity for threonine over serine(41). Fittingly, TAK1 contains a threonine at this position, T178. Although only one substrate, Rab1, was studied in depth in this study, a number of these substrates fit with known characteristics of TAK1 signaling. Filamin A (FLNA) functions as a scaffold for MKK4 and JNK association and activation of JNK(42, 43). MKK4 is a direct substrate of TAK1, thus it is possible TAK1 also associates with Filamin A to stimulate MKK4/JNK signaling. Additionally, TAK1 is known to be a client of HSP90(44). TAK1 mediated phosphorylation of a close relative, endoplasmin (HSP90B1), suggests TAK1 is capable of interacting with additional heat shock proteins.

We focused in particular on a novel TAK1 substrate, the GTPase Rab1. We demonstrate TAK1 phosphorylates Rab1 at a single site within the dynamic switch II region *in vivo*. Given the preference of TAK1 for GDP-bound Rab1 *in vitro*, we believe phosphorylation of Rab1 occurs in the inactive state. However, the GTP affinity of phosphorylated Rab1 is unchanged, GEF DrrA catalyzes nucleodite exchange of Rab1T75E efficiently, and Rab1T75E can perform GAP catalyzed GTP hydrolysis normally, and phosphorylation is present only on membrane associated Rab1, suggesting phosphorylated Rab1 has a normal catalytic cycle and associates with membranes. We find phosphorylation of Rab1 disrupts interaction with GDI1, an interaction

which is stabilized by the residues of switch II (45). Combined, these results suggest phosphorylation of Rab1 may serve to disrupt association with the GDI, and perhaps push Rab1 toward membrane association and activation rather than sequestration. A strong Golgi fragmentation phenotype was observed by immunofluorescence upon over expression of non-phosphorylatable but not phosphomimetic Rab1 as well as inhibition of TAK1, suggesting that the ability to be phosphorylated is necessary for Rab1 function in ER to Golgi vesicle transport. Thus, we propose that TAK1 phosphorylation of Rab1 is a priming step for Rab1 activation and integral component of the Rab1 activity cycle.

We believe this is the first evidence of regulation of Rab1 function by endogenous post-translational modification within the catalytic domain of the protein. Seen in the context of recent studies and existing data, modification, especially phosphorylation, of switch II may be a widespread endogenous mechanism of Rab family regulation. The Phosphosite.org database contains phosphoproteomic evidence for switch II phosphorylation of at least 15 additional Rab GTPases, and several other small GTPases. Recent work from the Mann group(46), identified phosphorylation by LRRK2 of the switch II regions of Rab3a, Rab8a, Rab10 and Rab12 as a driver of membrane localization. In addition, a few GTPases outside the Rab family including Cdc42, Rac1 and Ran are thought to be regulated by modification of switch II(47–49). Switch II has long been recognized for its importance in dictating Rab activation state, it is now becoming clear that post-translational modification of this region allows further, external control of Rab function.

Our interest in Rab1 stemmed from the extensive literature describing the ability of *Legionella pneumophila* to manipulate Rab1 function by post-translational modifications to ensure maturation of the *Legionella* replication vacuole within the host cell(35, 38). Here, we suggest that a similar and endogenous mechanism, TAK1 mediated phosphorylation of Rab1, serves to

regulate Rab1 function in normal conditions. We also show that phosphorylation of Rab1 is stimulated by secretion-deficient *Legionella* (Δ*dotA)* infection, yet is reduced during wild type infection. We believe that TAK1 phosphorylation is outcompeted by secreted *Legionella* factors, as evidenced by the observed reduction of TAK1 driven phosphorylation of Rab1 exposed to GEF DrrA and the rescue of pT75 Rab1 levels in Δ*ankX,drrA* infected cells. Interestingly, *Legionella* also stimulate NF-kB, p38 and JNK signaling through TLR independent mechanisms during infection(50, 51). TAK1 normally serves to respond to TLR signaling and activate these same pathways during infection. In addition, *Yersinia pestis* has been shown to inhibit innate immune signaling through acetylation and inactivation of TAK1(52). Thus, we hypothesize that *Legionella* has evolved mechanisms to mimic, or perhaps directly manipulate, TAK1 function during infection in order to control the innate immune response, as evidenced by activation of NF-kB, p38 and JNK, and now by modification of Rab1. The unbiased identification of TAK1 substrates has revealed phosphorylation of Rab1 switch II, a hotspot for post-translational modification, as a novel regulatory mechanism and potential unique component of innate immunity.

Materials and Methods

Cell lines, Plasmids, Antibodies, other reagents:

All cell lines were grown using standard conditions in DMEM (Gibco) containing 10% fetal bovine serum (FBS, Gibco). Cells were harvested at 80-90% confluence. Cell lysis for covalent capture was performed in lysis buffer 1(20mM Tris at pH7.5, 100mM NaCl, 10mM MgCl2, 0.5 mM DTT, 0.25% NP-40 and 1x Roche Complete protease inhibitor cocktail). All other cell lysis was performed in lysis buffer 2 (50 mM Tris at pH 8.0, 200 mM NaCl, 1 mM DTT, 1mM MgCl2, 0.5% Triton, 1x Roche Complete protease inhibitor cocktail, and 1x PhosStop phosphatase inhibitor (Roche)). 5z-7-oxozeaenol was purchased from Tocris.

WT-TAK1[f] fusion protein cDNA was synthesized by DNA 2.0 and cloned into pFastBac (Invitrogen) with a N-terminal 6xHis tag. pDONOR plasmids containing cDNA of MKK6, PSMC4, POLR3D, AP2B1, ADD1, Vinexin, EIF4B, EIF3I, TAK1, TAB1 and Rab1 were purchased from DNASU. Rab1, EIF4B, EIF31 were cloned into gateway vector pDEST with N-terminal GST fusion. TAK1 and TAB1 were cloned into pcDNA3 vector with N-terminal V5 or Myc tags, respectively. The remaining genes were cloned into pcDNA3 with N-terminal Flag tags. Constructs for His-DrrA, His-LepB, pcDNA4/TO-Flag-Rab1 and pGEX-GST Rab-1 were gifts from Shaeri Mukherjee, as were HEK-293 stably expressing FCγRII receptor and Flag-Rab1. All point mutants, including AS-TAK1[f], were generated by site directed mutagenesis of the wild-type construct.

Antibodies used with product number: Cell Signaling Technologies:TAK1 (4505), TAB1 (3226), B-Tubulin (2146), CoxIV (4850). ThermoFisher Scientific: Myc (21316), His (21315), Flag(91878). Sigma: V5 (V8012), GDI1 (AV13086). Abcam: Anti-thiophosphate ester (ab92570).

The pT75 Rab1 rabbit polyclonal antibody was raised by GenScript and is available by request. The anti-AMPylated Rab1 antibody was a gift from the Itzen laboratory.

Transfection, western blotting and immunoprecipitation:

Fugene HD (Promega) was used for transfection of HeLa cells for immunofluorescence. For immunoprecipitation prior to kinase assays in Figure 2A,B,C , HEK-293Ts were transfected with Lipofectamine (Invitrogen). All other HEK-293T transfections were done with Fugene HD. Cells were transfected at 60% confluence for 24 hours. For western blots or immunoprecipitation, cells were lysed in lysis buffer 2 with sonication. Protein concentrations were measured using a BCA assay (Thermo). 20-30 micrograms of protein was separated by SDS-Page and transferred to nitrocellulose. Membranes were incubated with antibody per manufacturer's guidelines and imaged on a Licor system. All immunoprecipitation of proteins was performed on 500ug-1mg lysate per sample with anti-Flag magnetic beads (Sigma) or glutathione magnetic beads (Thermo) as appropriate for 2 hours at 4 degrees. For use in in vitro kinase assays, samples were washed 3x in 500ul lysis buffer and eluted with 3xFlag-tide or 10mM glutathione. For LC-MS/MS analysis, samples were run on SDS-Page, coomassie stained, subject to a standard in gel trypsin digestion protocol. For co-immunoprecipitations, samples were washed 3x in PBS before elution by heating in SDS gel loading buffer.

Purification of TAK1[f] and Rab1

TAK1[f] was purified as previously described (17). Briefly, His-tagged WT- TAK1[f] and AS- TAK1[f] were over-expressed using a baculovirus expression system in SF9 insect cells and purified using Ni/NTA agarose resin (Qiagen). The tagged protein was further purified by size exclusion chromatography on a Superdex 75 column (Amersham Biotech) and concentrated prior to the addition of glycerol to 10% and snap freezing.

Rab1 was purified as previously described(53). Purification for DrrA, DrrA$_{340-533}$, and LepB followed the same conditions. Briefly, *E. coli* BL21 cells transformed with vectors for GST-Rab1 mutants were grown in LB broth at 37 degrees to an OD=0.4. 0.1mM IPTG was added to induce protein expression and cells were incubated for 4 hours at 30 degrees. Cells were harvested by centrifugation and mechanically lysed via microfluidizer in buffer containing 50mM Tris at pH 8.0, 200mM NaCl, 1mM DTT, 1mM MgCl2 and 1x Roche Complete protease inhibitor cocktail. Cleared lysate was incubated with 1mL per liter of culture of glutathione sepharose resin (GE Healthcare) or Nickel-NTA resin (Qiagen) for 2 hours at 4 degrees. Bound proteins were washed with lysis buffer and eluted in buffer containing 10mM glutathione or 50mM imidazole. All GST-Rab1 proteins were further purified by size exclusion chromatography on a Superdex 200 column (Amersham Biosciences).

Rab1 Nucleotide Exchange

Rab1 proteins were loaded with the indicated nucleotides (GTPγS, GDP or 1'(3)-bis-O-(N-methylanthraniloyl) GDP (mant-GDP, Molecular Probes) by incubation for 1 hour at 37 degrees in buffer containing 50mM Tris at pH 8.0, 200mM NaCl, 1mM DTT, 1mM MgCl2, 5mM EDTA and 25mM excess of the indicated nucleotide. The exchange reaction was quenched by addition of 10mM MgCl$_2$. For *in vitro* kinase assays, GST-Rab1 was purified away from excess nucleotide by size exclusion. For nucleotide affinity and GEF assays, protein was desalted and excess nucleotide removed on Zebra spin desalting columns (Thermo).

Thiophosphorylation and covalent capture.

Thiophoshorylation of MBP (dephosphorylated, EMD Milipore) with purified WT-TAK1[f] was performed in buffer containing 50mM Tris pH 7.5, 150mM NaCl, 10mM MgCl2 and 0.5mM of each ATPγS analog (6-Bn-ATP-γ-S, 6-PhEt-ATP-γ-S or 6-Furfuryl-ATP-γ-S, Axxora). Labeling experiments for covalent capture enrichment were performed on 2mg of protein lysate per

sample. Samples were incubated in lysis buffer 1 supplemented with 250µM FF-ATPγS, 250µM

ATP, 3mM GTP, 10mM MgCl2 and 20µg of purified TAK1 as indicated. Labeling reactions were

left at room temperature for 1 hour before quenching with 50mM EDTA. 30µL aliquots of each

reaction were alkylated with 2uL of 100mM p-nitro mesylate (PNBM) for 30 minutes at room

temperature. Thiophosporylation was detected by western blot with the anti-thiophosphate ester

antibody.

Covalent capture of thiophosporylated proteins was performed as describe previously(9).

Briefly, lysates were denatured by adding 60% w/v solid urea, 10mM final TCEP and incubating

at 55 degrees C for 30 minutes. Samples were diluted to 2M urea with 50mM ammonium

bicarbonate and digested overnight at 37 degrees C with typsin (Promega) at a 1:20 ratio.

Peptides were acidified with triflouroacetic acid, desalted on a SepPak C18 column (Waters)

and speedvaced to dryness. Peptides were resuspended in 50mM HEPES and 50% acetonitrile

and adjusted to pH 7. The peptide solution was incubated overnight rocking with 100µL of

iodoacetyl sepharose resin in the dark (Thermo). Beads were washed by gravity flow with

water, 5M NaCl, 50% Acetonitrile, 5% formic acid and 10mM DTT followed by elution with

1mg/mL oxone (Sigma). Peptides were desalted with ZipTips (Milipore) and speedvacuumed to

dryness.

LC-MS/MS analysis and data processing

All desalted peptides were resuspended into 10µL of 0.1% formic acid . Peptides were loaded

on to a nanoACQUITY (Waters) UPLC instrument for reversed-phase chromatography with a

C18 column (BEH130, 1.7µm bead size, 100µm × 100mm) in front of an LTQ Orbitrap Velos.

The LC was operated at a 600nL/min flow rate and peptides were separated over an 80 minute

gradient from 2-50% Buffer B (Buffer A: water and 0.1% formic acid, Buffer B: acetonitrile and

0.1% formic acid). Survey scans were recorded over a 350 – 1800 m/z range and MS/MS

fragmentation was performed using HCD on the top 8 peaks. A second injection, i.e. technical replicate, of each sample was performed using ETD fragmentation on the top 6 peaks. Peaklists were generated with an in-house software called PAVA and searched against the SwissProt Homo Sapiens database (downloaded June 27, 2013, 20,264 entries) using Protein Prospector (version 5.10.10). Data was searched with a 20 ppm tolerance for parent and fragment ions (HCD or 20ppm/0.6Da ETD), allowing for standard variable modifications and S/T/Y phosphorylation. Filtering of background peptides and phosphopeptides was accomplished using an in-house R script described previously(21). Individual phosphopeptide abundance, when noted, was manually extracted using the extracted ion chromatogram functions built into Xcalibur Qual Browser (Thermo). Raw LC-MS/MS data and matched search results have been deposited to the ProteomeXchange Consortium via the PRIDE(54) partner repository with the dataset identifier PXD004213. Searched peptide identifications from all runs are also available in Datasets 1 through 4. Each Dataset is all runs for a single cell type, with individual sheets containing all identifications for a single injection.

In Vitro Kinase Assays with γ^{32}P-ATP

Purified kinase to a final concentration of 100-300nM was added into immunoprecipitated substrate or purified GST-Rab1 in 50mM Tris pH 7.5, 150mM NaCl and 10mM MgCl2. A small aliquot of this mixture was removed to check loading by western blot. 1-2ul of a mixture of cold ATP and γ^{32}P-ATP, for a final concentration of 100uM ATP and 1-5uCi γ^{32}P-ATP per sample, was added to start each reaction. Reactions were quenched by adding gel loading buffer and heating to 95 degrees C prior to SDS-Page separation. Gels were washed, dried and detected by autoradiography.

Cell Fractionation

Cell fractionation experiments were performed using 1 confluent well of a 6 well plate of HEK-293Ts per sample. Fractionation was performed according to the Subcellular Protein Fractionation Kit protocol (Thermo).

Immunofluoresence

HeLa cells were plated on glass coverslips and grown to 50% confluency. Cells were transfected and grown for 24 hours, then fixed. For immunofluorescence experiments with TAK1 inhibition, cells were transfected (or left untransfected), grown for 24 hours, then treated with 2.5μM 5z-7-oxozeanol for 6 hours and fixed. Cells were fixed with paraformaldehyde, permiablized with saponin, and stained with rabbit anti-GFP and mouse anti-GM130 (BD biosciences) for 1 hour. Coverslips were washed and stained with anti-rabbit and anti-mouse antibodies conjugated to alexa-488 and alexa-568, respectively. Coverslips were then stained with Hoechst reagent, fixed to slides, imaged and quantified manually.

Legionella Infection Experiments

HEK-293 expressing FCγRII and Flag-Rab1 were infected as described previously(15). Cells were grown to near confluency in 10cm dishes and infected with *Legionella pneumophila* strain LP01 or isogenic mutants at an estimated multiplicity of 100 bacteria to 1 host cell. Cells were harvested and snap frozen at the indicated time points.

GDP/GTP preference and GEF assays

First, GST-Rab1 mutants were loaded with mant-GDP as described above. The complex of mant-GDP and Rab1 fluoresces when excited, but not mant-GDP alone. The GDP/GTP affinity assay was performed as described previously(29).Briefly, mant-GDP loaded Rab1 (1μM final concentration) was incubated with EDTA (5mM final concentration) in the presence of varying concentrations of GTP or GDP as indicated. In a 384 well low volume black plate, 5μL of

EDTA/nucleotide mixture was added to the 10 µL of Rab1 to start the reaction. The presence of

EDTA in the reaction mixture helps displace mant-GDP from Rab1, which is then free to bind

any nucleotide in solution, and is read out as a decrease in fluorescence. The amount of

displacement in the presence of free nucleotide can be used to determine nucleotide

preference. Where indicated, WT-TAK1[f] was also present in the reaction at 100nM and ATP at

and 200uM, and allowed to react for 15 minutes prior to the addition of EDTA and GDP/GTP.

This reaction was allowed to reach equilibrium during a 1 hour incubation. The amount of

remaining mant-GDP bound Rab1 was determined by fluorescence Spectramax M5 plate

reader (Molecular Devices, 360 nm excitation, 440 nm emission). For the determination of

nucleotide IC_{50}, a sigmoidal curve fit was used for each nucleotide and mutant (Prism).

The GEF assay followed similar conditions to the above nucleotide affinity assay, using the

same plate set up and reader. Briefly, GST-Rab1 mutants were loaded with mant-GDP as

described above. 10µM of Rab1 was added to each well (final concentration 1µM). To trigger

the reaction, 5µL of His-DrrA$_{340-533}$, EDTA, or buffer with excess GTPγS (final concentration

200µM) was added to the reaction and the fluorescence monitored for 2 hours at 60-second

intervals. K_{obs} values were determined using a single exponential decay fit (Prism).

GAP assay

The GTPase-Glo system (Promega)(34) was used to measure the GTP remaining after

incubation of GST-Rab1 with varying concentrations of His-LepB. 10uL of a solution containing

2µM Rab1 in assay buffer (50mM Tris, 200mM NaCl, 1mM DTT, 5mM $MgCl_2$, 20mM EDTA)

was dispensed into a low volume white 384 well plate. LepB was serially diluted in assay buffer

with 10µM GTP and 5µL of this mixture was added to each well to trigger the reaction. The

reaction was incubated at room temperature protected from light for 1 hour. At one hour, 10µL

of GTPase-Glo Reagent mix was added to each well and incubated while shaking for 30 min at

room temperature. Finally 20µL of Detection Reagent was added to each well, incubated for 5

minutes at room temperature, and luminescence was measured on a Spectramax M5 Plate

reader (Molecular Devices, 500 ms read time). For the determination of LepB EC_{50},

concentrations of LepB were plotted against Relative Fluorescence Units and a sigmoidal curve

fit was performed (Prism).

In Vitro Labeling of Rab1 by DrrA and TAK1

15 µg of Rab1 was diluted in 30µL of 50mM Tris pH 7.5, 150mM NaCl and 10mM MgCl2 with

200µM ATP and 30µM GTP or 30µM GDP. At 0 min a 10µL portion was removed and

quenched with gel loading buffer. 1 µg of TAK1 or 0.5 µg of DrrA was added to the reaction and

allowed to react for 15 minutes. At 15 minutes, a 10µL portion was removed and quenched.

0.25µg of full length His-DrrA was then added to the TAK1 labeled sample and 0.5µg of TAK1 to

the DrrA labeled sample and allowed to react for an additional 15 minutes (30 min total) before

quenching with SDS sample loading buffer and analysis by western blot.

References

1. Shim J-H, et al. (2005) TAK1, but not TAB1 or TAB2, plays an essential role in multiple signaling pathways in vivo. *Genes Dev* 19(22):2668–81.
2. Zhang J, Clark K, Lawrence T, Peggie MW, Cohen P (2014) An unexpected twist to the activation of IKKβ: TAK1 primes IKKβ for activation by autophosphorylation. *Biochem J* 461(3):531–537.
3. Emmerich CH, et al. (2013) Activation of the canonical IKK complex by K63/M1-linked hybrid ubiquitin chains. *Proc Natl Acad Sci U S A* 110(38):15247–52.
4. Dai L, Aye Thu C, Liu X-Y, Xi J, Cheung PCF (2012) TAK1, more than just innate immunity. *IUBMB Life* 64(10):825–34.
5. Momcilovic M, Hong S-P, Carlson M (2006) Mammalian TAK1 activates Snf1 protein kinase in yeast and phosphorylates AMP-activated protein kinase in vitro. *J Biol Chem* 281(35):25336–43.
6. Sumiya E, et al. (2015) Phosphoproteomic analysis of kinase-deficient mice reveals multiple TAK1 targets in osteoclast differentiation. *Biochem Biophys Res Commun* 463(4):1284–1290.
7. Kajino-Sakamoto R, et al. (2010) TGF-beta-activated kinase 1 signaling maintains intestinal integrity by preventing accumulation of reactive oxygen species in the intestinal epithelium. *J Immunol* 185(8):4729–4737.
8. Blethrow JD, Glavy JS, Morgan DO, Shokat KM (2008) Covalent capture of kinase-

specific phosphopeptides reveals Cdk1-cyclin B substrates. *Proc Natl Acad Sci U S A* 105(5):1442–7.

9. Hertz NT, et al. (2010) Chemical genetic approach for kinase-substrate mapping by covalent capture of thiophosphopeptides and analysis by mass spectrometry. *Curr Protoc Chem Biol* 2(1):15–36.

10. Ding J, Soule G, Overmeyer JH, Maltese W a (2003) Tyrosine phosphorylation of the Rab24 GTPase in cultured mammalian cells. *Biochem Biophys Res Commun* 312(3):670–5.

11. Bailly E, McCaffrey M, Touchot N, Zahraoui A (1991) Phosphorylation of two small GTP-binding proteins of the Rab family by p34cdc2. *Nature*.

12. Lewandowska A, Macfarlane J, Shaw JM (2013) Mitochondrial association, protein phosphorylation, and degradation regulate the availability of the active Rab GTPase Ypt11 for mitochondrial inheritance. *Mol Biol Cell* 24(8):1185–95.

13. Sluijs P Van Der, et al. (1992) Reversible phosphorylation dephosphorylation determines the localization of rab4 during the cell cycle. 11(12):4379–4389.

14. Fentress SJ, et al. (2010) Phosphorylation of immunity-related GTPases by a Toxoplasma gondii-secreted kinase promotes macrophage survival and virulence. *Cell Host Microbe* 8(6):484–95.

15. Mukherjee S, et al. (2011) Modulation of Rab GTPase function by a protein phosphocholine transferase. *Nature* 477(7362):103–6.

16. Müller MP, et al. (2010) The Legionella effector protein DrrA AMPylates the membrane traffic regulator Rab1b. *Science* 329(5994):946–949.

17. Brown K, et al. (2005) Structural basis for the interaction of TAK1 kinase with its activating protein TAB1. *J Mol Biol* 354(5):1013–20.

18. Singh A, et al. (2012) TAK1 inhibition promotes apoptosis in KRAS-dependent colon cancers. *Cell* 148(4):639–50.

19. Melisi D, et al. (2011) Modulation of pancreatic cancer chemoresistance by inhibition of TAK1. *J Natl Cancer Inst* 103(15):1190–204.

20. Schaffer BE, et al. (2015) Identification of AMPK Phosphorylation Sites Reveals a Network of Proteins Involved in Cell Invasion and Facilitates Large-Scale Substrate Resource Identification of AMPK Phosphorylation Sites Reveals a Network of Proteins Involved in Cell Invasion and Facilitates Large-Scale Substrate Prediction. 907–921.

21. Lipp JJ, Marvin MC, Shokat KM, Guthrie C (2015) SR protein kinases promote splicing of nonconsensus introns. *Nat Struct Mol Biol* 22(8):611–617.

22. Crooks GE, Hon G, Chandonia J-M, Brenner SE (2004) WebLogo: A Sequence Logo Generator. *Genome Res* 14(6):1188–1190.

23. Hutagalung AH, Novick PJ (2011) Role of Rab GTPases in Membrane Traffic and Cell Physiology. *Physiol Rev* 91(1):119–149.

24. Ninomiya-Tsuji J, et al. (1999) The kinase TAK1 can activate the NIK-I kappaB as well as the MAP kinase cascade in the IL-1 signalling pathway. *Nature* 398(6724):252–256.

25. Wu J, et al. (2013) Mechanism and In Vitro Pharmacology of TAK1 Inhibition by (5Z)-7-Oxozeaenol. *ACS Chem Biol*. doi:10.1021/cb3005897.

26. Nuoffer C, Davidson HW, Matteson J, Meinkoth J, Balch WE (1994) A GDP-bound of rab1 inhibits protein export from the endoplasmic reticulum\rand transport between Golgi compartments. *J Cell Biol* 125(2):225–237.

27. Tisdale EJ, Bourne JR, Khosravi-Far R, Der CJ, Balch WE (1992) GTP-binding mutants of rab1 and rab2 are potent inhibitors of vesicular transport from the endoplasmic reticulum to the Golgi complex. *J Cell Biol* 119(4):749–761.

28. Tan Y, Arnold RJ, Luo Z-Q (2011) Legionella pneumophila regulates the small GTPase Rab1 activity by reversible phosphorylcholination. *Proc Natl Acad Sci* 108(52):21212–21217.

29. Ostrem JM, Peters U, Sos ML, Wells JA, Shokat KM (2013) K-Ras(G12C) inhibitors allosterically control GTP affinity and effector interactions. *Nature* 503(7477):548–551.
30. Goody PR, et al. (2012) Reversible phosphocholination of Rab proteins by Legionella pneumophila effector proteins. *EMBO J* 31(7):1774–84.
31. Oesterlin LK, Goody RS, Itzen A (2012) Posttranslational modifications of Rab proteins cause effective displacement of GDP dissociation inhibitor. *Proc Natl Acad Sci* 109(15):5621–5626.
32. Suh H-Y, et al. (2010) Structural insights into the dual nucleotide exchange and GDI displacement activity of SidM/DrrA. *EMBO J* 29(2):496–504.
33. Ingmundson A, Delprato A, Lambright DG, Roy CR (2007) Legionella pneumophila proteins that regulate Rab1 membrane cycling. *Nature* 450(7168):365–9.
34. Mondal S, Hsiao K, Goueli S (2015) A Homogenous Bioluminescent System for Measuring GTPase, GTPase Activating Protein, and Guanine Nucleotide Exchange Factor Activities. *Assay Drug Dev Technol* 13(8):444–455.
35. Barr FA (2013) Rab GTPases and membrane identity: Causal or inconsequential? *J Cell Biol* 202(2):191–199.
36. Aizawa M, Fukuda M (2015) Small GTPase Rab2B and Its Specific Binding Protein Golgi-associated Rab2B Interactor-like 4 (GARI-L4) Regulate Golgi Morphology. *J Biol Chem* 290(36):22250–22261.
37. Wilson BS, et al. (1994) A Rab1 mutant affecting guanine nucleotide exchange promotes disassembly of the Golgi apparatus. *J Cell Biol* 125(3):557–571.
38. Hardiman CA, Roy CR (2014) AMPylation is critical for Rab1 localization to vacuoles containing Legionella pneumophila. *MBio* 5(1). doi:10.1128/mBio.01035-13.
39. Goody PR, et al. (2012) Reversible phosphocholination of Rab proteins by Legionella pneumophila effector proteins. *EMBO J* 31(7):1774–1784.
40. Tan Y, Luo Z-Q (2011) Legionella pneumophila SidD is a deAMPylase that modifies Rab1. *Nature* 475(7357):506–509.
41. Chen C, et al. (2014) Identification of a Major Determinant for Serine-Threonine Kinase Phosphoacceptor Specificity. *Mol Cell* 53(1):140–147.
42. Nakagawa K, et al. (2010) Filamin associates with stress signalling kinases MKK7 and MKK4 and regulates JNK activation. *Biochem J* 427(2):237–245.
43. Shirakabe K, et al. (1997) TAK1 mediates the ceramide signaling to stress-activated protein kinase/c-Jun N-terminal kinase. *J Biol Chem* 272(13):8141–8144.
44. Liu XY, Seh CC, Cheung PCF (2008) HSP90 is required for TAK1 stability but not for its activation in the pro-inflammatory signaling pathway. *FEBS Lett* 582(29):4023–4031.
45. Rak A, et al. (2003) Structure of Rab GDP-Dissociation Inhibitor in Complex with Prenylated YPT1 GTPase. 302(October).
46. Steger M, et al. (2016) Phosphoproteomics reveals that Parkinson's disease kinase LRRK2 regulates a subset of Rab GTPases. *Elife* 5(e12813). doi:10.7554/eLife.12813.
47. Tu S, Wu WJ, Wang J, Cerione R a. (2003) Epidermal growth factor-dependent regulation of Cdc42 is mediated by the Src tyrosine kinase. *J Biol Chem* 278(49):49293–49300.
48. Kwon T, Kwon DY, Chun J, Kim JH, Kang SS (2000) Akt protein kinase inhibits Rac1-GTP binding through phosphorylation at serine 71 of Rac1. *J Biol Chem* 275(1):423–428.
49. de Boor S, et al. (2015) Small GTP-binding protein Ran is regulated by posttranslational lysine acetylation. *Proc Natl Acad Sci* 112(28):E3679–E3688.
50. Ge J, et al. (2009) A Legionella type IV effector activates the NF-kappaB pathway by phosphorylating the IkappaB family of inhibitors. *Proc Natl Acad Sci U S A* 106(33):13725–13730.
51. Shin S, et al. (2008) Type IV secretion-dependent activation of host MAP kinases induces an increased proinflammatory cytokine response to Legionella pneumophila. *PLoS*

Pathog 4(11). doi:10.1371/journal.ppat.1000220.

52. Thiefes A, et al. (2006) The Yersinia enterocolitica effector YopP inhibits host cell signalling by inactivating the protein kinase TAK1 in the IL-1 signalling pathway. *EMBO Rep* 7(8):838–44.

53. Murata T, et al. (2006) The Legionella pneumophila effector protein DrrA is a Rab1 guanine nucleotide-exchange factor. *Nat Cell Biol* 8(9):971–977.

54. Rigden DJ, Fernández-Suárez XM, Galperin MY (2016) The 2016 database issue of Nucleic Acids Research and an updated molecular biology database collection. *Nucleic Acids Res* 44(Database issue):D1–D6.

Chapter 4

Establishing the Multiplexed Kinase Inhibitor Beads (MIBs) technique and use on collaborative projects

Introduction

The study of kinase in normal and disease context has benefited immensely from the drive to produce specific and sensitive kinase inhibitors. These inhibitors are often developed with therapeutic intentions, however few advance into the clinic. Although inadequate for use in patients, these tool compounds have been use extensively for the precise study of kinase signaling in cell culture and mouse models of disease. These compounds have also found a new use as scaffolds for the purification of kinases from biological samples. When coupled to a sepharose resin, initial experiments demonstrated that these inhibitors could selectively enrich for multiple classes of kinase, depending on the specificity of the inhibitors used. Thus, specificity of kinase inhibitors could be tested, either by coupling the inhibitor and fishing out kinases to which it binds, or by treating a biological sample with the test compound and looking for a reduction in kinase enrichment using inhibitor-coupled resin targeted at wide swath of kinase families(1).

Furthermore, these inhibitor-coupled resins can also be used to assess the activity of kinases in the proteome. When inhibitors that bind exclusively to active kinases, termed Type I inhibitors, are used to pull down kinases from a lysate, this biases the pull down toward kinases in the active state. This can be used to assess broad changes in kinase activity between conditions, for example drug treated versus control, or stimulated versus unstimulated cells. Often, alternative kinase pathways will activate in response to inhibition of common tumor driver

kinases, and this activation can be detected with this method. While many labs had pursued

kinase enrichment strategies using kinase inhibitors as bait(1), the Johnson lab was the first to

publish the activation state biased enrichment technique, referred to as Multiplexed Inhibitor

Beads (MIBs)(2). The Johnson group used this technique to study drug induced reprograming of

the kionome in breast cancer and leukemia(2–4). Given the interest of the Shokat lab in the

development and use of kinase inhibitors, we worked extensively to adapt the MIBs

methodology for use in our laboratory. Described in this chapter is the approach to MIBs

developed in the Shokat lab as well as examples of projects using the MIBs approach. Chapter

5 describes specific proteomic technological advancements for increasing the sensitivity and

robustness of the MIBs approach.

Adaptation of MIBs to the Shokat Lab

In the Shokat lab, we first began by determining the optimal coupling reactions and inhibitors to

couple to beads. Dr. John Gordan drove the chemistry arm of the project, selecting inhibitors,

running coupling reactions, and synthesizing compounds as needed. To test inhibitor

conjugated resin, we first ran single inhibitor-coupled resin (or "single bead") pull downs from

cell lysates to check for enrichment. Pull downs were done in the batch style, as one does for

any immunoprecipitation experiment. Eluate for these was run on a gel and subject to in gel

digestion and LC-MS/MS analysis. Criteria for including a particular inhibitor resin in further

experiments included high levels (greater than 30) of kinase identifications, as well as

identification of known targets of the inhibitor. We developed a number of new inhibitor resins,

including compounds developed in the Shokat lab as well as clinical compounds not previously

used in the MIBs approach(5). The best performing beads were selected for use in the multiplex

system, with multiple layers of individual inhibitor-coupled resin stacked in a gravity column.

Inhibitor combinations were selected to give the broadest possible coverage of the kinome.

Previous publications using MIBs(2) relied on the use of isobaric tags for quantitation.

Experiences in the Burlingame lab with isobaric tags had previously been quite negative, with low levels of identification and disruption of instrument function. Thus we instituted a label free quantitation system to assess kinase abundance in enriched samples (Figure 1), which does not require any additional processing of samples or expensive reagents. Individual MIBs columns are run for each sample, proteins are eluted by denaturation, digested with trypsin and identified by a standard 2 hour data dependent LC-MS/MS run. Skyline software(6) was used to extract ion chromatograms for identified peptides, or the MS1 intensity of individual peptides in all samples. MSstats(7) along with an in house processing script, as written by collaborator James Webber, was used to normalize peptide abundance and provide statistics on the relative abundance of proteins between samples. This platform proved to be a very robust means of assessing kinase abundance, and requires no special bench or proteomics techniques. In collaboration with Anatoly Urisman, we developed an even more sensitive and robust means of label free quantification of MIBs samples through the use of a super long monolithic liquid chromatography column and targeted mass spectrometry protocol, termed parallel reaction monitoring. While this new method does provide significant gains in sensitivity, we have found that the standard label free quantitation using MS1 filtering with Skyline is more than adequate for most MIBs experiments.
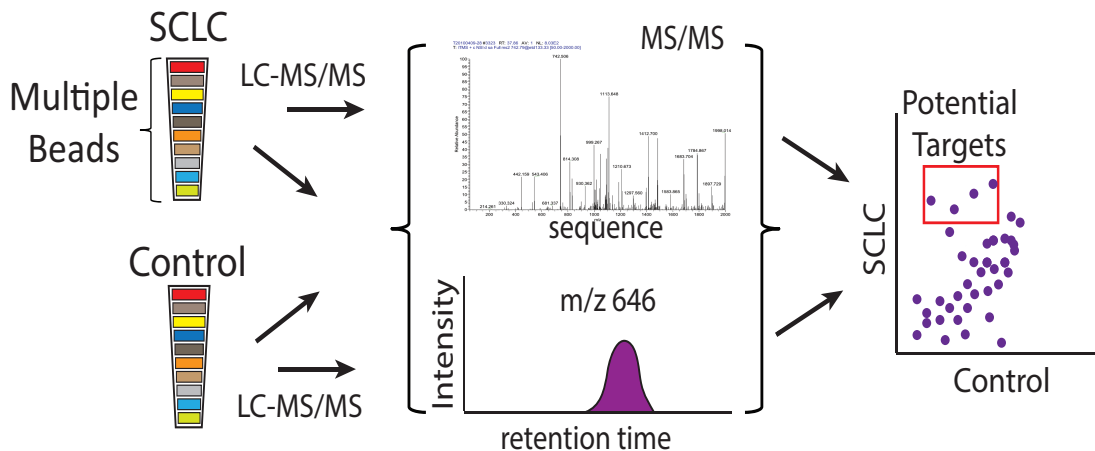
Figure 1. The Shokat MIBs approach. Samples are run on individual columns and in individual LC-MS/MS runs. Protein idenfications and relative peptide abundance are derived from these runs, and translated into relative protein abundance using MSstats.

During my time in the Shokat lab, I was fortunate to collaborate on many projects using this MIBs platform. Collaborators, often recruited by Dr. Gordan, usually had specific areas they were interested in analyzing. Much of this work remains unpublished to date, but the projects spanned from examining biomarkers of sensitivity to drug, identifying non-mutated kinase drivers of cancer, and identifying synthetic lethal relationships between kinases and specific genetic drivers of cancer. For these studies, I processed MIBs samples and analyzed data, and in some instances designed MIBs experiments as well as follow up.

As an example of the power of MIBs, the following section is adapted from a study(8) lead by Dr. Martin Sos, a postdoc in the group, and performed by Dr. Sos, myself and many contributors from the Shokat lab. This study is a perfect example of the complementary nature of MIBs to quantitative phosphoproteomics. Here, we use MIBs to understand the basic mechanisms of resistance to kinase-targeted therapeutics. A parallel quantitative phosphoproteomics study identified specific phosphosites and targets of this kinase activity, leading to the discovery of a novel mechanism of autocrine stimuli driven resistance to MEK inhibition. For this project, I

assisted in the MIBs enrichment, performed the MIBs mass spectrometry and data analysis, participated in the design of the phosphoproteomics and executed the enrichment and analysis of phosphopeptides. The project was conceptualized and lead by Dr. Martin Sos.

Oncogene mimicry as a mechanism of primary resistance to BRAF Inhibitors

Activating mutations in the S/T kinase BRAF are among the most common mutations across all cancers and lead to RAS-independent induction of mitogen-activated protein kinase (MAPK) signaling in these tumors (9, 10). Given the incidence of this mutation in cancer, much effort has been place in creating targeted inhibitors of mutant BRAF, such as vemurafinib, and the downstream kinases it activates, MEK and ERK, such as trametinib (11–13). These inhibitors should disrupt the activation of the RAS/MAPK pathway driven by the oncogenic mutations of BRAF, such as V600E, the most commonly observed mutation. These targeted approaches, although initially successful in treating the disease, are limited by the gradual selection of cells that are insensitive to the drug, termed acquired resistance. However, some BRAF mutant cancers never respond to targeted therapies, termed primary resistance(12, 14). The finding that BRAF^{V600E} present in different tissues exhibits drastically different sensitivity to vemurafenib suggests drastically different wiring diagrams and adds to the complexity of primary resistance to MAPK pathway inhibition in BRAF-mutant tumors(15). Activation of parallel kinase pathways (15) or relief of upstream negative feedback upon BRAF inhibition (16) had been previously identified as mechanisms of resistance to MAPK pathway inhibition in the context of BRAF activating mutations.

We initiated an effort to systematically map the signaling differences be- tween primary resistant and sensitive BRAFV600E-mutant cells originating from different tissues. Our approach relied on two complementary mass spectrometry platforms: (1) a kinase inhibitor bead-based affinity purification to profile active kinases within the MAPK pathway and parallel pathways, and (2) a

stable isotope labeling with amino acids in cell culture (SILAC)-based phosphoproteomic

analysis to capture the output of a wide variety of signaling outputs. To our knowledge, this is

the most comprehensive kinase and phosphoproteomic analysis of the primary resistant state of

BRAF^{V600E} mutant tumor cells.

We first assayed the dependency of a variety of BRAF mutant cell lines on BRAF through

siRNA depletion of RAF, which suggested that BRAF dependency is conserved across BRAF

mutant cells. However, pharmacologic perturbation of the BRAF pathway does not mimic this

dependence, with a variety of responses to chemical inhibition observed. A small subset of cells

displayed a phenotype of primary resistance. Through the use of a sorafenib coupled resin, we

showed that inhibition of MEK lead to increased binding of BRAF, CRAF and also KSR1 in

MAPK inhibitor resistant (SW1736), but not sensitive (SKMEL1) cells. This suggests that RAF

isoforms are activating in response to inhibition of downstream kinase MEK in the context of

resistance, and forming complexes with KSR1, likely stimulating signaling and survival even in

the presence of drug.

Encouraged by the utility of a single-inhibitor bead to reveal differential kinase activation

mechanisms, we next developed a custom-designed *m*ultiplexed kinase *i*nhibitor *b*eads (MIB)

library(2, 17) to systematically detect drug-induced perturbation of kinase signaling in MAPK

inhibitor primary resistant SW1736 cells at early (1 hr) and late (24 hr) time points after

treatment with MEK inhibitor PD325901. Using this enrichment method coupled to mass

spectrometry-based protein analysis described in the introduction to this chapter, we were able

to detect 128 unique kinases (Figure 2A) In the group of preferentially enriched kinases after

PD325901 treatment at both time points, we detected canonical MAPK pathway members

(MEK2 and ERK1) and five non-canonical MAPK pathway effectors (MP2K2, M3K2, TAOK2,

M4K5, and TAOK3) (Figure 2A, B). These results suggest the formation of activating complexes

between MAPK family members extends beyond those initially identified using our single-

inhibitor bead pull-downs and are part of a more global signaling adaptation to overcome the

initial inhibitory effect of the drug.
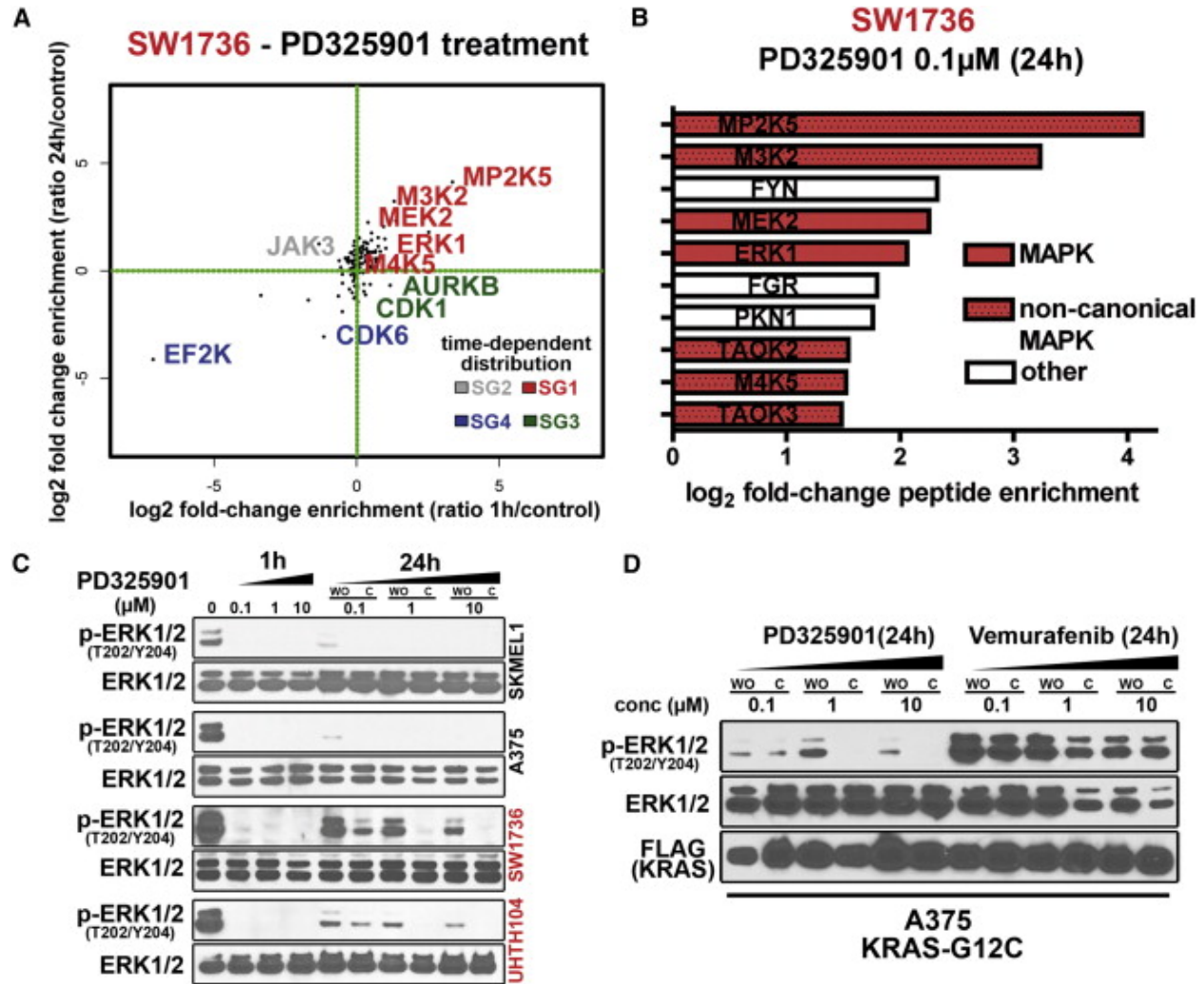
Figure 2. High-Dose MEK Inhibition Prevents Reactivation of MAPK in Primary Resistant Cells
(A) Mapping of all identified kinases (n = 128) according to the log2-change of enrichment as
compared to control for cells treated either for 1 hr (x axis) or 24 hr (y axis) with PD325901.
Selected proteins in the individual groups (red: SG1, immediate enrichment; gray: SG2, delayed
enrichment; blue: SG3, immediate decrease; green: SG4, delayed decrease) are highlighted.(B)
Fold-change enrichment of selected kinases binding to MIBs (log$_2$-scale) as detected by mass
spectrometry in resistant SW1736 cells treated with PD325901 (24 hr). MAPK components are
marked in red. (C) Cells (sensitive, black; resistant, red) were treated with increasing concentrations of
PD325901 (1 hr and 24 hr). Cells were either treated for 24 hr ("C") or compound was washed out ("WO")
with fresh media after 1 hr treatment. ERK and phospho-ERK levels were assessed in immunoblotting
assays.(D) A375 cells were transfected with FLAG-KRAS^{G12C} and were treated with either PD325901 or

vemurafenib for 24 hr ("C") or compound was washed out ("WO") with fresh media after 1 hr treatment. ERK and phospho-ERK levels were assessed in immunoblotting assays. Due to overlapping protein sizes, bands were not detected at the same membrane.

We speculated that the adaptive range of the increased MAPK pathway flux is finite and that high-dose MAPK inhibition may be able to override this primary resistance mechanism. To test this hypothesis, we steadily increased the concentration of PD325901 and measured the ability of the cells to reactivate MAPK signaling (Figure 2C). As expected, in both sensitive cells (A375 and SKMEL1), short-term and long-term MEK inhibition eliminates phospho-ERK, but in primary resistant (SW1736 and UHTH104) cells, phosphorylation of ERK recovers when cells are treated with low-dose (0.1 µM) PD325901 (Figure 2C). In contrast, high-dose (1–10 µM) MEK inhibition prevents recovery of phospho-ERK levels in these cells (Figure 2C). We observed the same pattern of ERK reactivation following treatment of A375 cells expressing a constitutively active $KRAS$[G12C] allele (Figure 2D) that mimics the feedback-induced effects of primary resistant cells Thus, we conclude that in a subset of $BRAF$-mutant tumors, primary resistance to MAPK inhibition is primarily driven by an increased flux of the MAPK signaling that can be overcome by high-dose MEK inhibition.

The MIB analysis revealed the set of kinases activated in inhibitor resistant cells. To capture the downstream consequences of kinase reactivation occurring in primary resistant MAPK pathway-reactivated cells, we conducted a SILAC-based mapping of cellular phosphopeptides in SW1736 cells treated with the MEK inhibitor PD325901 over time (0, 1, and 24 hr) (Figure 3A) We identified 3,481 unique phosphopeptides from 1,396 unique proteins. Not surprisingly, the abundance of many phosphopeptides decreased after kinase inhibition (Figure 3B). Gene Ontology (GO)-term analysis showed that proteins phosphorylated within 24 hr are significantly enriched in the category of "negative regulation of gene expression" (SG1, immediate increase) and "negative regulation of macromolecule biosynthetic process" (SG2, delayed increase)

(Figure 3B) Phosphoproteins decreasing in abundance within 24 hr of MEK inhibitor treatment were primarily involved in regulation of the cell cycle (SG3, delayed decrease) and DNA replication (SG4, immediate decrease) (Figure 3B) In line with previous reports, we found increased phosphorylation of two receptor tyrosine kinases, ERBB3 and MET (SG1), in the MEK inhibitor-treated SW1736 cells (Figure 3B)(15). Receptor tyrosine kinase (RTK) arrays confirmed MEK inhibitor-induced phosphorylation of not only ERBB3 and MET but also additional RTKs such as EGFR or AXL in resistant (SW1736 and BCPAP), but not in sensitive (A375), cells (Figure 3C). However, we did not observe an increased expression of ERBB3 and EGFR or their respective ligands EGF and NRG1 upon MAPK inhibition. Interestingly, the treatment with the MET inhibitor crizotinib or the HER2 inhibitor lapatinib (SW1736 and BCPAP) failed to prevent MEK inhibitor-induced reactivation of ERK phosphorylation. Furthermore, the combination of lapatinib and PD325901 had only a minor effect on the induction of apoptosis in primary resistant cells. These data suggest that the feedback-induced RTK phosphorylation pattern is not uniform across resistant cells and that inhibition of single nodes of RTK signaling may not be sufficient to prevent feedback-induced MAPK reactivation in *BRAF*-mutant cancer.
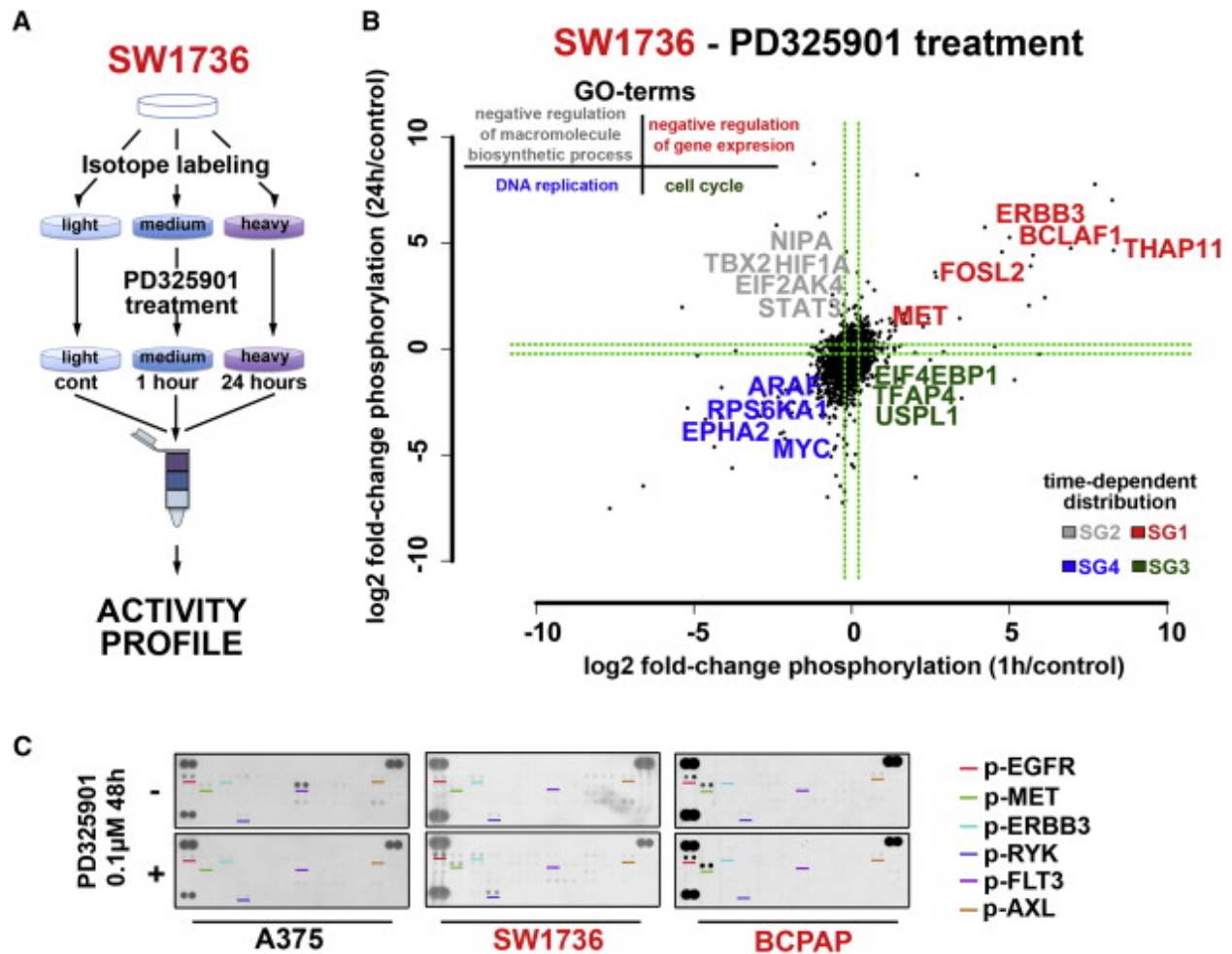
Figure 3. Mapping of Global Phosphoproteome Perturbation Reveals Effectors of Primary Resistance in BRAF-Mutant Cells (A) Graphic overview of the isotope-labeling strategy for SILAC-based detection of phosphoproteome activity.(B) Mapping of all identified phosphopeptides according to the log2-change of phosphorylation levels as compared to control for cells treated for either 1 hr (x axis) or 24 hr (y axis) with PD325901. Selected proteins in the individual groups (red, SG1; gray, SG2; blue, SG3; green, SG4) are highlighted. Inlay panel (upper left corner) shows the top-scoring GO-term annotation for the individual groups.(C) Sensitive (black; A375) and resistant (red; SW1736, BCPAP) cells were treated with PD325901 (0 and 48 hr), and phosphorylation status of 49 RTKs was detected using RTK arrays. Selected RTKs are highlighted.

To further explore the signaling fingerprint of primary resistant SW1736 cells, we focused on the delayed induction of phosphorylation of signal transducer and activator of transcription 3 (STAT3) at Tyr705. Of note, the activation pattern of STAT3 identified in the SILAC assay (Figure 3B) corresponds to the delayed enrichment of JAK3 binding in the MIB assay (Figure 2A), suggesting that the time-dependent reactivation of JAK/STAT signaling is a conserved

response to MEK inhibition in these cells. Through multiple experiments, we demonstrated that inhibition of MEK in resistant cell lines lead to phosphorylation of STAT3. Because cytokines such as IL-6 are known activators of STAT3 signaling, we hypothesized that an autocrine loop might be responsible for the time-dependent activation of JAK/STAT signaling. Indeed, cell lines resistant to MEK inhibition demonstrate much higher levels of IL-6 secretion. Further, the addition of IL-6 into media of sensitive cells significantly reduced the sensitivity of the cells to MEK inhibitors, while depletion of IL-6 with siRNA increases sensitivity in resistant cells.

Our chemical proteomics approach to dissect global signaling networks in *BRAF*-mutant cells revealed two major mechanisms that contribute to primary resistance: (1) in primary resistant cells, MAPK pathway inhibition can induce RAS-RAF-MEK complex formation that buffers inhibition of the pathway and shifts cellular sensitivity to high-dose MEK inhibition; and (2) autocrine IL-6 secretion and subsequent activation of JAK/STAT signaling represent an unexpected route to overcome targeted inhibition of the MAPK pathway. Both strategies resemble the adaptation mechanisms by which *KRAS*-mutant cells escape targeted inhibition of MAPK signaling, and thus we propose to name this primary resistance concept "oncogene mimicry."

References

1. Daub H (2015) Quantitative Proteomics of Kinase Inhibitor Targets and Mechanisms.
2. Duncan JS, et al. (2012) Dynamic reprogramming of the kinome in response to targeted MEK inhibition in triple-negative breast cancer. *Cell* 149(2):307–21.
3. Cooper MJ, et al. (2013) Application of multiplexed kinase inhibitor beads to study kinome adaptations in drug-resistant leukemia. *PLoS One* 8(6):e66755.
4. Stuhlmiller TJ, et al. (2015) Inhibition of lapatinib-induced kinome reprogramming in ERBB2-positive breast cancer by targeting BET family bromodomains. *Cell Rep* 11(3):390–404.
5. Saha SK, et al. (2016) Isocitrate dehydrogenase mutations confer dasatinib hypersensitivity and SRC-dependence in intrahepatic cholangiocarcinoma. *Cancer Discov* (july). doi:10.1158/2159-8290.CD-15-1442.
6. Schilling B, et al. (2012) Platform-independent and label-free quantitation of proteomic

data using MS1 extracted ion chromatograms in skyline: application to protein acetylation and phosphorylation. *Mol Cell Proteomics* 11(5):202–14.

7. Choi M, et al. (2014) MSstats: an R package for statistical analysis of quantitative mass spectrometry-based proteomic experiments. *Bioinformatics* 30(17):1–2.

8. Sos M, et al. (2014) Oncogene Mimicry as a Mechanism of Primary Resistance to BRAF Inhibitors. *Cell Rep* 8(4):1037–1048.

9. Davies H, et al. (2002) Mutations of the BRAF gene in human cancer. *Nature* 417(6892):949–954.

10. Bamford S, et al. (2004) The COSMIC (Catalogue of Somatic Mutations in Cancer) database and website. *Br J Cancer* 91(2):355–8.

11. Falchook GS, et al. (2012) Activity of the oral MEK inhibitor trametinib in patients with advanced melanoma: A phase 1 dose-escalation trial. *Lancet Oncol* 13(8):782–789.

12. Chapman PB, et al. (2011) Improved survival with vemurafenib in melanoma with BRAF V600E mutation. *N Engl J Med* 364(26):2507–16.

13. Janne PA, et al. (2013) Selumetinib plus docetaxel for KRAS-mutant advanced non-small-cell lung cancer: a randomised, multicentre, placebo-controlled, phase 2 study. *Lancet Oncol* 14(1474-5488 (Electronic)):38–47.

14. Kudchadkar R, Paraiso KHT, Smalley KSM (2012) Targeting mutant BRAF in melanoma: current status and future development of combination therapy strategies. *Cancer J* 18(2):124–31.

15. Prahallad A, et al. (2012) Unresponsiveness of colon cancer to BRAF(V600E) inhibition through feedback activation of EGFR. *Nature* 483(7387):100–3.

16. Lito P, Rosen N, Solit DB (2013) Tumor adaptation and resistance to RAF inhibitors. *Nat Med* 19(11):1401–1409.

17. Graves LM, Duncan JS, Whittle MC, Johnson GL (2013) The dynamic nature of the kinome. *Biochem J* 450(1):1–8.

Chapter 5

An optimized chromatographic strategy for multiplexing in parallel reaction monitoring mass spectrometry: Insights from quantitation of activated kinases

Anatoly Urisman *[1,2], Rebecca S. Levin *[2,3], John D. Gordan [3,4], James T. Webber [5], Hilda Hernandez [2], Yasushi Ishihama [6], Kevan M. Shokat [3,7], Alma L. Burlingame [2].

* These authors contributed equally to this publication

1. Department of Pathology, University of California San Francisco, San Francisco, CA, USA.
2. Department of Pharmaceutical Chemistry, University of California San Francisco, San Francisco, CA, USA.
3. Department of Cellular and Molecular Pharmacology, University of California San Francisco, San Francisco, CA, USA.
4. Department of Medicine, University of California San Francisco, San Francisco, CA, USA.
5. Department of Bioengineering and Therapeutic Sciences, University of California San Francisco, San Francisco, CA, USA.
6. Graduate School of Pharmaceutical Sciences, Kyoto University, Kyoto, Japan.
7. Howard Hughes Medical Institute, University of California San Francisco, San Francisco, CA, USA.

Abstract

Reliable quantitation of protein abundances in defined sets of cellular proteins is critical to numerous biological applications. Traditional immunodetection-based methods are limited by the quality and availability of specific antibodies, especially for site-specific post-translational modifications. Targeted proteomic methods, including the recently developed parallel reaction monitoring (PRM) mass spectrometry, have enabled accurate quantitative measurements of up to a few hundred specific target peptides. However, the degree of practical multiplexing in label-free PRM workflows remains a significant limitation for the technique. Here we present a strategy for significantly increasing multiplexing in label-free PRM that takes advantage of the superior separation characteristics and retention time stability of meter-scale monolithic silica-C18 column-based chromatography. We show the utility of the approach in quantifying kinase abundances downstream of previously developed active kinase enrichment methodology based

on multidrug inhibitor beads. We examine kinase activation dynamics in response to three different MAP kinase inhibitors in colorectal carcinoma cells and demonstrate reliable quantitation of over 800 target peptides from over 150 kinases in a single label- free PRM run. The kinase activity profiles obtained from these analyses reveal compensatory activation of TGF-b family receptors as a response to MAPK blockade. The gains achieved using this label-free PRM multiplexing strategy will benefit a wide array of biological applications.

Introduction

Kinases are involved in the regulation of most cellular processes and are implicated in numerous human disease states. Five hundred and eighteen human kinases are known, and between 200 and 400 are typically expressed in a given cell type (1–3). Quantitative measurement of kinase activity is of critical importance in numerous biological applications, including studies of cellular signaling, cancer biomarker discovery, and drug development. An ideal strategy for functional kinase analysis must combine an active state kinase enrichment component and a methodology to quantify their levels of activation, since kinase regulation is a major determinant of cellular function and disease phenotypes.

We and other groups have previously reported on the development and use of Multidrug Inhibitor Beads (MIB) strategy for active kinase enrichment (4–8). In this approach, kinase affinity enrichment scaffolds based on known kinase inhibitor structures targeted to conformationally active kinases are chemically coupled to a resin, which is used to capture broad classes of kinases from cell lysates (see recent review of this and related approaches by Daub (4)). When coupled to quantitative mass spectrometry-based proteomics, MIB enrichment can be used to determine kinase inhibitor specificity by comparing relative abundances of particular kinases enriched from drug treated and untreated samples or to study kinase activation dynamics as response to clinical therapy or various biological perturbations. For

example, MIB experiments have demonstrated on-target suppression of kinase activity and activation of compensatory kinase signaling pathways driving resistance to therapy in triple negative breast cancer (5), drug-resistant leukemia (6), and ERBB2-positive breast cancer (7).

Despite significant kinase enrichment afforded by MIB, the eluates are still highly complex peptide mixtures in which reliable quantitative detection of low-abundance species remains challenging. To date, several workflows focused on this task have been described. Typically, around 110-125 kinases can be uniquely quantified by DDA LC-MS/MS in any single MIB enrichment with stringent exclusion of peptides shared by multiple kinases. In addition, isobaric tags for relative and absolute quantitation (iTRAQ) (9), have been used downstream of MIB enrichment. However, this particular strategy suffers from non-uniform labeling efficiency and artificial compression of measured peptide ratios (10) and requires sample fractionation prior to MS analysis for adequate kinome coverage (5).

Finally, selected reaction monitoring (SRM) is an established technique which allows quantitation of a selected set of desired target peptides with improved sensitivity of detection compared to DDA LC- MS/MS (11). For example, application of an SRM method downstream of ActiveX, a related total kinase enrichment strategy employing ADP and ATP analogs (12) allowed quantitation of 132 of 196 targeted kinases represented by 790 unique peptides (13). However, current SRM approaches require sufficient sample to carry out multiple runs of the same sample using conventional chromatography in order to overcome multiplexing limits and achieve broad kinase coverage. Given the pitfalls of the current approaches, development of an improved strategy for one-shot label-free MS quantitation in complex biological mixtures, including MIB-enriched samples, is necessary.

Parallel reaction monitoring (PRM) is a recently introduced targeted proteomic methodology that

takes advantage of the unique capabilities of quadrupole-Orbitrap mass spectrometers (14, 15).

PRM provides improved sensitivity, reproducibility, and quantitative dynamic range compared to

the techniques described above. Like the older SRM methodology (11), PRM relies on

scheduled precursor peptide selection by a quadrupole followed by analysis of fragment ions.

However, unlike SRM where a few individual fragments are analyzed sequentially using low-

resolution quadrupole-based measurement, PRM utilizes the Orbitrap to record full-range high

mass resolution and high mass accuracy MS2 spectra. Thus, use of high resolution in selection

of target precursor ions is coupled with high-accuracy MS2-level quantitation resulting in greatly

improved specificity of detection. Additionally, evaluation of the PRM advantages for complex

peptides mixtures has established that it achieves lower limits of detection and quantification

than SRM (14, 15), making it particularly useful for analysis of unfractionated biological samples

such as whole cell lysates.

Despite these inherent advantages of PRM, its multiplexing capacity, i.e. the ability to detect

multiple targets simultaneously, remains a significant limitation of the technique. Detection of

more than a few hundred targets, or roughly 100 proteins, in a single PRM run has been difficult

to achieve in a reproducible and robust manner. Although a strategy for improved PRM

multiplexing that takes advantage of real-time detection of synthetic isotope-labeled (SIL)

peptide standards has been recently proposed (16), its utility is limited in applications where

having a SIL standard for each target peptide is not practical, most notably in detection of

peptides with post-translational modifications. Therefore, alternative strategies for improved

PRM multiplexing that would allow a wider adoption of the methodology for large-scale

quantitative targeted proteomic applications are needed.

Recently, remarkable gains in sensitivity and depth of peptide/protein detection have been

achieved for DDA LC-MS/MS through the use of meter-scale monolithic silica-C18 silica

capillary columns with ultra- long (up to 24-hr) chromatographic gradients (17, 18). This

approach is the current state of the art in chromatographic separation capabilities available for

one-shot proteomics. Given the superb separation characteristics of the monolithic silica-C18

columns in long reverse phase chromatographic gradients (19, 20), we sought to exploit the

performance characteristic of monolithic silica-C18 columns to greatly increase PRM

multiplexing and evaluate the effectiveness of this strategy by specifically detecting activated

kinases downstream of MIB enrichment (Figure 1).

Figure 1
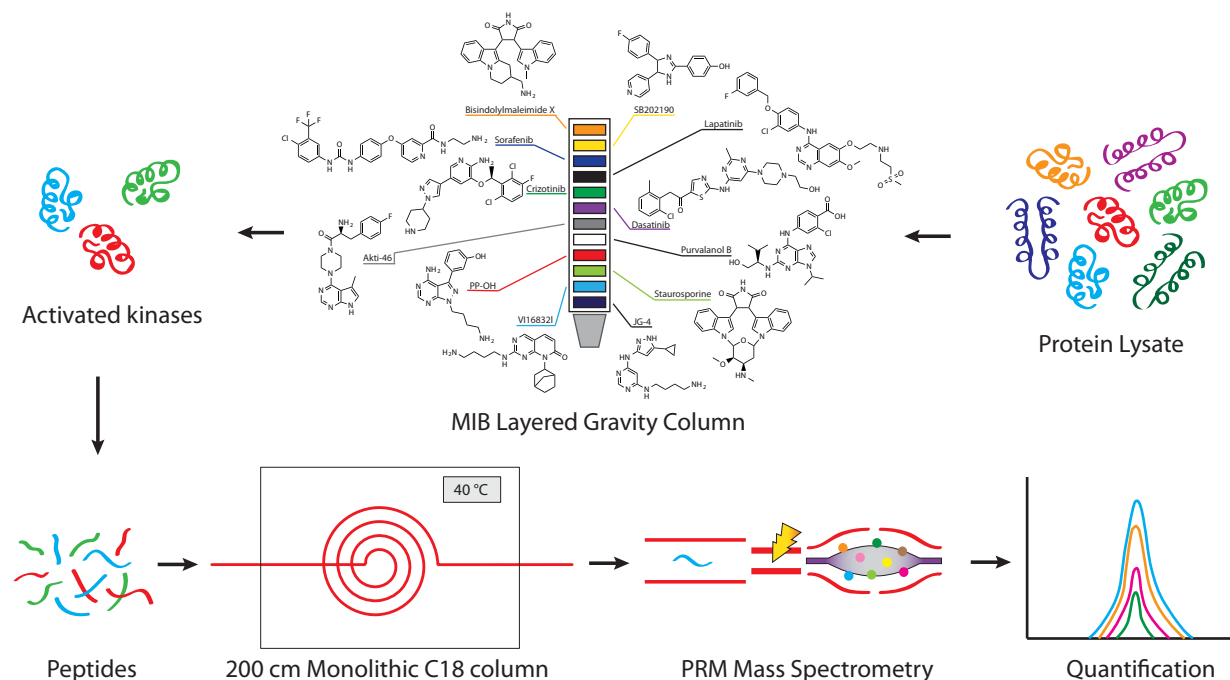
Figure 1: MIB-PRM workflow. Undigested protein lysate is passed through a gravity layered multidrug inhibitor beads column. Broad classes of activated kinases are preferentially enriched in the eluate. A tryptic digest of the eluate is loaded on a meter-scale monolithic silica-C18 column and resolved using a 6-hr reverse phase chromatography gradient at a constant temperature of 40 °C. Online targeted detection of endogenous kinases by a highly multiplexed label-free PRM method provides high sensitivity and specificity of detection compatible with automated data processing.

Results

Monolithic silica-C18 column performance in 6-hr DDA gradients

As the first step toward developing a highly multiplexed PRM pipeline, we examined the

performance of a 200 cm monolithic silica-C18 column in a variety of conditions by considering three factors: estimating its peak capacity (PC), peak width, retention time (RT) reproducibility, and sensitivity of detection (Figure 2). PC is defined as the number of elution peaks that can be separated from baseline over the total duration of a given gradient. RT refers to the elapsed time between sample injection and detection of a given peak.

Temperature is an important determinant of separation efficiency in reverse phase chromatography and ion spray performance, where even small changes in temperature can introduce significant variation in RTs of individual analytes (21, 22). Thus, we evaluated the performance of the monolithic column at different temperatures. For this purpose, a tryptic digest of mouse bone marrow lysate was used in triplicate DDA runs employing 6-hr HPLC gradients while maintaining the column at 25 °C, 40 °C, 60 °C, or 80 °C. In general, peak widths (Figure 2a) and PCs (Figure 2b) observed were similar to the results previously reported for the meter-scale monolithic silica-C18 columns (19). Only minor changes in peak width and PC were observed as a function of temperature. However, the number of identified proteins and peptides was clearly superior at 40 °C (3,384 proteins/21,263 peptides), with more than doubling of identified peptides compared to 25 °C (2,262 proteins/9,537 peptides). Therefore, we chose 40 °C as the standard monolithic column temperature for the remainder of this study.

Figure 2

a

Median peak width

b

Median peak capacity

c

Identified proteins and peptides

d

Retention time reproducibility
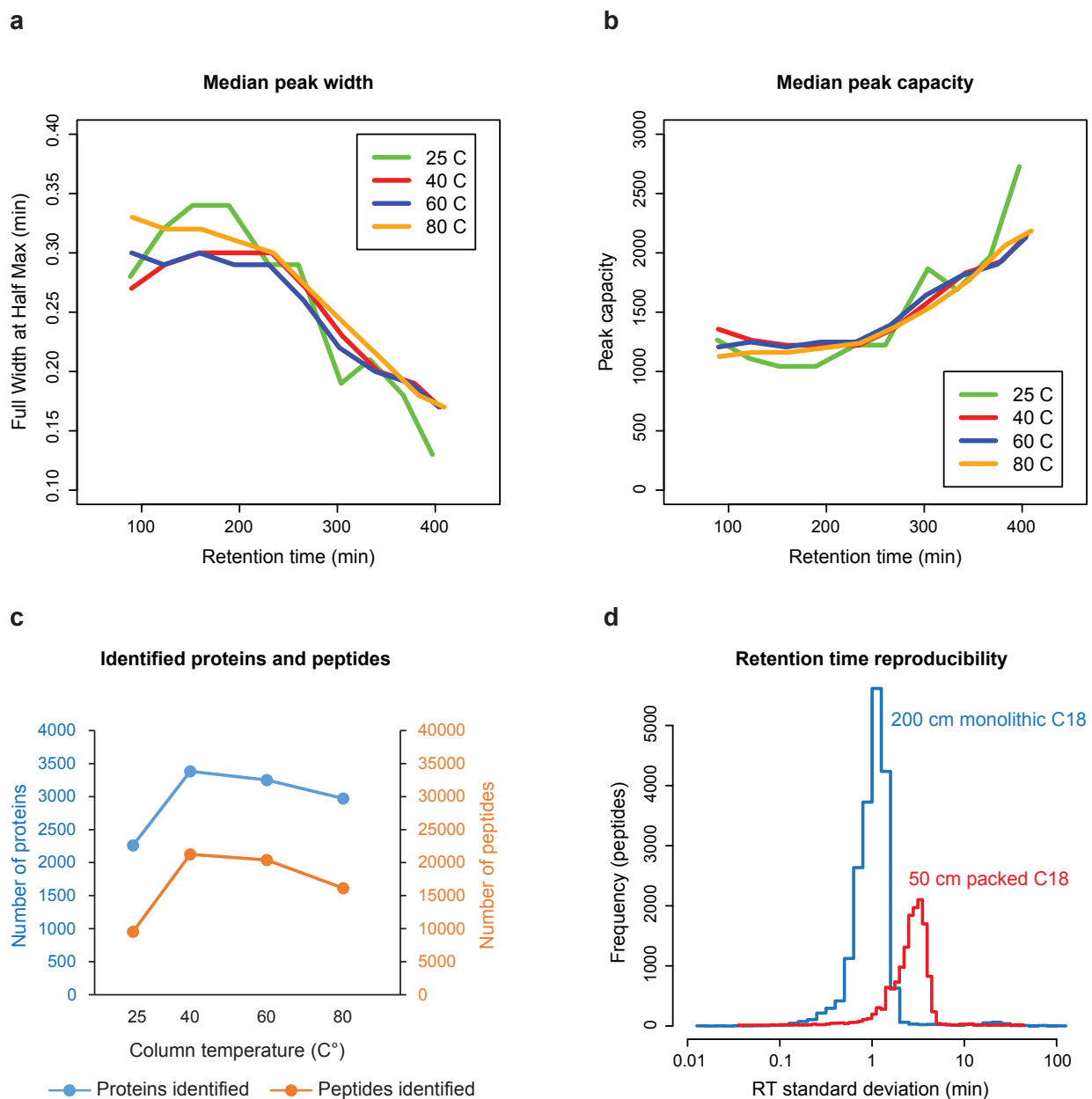
Figure 2: Performance characteristics of a meter-scale monolithic silica-C18 column desirable for targeted proteomic applications. Tryptic digest of mouse bone marrow lysate was separated on the 200 cm monolithic silica-C18 column at 25, 40, 60, and 80 °C and analyzed by LC-MS/MS. (a) Peak width as a function of gradient time is calculated as a running median of full width at half maximum. (b) Peak capacity as a function of gradient time is calculated as the running median of peak width divided by gradient duration. (c) Number of peptides and proteins identified at each temperature. (d) Triplicate runs of the mouse bone marrow lysate sample were performed on the 200 cm monolithic silica-C18 column (at 40 °C) and 50 cm C18 silica particle-packed column (at 45 °C). Histogram of RT standard deviations for peptides identified in all replicates is plotted.

We next examined RT reproducibility, a prerequisite for high multiplexing, on the monolithic silica-C18 column as compared to a conventional C18 silica particle-packed column. The same biological sample was analyzed in triplicate on the monolithic column at 40 °C and on a widely used 50 cm Thermo EasySpray C18 silica particle-packed column maintained at 45 °C (previously identified as the optimal temperature, data not shown) using the same gradient (Figure 2d). Results obtained using the monolithic column established significantly lower RT variability. RT standard deviations under 3 min were documented for over 95% of all identified peptides, while on the packed column, close to 50% of peptides had RT standard deviations above 3 minutes (t-test p <1e-15). Consistent with prior reports (19), approximately 25% more proteins and peptides were identified on the monolithic silica-C18 column compared to the C18 silica particle-packed column (Appendix 2, Figure S1). Both improved sensitivity, as indicated by the increased depth of peptide detection, and lower RT variability afforded by the monolithic silica-C18 column are very desirable characteristics for developing highly multiplexed 16 targeted proteomic applications. In particular, based on the observed low RT variability characteristic of the monolithic column, we deduced that target detection windows of +/-4 minutes would permit the detection of well over 95% of target peptides in a PRM assay.

PRM multiplexing with monolithic silica-C18 columns

Based on our experience and consistent with prior reports (14, 15), optimal PRM sensitivity in complex biological samples on currently available instruments such as Q Exactive Plus (Thermo) requires Orbitrap injection times between 100 and 300 ms. Assuming a cycle time of 6 s, where cycle time is the time delay between adjacent MS2 scans of the same target peptide, is required for 5 measurements over a 30 s elution peak and injection time of 120 ms, no more than 50 targets can be scheduled at any given time (Appendix 2, Figure S2). Furthermore, based on the typical distributions of overlapping target detection windows in the long gradient

runs of complex peptide digests, we estimated that use of target windows of +/-4 minutes (see above) would be adequate to permit scheduling of around 1,000 target peptides in a single run.

To test this possibility, we used a subset of peptides identified in the DDA runs of the mouse bone marrow lysate sample to schedule a highly multiplexed PRM assay (Figure 3). In order to minimize bias for high abundance targets, all detected proteins belonging to Gene Ontology (GO) (23) category "cellular process" were included, independent of the observed intensity in the DDA runs. A total of 1067 target peptides from 325 proteins were selected and scheduled for detection by a single PRM method with variable length detection windows ranging from +/-3.8 min in the most complex part of the gradient (150-350 min) up to +/-8 min in the less complex tail portions (<150 min and >350 min) (Figure 3a). PRM was performed on the same mouse sample and using the same LC gradient as in the DDA runs. Spectra were analyzed with Skyline software, which allows automated detection of extracted MS2 chromatographic peaks (24). Three metrics available in Skyline to monitor specificity of target detection (25) were used to assess the quality of all peaks auto-detected by the software. The distributions of library dot product, a measure of similarity between the observed MS2 spectra and those in the reference DDA library, showed that over 90% of peptides had a dot product > 0.5, where a perfect match equals 1. The distribution of peaks found ratio, the fraction of MS2 component peaks detected of those monitored by PRM, showed that over 95% of peptides had a peaks found ratio > 0.6 (Figure 3b). The high median library dot product and peaks found ratios support a high overall specificity of detection. Similarly, fragment ion mass error distribution demonstrated that more than 90% of all detected peaks were within +/-20 ppm of expected (Figure 3c). Based on these results, we chose a combination of the following three parameters as the threshold for classifying a given target peptide as successfully detected: library dot product > 0.5, peak found ratio > 0.5, and mass error < +/-20 ppm.

Figure 3
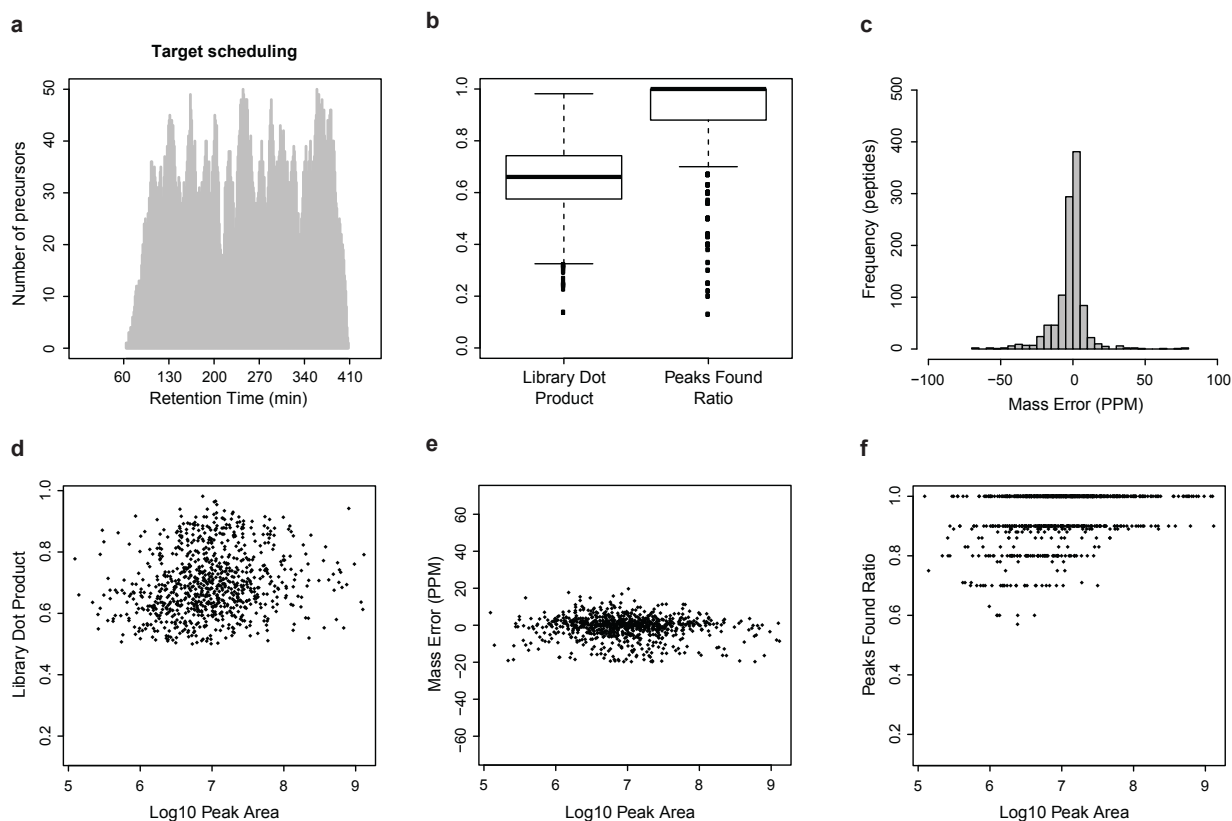
Figure 3: Highly multiplexed label-free PRM is achieved with long gradient chromatography on meter- scale monolithic silica-C18 column. 1,067 peptides from 325 mouse proteins belonging to GO category "Cellular Process" were included in a single PRM method utilizing a 6-hr reverse phase chromatography gradient on the 200 cm monolithic silica-C18 column. Tryptic digest of the mouse bone marrow lysate was used to test the method. Data were analyzed in Skyline using automated peak detection. **(a)** Scheduling diagram shows the expected maximum number of targets as a function of time along the gradient based on the overlap of target detection windows. **(b)** Distributions of library dot product and peaks found ratio, two metrics of detection specificity calculated by Skyline, are shown as box plots (solid line = median, box = interquartile range, whiskers = 1.5 x interquartile distance, dots = individual observations outside whiskers). **(c)** Histogram of MS2 fragment mass accuracy in parts per million (ppm) calculated by Skyline. **(d-f)** Specificity of detection in relationship to protein abundance is estimated by library dot product (d), MS2 fragment mass accuracy (e), and peaks found ratio (f) as a function of peak area.

Employing these strict specificity criteria, a total of 856 target peptides (80%) from 293 proteins

(90%) were successfully detected. Considering only these successfully detected peptides and

using integrated peak areas as a rough estimate of their abundance, we found no significant

correlation between abundance and library dot product (Figure 3d) or mass error (Figure 3e). However, a trend for lower peak found ratio with decreasing abundance was observed (Figure 3f), consistent with loss of lower- intensity peaks in the MS2 spectra recorded at the limits of detection. Additionally, we saw no apparent relationship between abundance and the number of peptides per protein detected among those scheduled (Appendix 2, Figure S3). A comparison of relative intensities of the MS1 precursor ion intensities obtained in the DDA runs to the measured by PRM total MS2 fragment ion intensities demonstrated that the MS1-level and MS2-level quantitation were highly correlated (Appendix 2, Figure S4). Collectively, these results indicate that PRM multiplexing approaching 1,000 target peptides per single 8-hr (6-hr gradient) run on a 200-cm monolithic silica-C18 column is appropriate for routine quantitative PRM detection of label-free endogenous peptides in complex biological samples, providing high sensitivity and specificity of detection.

Monolithic silica-C18 column-coupled PRM for high-coverage kinase detection after MIB enrichment

Quantitative detection of a broad spectrum of kinase activity is needed for comprehensive studies of cellular signaling mechanisms as well as in cancer biomarker discovery and drug development applications. To achieve high coverage of kinases in a quantitative fashion, we developed and validated a highly multiplexed PRM method for detecting human kinases following MIB kinase enrichment. Target precursors were chosen from DDA spectral libraries representing approximately 150 diverse MIB samples, analyzed in pools of 30 to 40 samples each using a 6-hr gradient on the monolithic silica-C18 column. Initial scheduling runs used two injections per sample with ~465 targets per injection and target windows of +/-10 min. In these runs, detection of up to 79% of target precursors was achieved in several independent pools of approximately 30 unrelated MIB samples each (Appendix 2, Figure S5a). A single-injection method was then created by reducing target windows to +/-3.5 min, which successfully detected

>99% of targets (up to 738 peptides from 152 kinases in a single sample) previously detected by the 2-injection method (Appendix 2, Figures S5b,c). The final method employed a 6-hr gradient on the 200-cm monolithic column and targeted 929 unique precursors (peptides of specific charge) from 182 human kinases. Having validated the efficiency of the MIB-PRM platform for detecting a broad set of kinases, we next sought to use the single injection MIB-PRM method to profile kinase regulation in a biologically relevant context.

MIB-PRM identifies activation of TGF-b signaling as a compensatory response to MAPK signaling blockade

The RAS/RAF/MEK/ERK MAP kinase (MAPK) signaling pathway is an important regulator of cell proliferation and survival (26). Activating driver mutations in the pathway are present in over 20% of all human malignancies, including BRAF mutations in ~60% of melanomas and RAS mutations in ~30% of lung and over 50% of colorectal and pancreatic adenocarcinomas (27, 28). Thus, inhibition of MAPK signaling is of significant therapeutic interest (29, 30). Interestingly, recent studies have shown that different classes of inhibitors of MEK and ERK have varying degrees of effectiveness depending on the oncogenic genotype (31, 32). GDC-0973, or cobimetinib, has demonstrated effectiveness in *BRAF* V600E melanomas by inhibiting MEK, but it also stabilizes MEK in its active confirmation. In contrast, GDC-0623 also inhibits MEK but preferentially stabilizes its inactive confirmation. As GDC-0973 and GDC-0623 are both allosteric inhibitors of MEK, they are potentially sensitive to signaling bypass mechanisms that occur within complexes containing inhibited MEK, with complex composition and activity often determined by genotype. The stabilization of an inactive confirmation of MEK by GDC-0623 blocks cell growth and disrupts this feedback mechanism effectively in *KRAS*-mutant cell lines, while GDC-0973 is ineffective in *KRAS*-mutant cell line models (31). Inhibition of ERK, which has no direct interaction with either RAS or RAF, with SCH772984 shows broad effectiveness in *BRAF*, *NRAS* and *KRAS* mutant cell lines, and MEK-inhibitor resistant cells

(32). Given the distinct mechanisms of target inhibition by GDC- 0973, GDC-0623 and

SCH772984, we hypothesized that an evaluation of the kinome response to these inhibitors by

MIB-PRM, in addition to the known patterns of MEK and ERK activation, would likely highlight

unique signatures of kinase response to feedback regulation and crosstalk with other signaling

pathways.

We first validated this approach by western blotting for known kinase regulation phenotypes in

response to the three inhibitors in HCT116 *KRAS* mutant colorectal cancer cells (Figure 4). As

previously reported (31), GDC-0973 maintained MEK phosphorylation, while inhibiting

phosphorylation of downstream kinases ERK and RSK. In contrast, GDC-0623 stabilized

inactive dephosphorylated form of MEK, while similarly inhibiting phosphorylation of ERK and

RSK. SCH772984 eliminated ERK phosphorylation, but feedback activation of MEK was

observed (31, 33). We next used the MIB-PRM approach to identify differences in kinome

activation in response to the three types of MAPK pathway inhibitors in HCT116 cells.

Figure 4
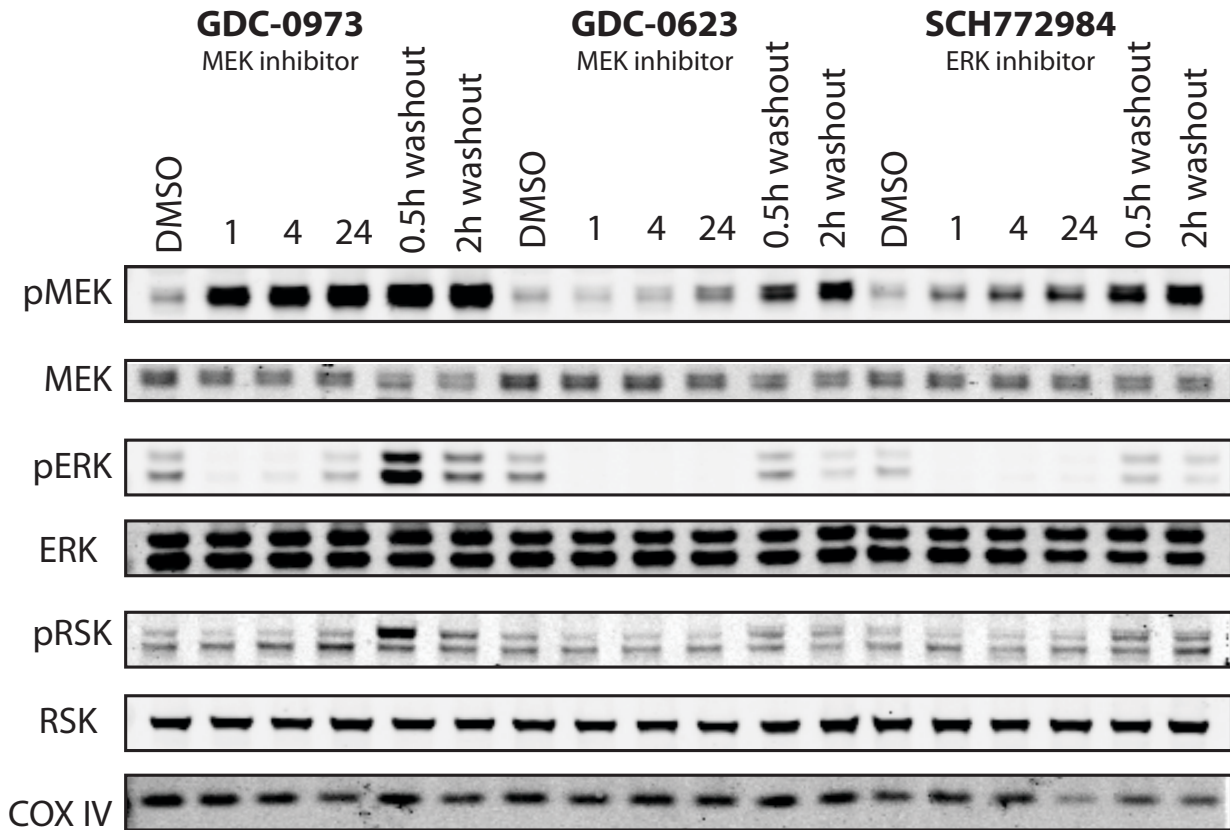
Figure 4: Three types of selective inhibitors of MAPK signaling produce expected differential kinase inhibition and activation responses in HCT116 colorectal cancer cells. HCT116 cells were treated with 250nM of GDC-0973, GDC-0623, SCH772984 or DMSO for 1, 4, or 24 hours. In the washout samples, cells were drug treated for 24 hours, then changed into fresh media and harvested after 0.5 or 2 hours. Lysates were used for western blots of total and phosphorylated MEK, ERK and RSK; blotting for COX IV was used as the loading control.

The validated single-injection PRM method was used to quantify kinase abundance in the eight experimental samples from 2 biological replicates of 4 experimental conditions. To ensure high specificity, targets were considered successfully detected using the same criteria as those used in the mouse digest highly multiplexed PRM validation experiments with a library dot product > 0.5, peak found ratio > 0.5, and mass error < +/-20 ppm. No additional individual fragment ion filters were used (such as threshold signal-to-noise ratio or coefficient of variance in repeat experiments) based on the observation that total areas (i.e. sum of the peak areas of all detected fragments) and sum area of only the top 3 most intense fragments with highest signal-

to-noise separation are highly correlated (r >0.97) (Appendix 2, Figure S6). Overall, 814 target

precursors, 88% of the 929 scheduled, from 154 kinases were quantified (Appendix 2, Figure

S7). A lower than 100% detection rate is expected in MIB experiments, given the preferential

enrichment of activated kinases and cell- specific variation in expression of individual kinases.

Comparison of PRM measurements in biological replicates revealed variable condition-

dependent heterogeneity, with correlation coefficients ranging between 0.47 and 0.86 (Appendix

2, Figure S8). This heterogeneity was attributed mainly to biological differences between the

samples, given the almost negligible in comparison differences between technical repeats

(Appendix 2, Figure S5C). MSStats software (34) was used to normalize the data and assign

statistical significance to the observed differences among the three drug conditions and DMSO

control (Appendix 2, Figure S9).

As expected, the PRM results demonstrated a highly significant reduction in detectable MAPK1

(ERK2) and MAPK3 (ERK1) following SCH772984 treatment compared to DMSO control

(Figure 5a), consistent with inhibition of the two ERK proteins by the compound. Furthermore,

increased abundance of MAP2K1 (MEK1) was observed in both GDC-0973 and SCH772984

treatments (Figure 5c), consistent with the concurrent increase in MEK phosphorylation

measured by Western blot in these two conditions (Figure 4) and in agreement with prior

evidence that both inhibitors induce compensatory activation of MEK1 (31–33). Consistent

enrichment of MAP2K1 (MEK1) and MAP2K2 (MEK2) remains an area for further optimization

of MIB proteomics and is likely the root cause of the less than statistically significant quantitation

of these kinases.

A total of 23 kinases demonstrated significant changes of abundance in MIB eluates as

measured by PRM in at least one of the three inhibitor treatments relative to the DMSO control

and using a conservative threshold of significance set at log2 fold change of >4 and MSStats

estimated p-value of <0.05 (Figure 5b and Appendix 2, Figure S10). Overall, while negative

changes (loss of kinase detection) produced by the three inhibitors were almost entirely non-overlapping, 5 of 11 kinases that showed significant positive changes (gain of detection) were shared by all three inhibitors. This suggests, that while negative changes reflect largely direct inhibition of target and off-target kinases, positive changes are more likely to represent shared compensatory effects in response to inhibition of MAPK signaling. The data further suggest very high specificity of SCH772984 with only on-target inhibition of MAPK1 and MAPK3 detected, as well as higher specificity of GDC-0623 compared to GDC-0973 based on the higher number of off-target inhibited kinases detected for the latter.

Figure 5

a
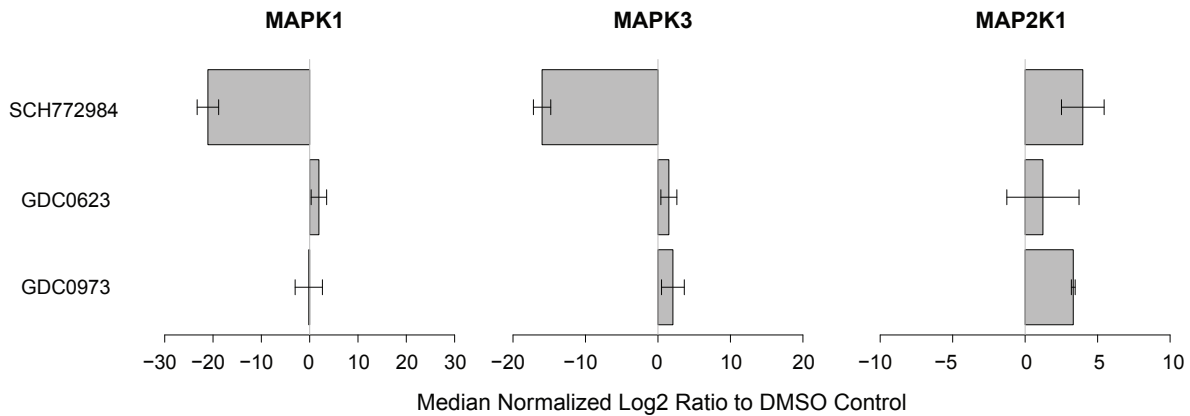
b
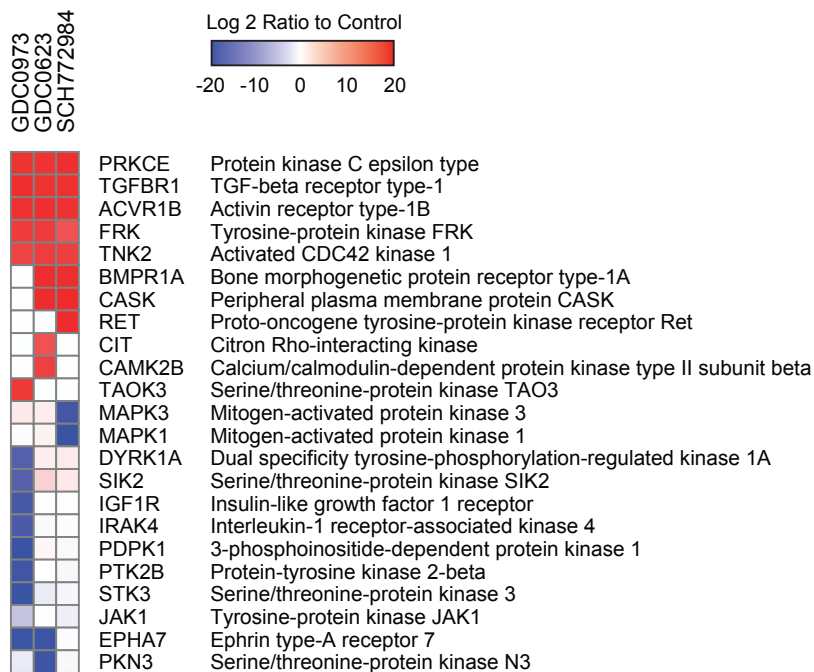
c
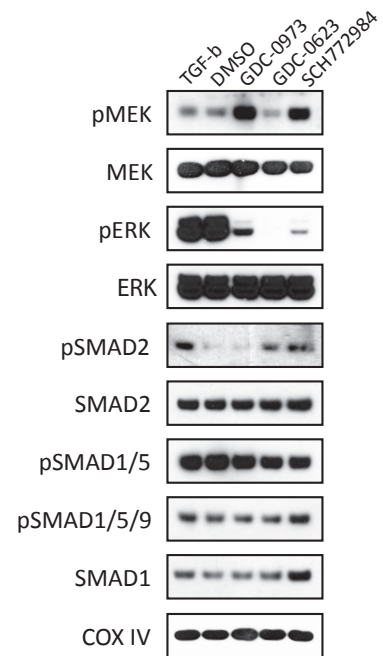
Figure 5: Highly multiplexed PRM method downstream of MIB kinase enrichment quantifies kinome response to three types of MAPK signaling inhibitors in HCT116 colorectal cancer cells. HCT116 cells were treated with 250nM GDC-0973, GDC-0623, SCH772984 or DMSO for 90 minutes. The lysates were collected and passed over MIB columns. The eluates enriched for activated kinases were digested with trypsin and analyzed by a single PRM method utilizing the long monolithic silica-C18 column and targeting 929 precursor peptides from 182 kinases. A total of 814 precursors from 154 kinases were quantified using strict specificity criteria. (a) Abundance of MAPK1 (ERK2), MAPK3 (ERK1) and MAP2K1 (MEK1) in MIB eluates measured by PRM are plotted as log2 ratios to DMSO control. (b) All kinases with statistically significant

inhibition or activation relative to DMSO control were ordered by hierarchical clustering of the corresponding log2 ratios. (c) HCT116 cells were treated with 250nM of GDC-0973, GDC-0623, SCH772984 or DMSO for 90 minutes, or with TGF-b at 50 pg/mL for 30 minutes, followed by western blotting.

Among the kinases with shared activation in response to the three inhibitors of MAPK signaling in the HCT116 cells were TGF-b superfamily receptors TGF-b receptor 1 (TGFBR1), activin receptor type 1B (ACTR1B), and bone morphogenic protein receptor type 1A (BMPR1A). These closely related receptors are activated upon binding of TGF-b and TGF-b-like ligands and are involved in diverse cellular processes such as cell migration and differentiation in response to paracrine signals (35). All three receptors function through downstream activation of SMAD2/3 and/or SMAD1/5 pathways, depending on cell type-specific context (36, 37). In our experiments, the apparent activation of all three receptors (TGFBR1, ACTR1B, and BMPR1A) was observed by PRM in response to GDC-0623 and SCH772984 and was accompanied by a concurrent increase in phosphorylation of SMAD2 (Figure 5c). In contrast, GDC- 0973 treatment resulted in activation of TGFBR1 and ACTR1B but not BMPR1A, and no changes in SMAD2 phosphorylation were observed. Phosphorylation of SMAD1, SMAD5, and SMAD9 was not affected by any of the inhibitors (Figure 5c). Previously, increased expression of TGF-b was shown to be a predictor of recurrence and metastasis in colorectal cancer (CRC) (38). It is also known that activation of TGF-b signaling leads to SMAD-independent activation of MAPK signaling in multiple systems (39, 40). In this light, our findings suggest that activation of TGF-b signaling is a compensatory mechanisms that in addition to downstream activation of SMAD2 may include a SMAD-independent effect aimed at restoring MAPK signaling in the context of MAPK signaling blockade in these KRAS-dependent cells.

Discussion

We have developed a strategy for highly multiplexed PRM relying on ultra-long monolithic silica-C18 column based liquid chromatography and demonstrated its utility by quantifying the activity

of a broad segment of the human kinome in vivo in response to kinase inhibitor therapy. By coupling MIB with highly-multiplexed PRM, we eliminate the need for isobaric tagging reagents and off-line sample fractionation prior to LC-MS/MS, while maintaining broad coverage and highly specific, reproducible and sensitive quantitation.

Higher kinome detection coverage of up to 260 kinases by DDA LC-MS/MS has been reported in proof- of-principle experiments on pooled lysates comprised of diverse cell lines using *kinobead* enrichment approach (41), a strategy similar to MIB that is not activity-dependent. However, consistent and specific quantitation at such high kinome coverage has not been demonstrated in practical biological applications employing a single cell type. With the ability to specifically target kinases for quantitation across a large dynamic range, MIB-PRM has the advantage of higher sensitivity, reproducibility and quantitative accuracy in realistic biological applications.

A recently published report by Ruprecht et al. calls into question the reliability of MIB enrichment as a functional readout of kinase activity (42). In this work, the authors compare the state of kinase activation inferred from phosphorylation changes of the downstream substrate sites measured by phosphoproteomics to the patterns of kinase enrichment following MIB. We agree with the authors that MIB enrichment is not as comprehensive or sensitive as phosphoproteomics in detecting kinase activity changes. However, based on our experience and consistent with the authors' findings, the changes in kinase regulation that are detected by MIB are typically in good agreement with those observed by phosphoproteomics. Therefore, based on our studies, MIB strategy remains a biologically relevant assay of kinase activity, albeit less sensitive than phosphoproteomics. The MIB platform can also be preferable in applications where phosphoproteomics are not feasible, e.g. the workflow used by Ruprecht et al. required metabolic isotopic protein labeling by SILAC (43) and extensive offline fractionation

of the digested lysates prior to LC-MS/MS analysis.

We used the MIB-PRM approach to study the effects of MAPK signaling inhibition by two MEK inhibitors, GDC-0973 and GDC-0623, the former being less potent in mutant *KRAS* driven cells, and an ERK inhibitor, SCH772984, in *KRAS*-mutant HCT116 colorectal cancer cells and found that all three inhibitors produced activation of TGF-b family of receptors. While GDC-0623 and SCH772984 led to activation of TGFBR1, ACTR1B and BMPR1A with concurrent activation of SMAD2; GDC-0973 treatment resulted in activation of only TGFBR1 and ACTR1B (not BMPR1A), and no activation of SMAD2 was observed. Given prior evidence of SMAD-independent MAPK activation downstream of TGF-b signaling (39, 40), we hypothesize that the observed activation of TGF-b signaling might be a compensatory mechanism either partially or primarily aimed at SMAD-independent MAPK signaling activation upstream of RAS to counteract MAPK blockade produced by the inhibitors. These results provide further support for the argument that combination therapy with MAPK and TGF-b inhibitors may have potential benefits in the treatment of KRAS-driven cancers (44, 45).

In this report, we demonstrate the utility of a meter-scale monolithic silica-C18 column in targeted proteomic applications. Long monolithic silica-C18 columns have been previously shown to be highly effective in achieving unprecedented chromatographic separation of peptides in complex biological samples in long (>6 hr) gradients, enabling near-proteome-scale protein detection in one-shot DDA proteomics applications (18). Here, we used the superior chromatographic characteristics of the long monolithic silica-C18 columns, specifically high peak capacity and low RT variability, to address one of the principal challenges of PRM – its limited multiplexing capacity.
Furthermore, we demonstrate the feasibility of targeting approximately 1,000 endogenous target precursors with expected detection of over 85% in a single 8-hr PRM run in routine applications

not employing SIL standard peptides. Previously, Burgess et al., used an in-house 30 cm C18

silica particle- packed column with a 3-hr reverse phase gradient to test an 800-plex SRM assay

to detect 400 heavy and 262 counterpart light SIL peptides (46). A total of 257 peptide pairs

(514 total precursors) were detected in that effort, effectively defining the practical limits of SRM

multiplexing. More recently, Gallien et al. addressed the limits of PRM multiplexing using a novel

approach in which detection of endogenous target peptides is aided by real-time detection of

spiked in SIL standard peptides, which once detected trigger on the fly adjustments to

OrbitrapTM injection time, scan resolution, and target window duration to maximize sensitivity

and minimize overlap between multiple windows (47). This so- called standard-triggered PRM

used 600 SIL standard peptides and was capable of detecting up to 300 corresponding

unlabeled endogenous peptides in serum samples run on a conventional 15 cm C18 silica

particle-packed column with a 66-min reverse phase HPLC gradient.

Although, this approach is perfectly suited for clinical and other analytical applications for which

synthesis of SIL peptides is warranted, many biological applications in targeted proteomics

would not be feasible if SIL standards were required for each desired target.

Not using SIL standards in PRM applications puts particular emphasis on specificity of detection

and reliability of automated peak detection. We have demonstrated that high specificity can be

achieved via use of high-resolution discovery spectral libraries for accurate RT scheduling

followed by application of high-stringency criteria that simultaneously ensure similarity with

reference spectra, acceptable fraction of MS2 peaks detected, and high mass accuracy during

routine automated analysis in Skyline (24). Furthermore, the general PRM workflow and data

analysis strategy illustrated above do not require any custom software or hardware beyond a

PRM-enabled instrument, making it straight-forward to implement in most proteomic labs.

It should be acknowledged that workflows incorporating very long chromatographic gradients,

such as the 6-hr gradient used here, present a significant demand on instrument time and are

not practical in all PRM applications. The proposed workflow is chiefly intended to overcome the scan time limitations of the existing Quadrupole-Orbitrap instruments in order to achieve the highest possible multiplexing capacity in PRM runs. Coupled with the higher sensitivity of detection stemming from the superior separation achieved in the long gradients on the monolithic silica-C18 column, the described workflow is particularly beneficial in the most demanding applications characterized by high sample complexity, low starting protein amounts prohibiting multiple injections, and a desire for the highest possible target multiplexing.

The demonstrated high degree of PRM multiplexing without SIL standards, combined with high detection specificity achieved by routine automated data processing and the inherent highly quantitative nature of the methodology, opens unprecedented possibilities for biological applications. In particular, we foresee the strategy applied to large scale screens of protein function in hundreds of proteins simultaneously. In addition to the MIB platform described above, other kinase enrichment modalities would benefit from downstream PRM detection (4). Other attractive targets include functional classes of proteins that can be enriched via biochemical or biophysical methods, including transcription factors and other nucleic acid binding proteins, proteins restricted to specific subcellular compartments, or specialized extracellular structures. In addition, the approach is perfectly suited for studies of signaling regulation by post-translational modifications (PTM) in large signaling networks. For example, phosphorylation states at many hundreds of sites in hundreds of proteins can be quantified by highly multiplexed PRM following phosphopeptide enrichment. The approach is also well suited for "one-shot targeted proteomics" applications that require flexible on-demand detection of hundreds of precursors relevant to a specific biological question in minute samples such as fluorescence sorted subpopulations of specialized cells, difficult-to-scale organoid cultures, or amount-limited clinical materials.

Acknowledgments

Experimental Procedures

Online liquid chromatography

A prototype 200 cm fused silica monolithic silica-C18 column, 100 mm inner diameter, was used in all experiments. Columns with essentially identical characteristics are now available commercially from GL Sciences (Tokyo, Japan). Liquid chromatography was performed on a Waters NanoAcquity UPLC system (Waters, USA). The column was maintained at a constant temperature using Eppendorf CH30 column heater with TC50 temperature controller (Eppendorf, USA). Reverse phase 6-hr gradients for both DDA and PRM runs on the monolithic column were performed with a binary buffer system using 0.1% formic acid in water (buffer A) and 0.1% formic acid in acetonitrile (buffer B) as follows: load at 2% B at 600 nL/min for 20 min; gradient with 2-25% B over 288 min at 400 nL/minà25-32% B over 36 min at 400 nL/minà32-40% B over 18 min at 400 nL/minà40-60% B for 18 min at 400 nL/min; wash at 60-80% B over 10 min at 400 nL/min; equilibrate at 2% B at 600 nL/min. Six-hour gradients on the EasySpray 50 cm column (Thermo Fisher Scientific, USA) were performed as above, except the flow rate was maintained at 200 nL/min to adjust for high column back pressure according to the manufacturer's recommendations.

DDA mass spectrometry

Q Exactive Plus instrument (Thermo Fisher Scientific, USA) was used in Full-MS/ddMS2 mode with one survey scan (350-1500 m/z, R=70,000 at 200 m/z, AGC target of 3e6), followed by up to 10 data- dependent HCD MS2 scans (AGC target of 5e4, max IT 120 ms, R=17,500 at 200 m/z, isolation window 4.0 m/z, NCE 25%, 4% underfill ratio, and 10 s dynamic exclusion). Mouse bone marrow lysate sample was loaded at 100 ng per injection.

PRM mass spectrometry

Q Exactive Plus instrument (Thermo Fisher Scientific, USA) was used in PRM mode with the following parameters: positive polarity, R=17,500 at 200 m/z, AGC target 1e6, maximum IT 190 ms, MSX count 1, isolation window 3.0 m/z, NCE 35%. Mouse bone marrow lysate sample was loaded at 100 ng per injection. MIB pooled samples were loaded at 500 ng per injection. Experimental MIB enriched samples from HCT116 cells were loaded at estimated 200-500 ng per injection based on historical average yields determined in pooled samples using Peirce BCA protein assay kit (Thermo Fisher Scientific).

Mouse bone marrow lysate preparation and tryptic digest

Bone marrow cells were harvested by needle aspiration from femora and tibiae of wildtype C57BL/6 mice, snap-frozen in liquid nitrogen. Frozen cell pellets containing approximately 1×10e8 cells were resuspended in 0.5 ml of TRIzol reagent (Thermo Fisher Scientific) and protein extraction was carried out according to the standard manufacturer's protocol. Precipitated protein pellets were washed with ethanol and vacuum-dried briefly. The pellets were reconstituted in 300 µL of 8 M urea, 0.2 % Zwittergent 3-16 (Santa Cruz Biotechnology), and 50 mM Tris-HCl, pH 8.0. Twelve µL of 100 mM DTT were added and samples vortexed for 30 min at room temperature. The pellets were dissolved by microtip soniction (30 sec on/30 sec off on ice x3). Eighteen µL of 100 mM iodoacetamide was added, followed by water bath sonication for 30 min at room temperature. Two µL of resuspended protein sample were

quantified using Pierce BCA protein assay kit (Thermo Fisher Scientific) according to the standard manufacturer's protocol. Sample was diluted by adding 1.2 mL of 50 mM Tris-HCl, 1 mM CaCl2 (pH 8.0), and pH was adjusted to 8.0. Sequencing grade trypsin (Promega) was added at a ratio of 1:50 (trypsin/protein), and the samples were incubated with gentle agitation at 37°C overnight. Approximately 10 μL of formic acid per 1 mL of sample was added to adjust pH to ~3.5. Digested peptides were desalted with Sep-Pak C18 cartridges (Waters) according to the manufacturer's protocol, dried to remove solvent under vacuum centrifugation, and stored at -80°C for further use.

Cell culture and kinase inhibitor treatments

HCT116 cells obtained from the ATCC (www.atcc.org) were cultured in DMEM supplemented with 10% fetal bovine serum. GDC-0973, GDC-0623 and SCH772984 were purchased from Selleckchem (www.selleckchem.com). For time course experiments, cells were grown in 6 cm dishes until near confluency, then treated for the indicated time and dose. For MIB experiments, cells were plated in 15 cm plates and grown to near confluency, then treated with drug or equivalent amounts of DMSO for 90 minutes. Cells were washed twice with phosphate buffered saline (PBS) then harvested by scrapping cells into PBS and centrifuging for 5 minutes at 300 xg and 4 °C yielding pellets of ~0.5 mL, and the cell pellets were snap frozen.

Cell lysate preparation and western blotting

Cells were diluted in 3-5x pellet volume of lysis buffer (50mM HEPES pH 7.5, 150mM NaCl, 0.5% Trition X-100, 1mM EDTA, 1mM EGTA) with PhosStop phosphatase and cOmplete protease inhibitor cocktails (Roche). Cells were lysed on ice using two 3-second pulses in a water bath sonicator. Lysates were spin cleared and protein concentration was checked by a BCA assay (Thermo Fisher Scientific). For immunobloting the following antibodies from Cell Signaling Technology were used: MEK (4694), phospho-MEK (Ser217/221, 9154), ERK (9102),

phospho-ERK (Thr202/Tyr 204, 9106), RSK1 (8408), phospho-RSK (Ser380, 9341), Ret (14556), phospho-Ret (Tyr905, 3221), COX IV (4844), SMAD2 (5339), phospho-SMAD2 (Ser465/467, 3108), SMAD1 (6944), phospho SMAD1/5 (Ser463/465, 5753), and phospho-SMAD1/5/9 (Ser463/465/467, 13820).

MIB kinase enrichment and tryptic digestion

Compounds for Multiplex inhibitor beads were synthesized or commercially purchased and conjugated to resin as previously described(8). 10mg of total protein per condition from lysed cell pellets was diluted to 10mL final volume in high salt buffer (50mM HEPES pH 7.5, 0.5% Triton X-100, 1M NaCl, 1mM EDTA, 1mM EGTA) containing protease and phosphatase inhibitors (Roche). Lysates were pre-cleared over unconjugated resin in a gravity column before passing onto the MIB gravity column. The MIB column was prepared by layering 50-100uL slurry of each individual inhibitor-conjugated bead in BioRad Poly-Prep Chromatography Columns with a 10 mL reservoir and 2mL bed volume (BioRad, 731-1550). For binding and washing, a 26-guage needle was placed on the outlet of the MIB column to slow the flow rate. We estimate the flow rate to be around 0.3 mL/min. Lysate-bound columns were washed with 10mL high salt buffer, 10mL low salt lysis buffer (50 mM HEPES pH 7.5, 0.5% Triton X-100, 150 mM NaCl, 1mM EDTA, 1mM EGTA) and lastly 1mL of low salt buffer with 0.1% SDS. Samples were eluted off the MIB column with 2x incubations at 100°C for 5 minutes with 0.5mL of elution buffer (0.5% SDS, 1%BME in 0.1M Tris-HCl ph 6.8). Samples were reduced with 5mM DTT at 55°C for 30 min and alkylated at room temperature with 10mM iodoacetimide for 45 minutes in the dark. Samples were spin concentrated to 100 uL using Amicon Ultra 10KDa centrifugal filters (Milipore). Proteins from the concentrated eluate were precipitated using a methanol-chloroform extraction, suspended in 75 uL of 50mM ammonium bicarbonate and digested overnight with 3 ug sequencing grade modified trypsin (Promega, V5113). Samples were acidified to pH 3 with formic acid, desalted with C18 ZipTips (Millipore), speedvac evaporated to

dryness and stored at -80°C until resuspension in 0.1% formic acid for MS analysis.

Data analysis

1. Performance of monolithic silica-C18 column by DDA MS

Raw data files of the mouse bone marrow lysate runs at 25, 40, 60 and 80 °C were converted to peak files using PAVA (21) and searched in Protein Prospector (48, 49) version 5.14.0 against UniprotKB mouse proteome database (50) downloaded on 09/18/13 (51,219 protein entries) and corresponding random concatenated decoy database with default "ESI-Q-high-res" parameters, including trypsin as the protease, up to one allowed missed cleavage site, Carbamidomethyl-C constant modification, default variable modifications (Acetyl (Protein N-term); Acetyl+Oxidation (Protein N-term M); Gln->pyro-Glu (N- term Q); Met-loss (Protein N-term M); Met-loss+Acetyl (Protein N-term M); Oxidation (M)), up to 3 modifications per peptide, and 20 ppm precursor mass and fragment mass accuracy. False discovery rate of <1% was used as the cutoff for peptide expectation values. The same high-specificity search parameters were used for both monolithic column and EasySpray column runs to minimize inclusion of false positive spectra in the spectral libraries. Spectral libraries of these runs in *blib* format were generated in Protein Prospector and imported into Skyline v. 3.5 (24). All identified peptides were added as targets in Skyline and raw data imported in MS1 filtering mode with the following settings: only scans within 1.5 min of MS/MS IDs imported, 3 isotope precursor peaks included, and Orbitrap mass analyzer with resolution of 70,000 at 200 m/z. Only peptides identified by the search engine in all runs were retained for further consideration. Peak widths were exported from Skyline as full width at half maximum (FWHM), and median peak widths as a function of the gradient time were calculated by binning peptides into RT windows of 30 minutes. Similarly, median peak capacity as a function of the gradient time was calculated as median peak widths within 30 min windows divided by the total gradient time, defined as the time between the earliest and the latest identified peptides. Retention time reproducibility was determined by

evaluating RT standard deviations among triplicate runs of the bone marrow lysate sample at 40 °C.

2. PRM multiplexing in mouse bone marrow lysate

Spectral library generated in the DDA experiments was used as the reference library in Skyline. Target proteins were chosen based on the GO (23) category "Cellular Process". Up to 8 target peptides per protein were included by matching to the spectral library if the following criteria were met: RT standard deviation in the triplicate DDA runs is less than 2 min, peptide does not share identity with any other protein in the human SwissProt database (51), peptide length is between 9 and 26 residues, and no more than one miscleavage site is present. Up to 10 most intense y and b ions (with preference for y ions) were chosen as monitored transitions. A total of 1067 target peptides from 325 proteins were selected. Target RT for each peptide was the average RT from the triplicate DDA experiments. RT target windows were set at +/- 8 min between minutes 0 and 150, +/- 3.8 min between minutes 150 and 350 and -5/+6 min after minute 350. Larger windows at the tails of the gradient were used to accommodate greater degree of RT variation in those areas and were possible due to lower numbers of eluting precursors in these regions. Raw data files were imported into Skyline for automated peak detection using "targeted" MS/MS filtering mode with mass analyzer set to Orbitrap, R=17,000 at 200 m/z. Total peak area (sum of areas of all transition peaks), library dot product, peaks found ratio, and MS2 fragment mass accuracy were calculated by Skyline and used to generate the plots in Figure 3 (b-f). Skyline document with PRM data collected in mouse bone marrow lysate is available on Panorama Web (52), dataset ID 2980

(https://panoramaweb.org/labkey/targetedms/UCSF-MSF/MIB-PRM%20paper/showPrecursorList.view?id=2980).

3. PRM method for kinase detection

Approximately 150 MIB individual samples from prior unrelated diverse experiments in human cell lines were combined into four pools of 30-40 samples in each. The pools were separately analyzed using DDA runs on the Q Exactive instrument equipped with the monolithic silica-C18 column. Raw data files were converted to peak files using PAVA (53) and searched in Protein Prospector (48, 49)version 5.14.0 against human SwissProt database (51), downloaded on 07/29/2013 (39,457 entries), and corresponding random concatenated decoy database with default "ESI-Q-high-res" parameters. Protein Prospector search parameters were as above. FDR of <0.2% was used as the cutoff for peptide expectation values to ensure specificity. Spectral libraries of these runs in *blib* format were generated in Protein Prospector and imported into Skyline v. 3.5 (25). Raw data files have been uploaded to the ProteomeXchange Consortium (http://proteomecentral.proteomexchange.org) via the MassIVE partner repository (http://massive.ucsd.edu/ProteoSAFe/static/massive.jsp) with the data set identifiers PXD003934 and MSV000079644, respectively.

Target peptides matching a list of 509 human kinases (1) were selected from the discovery spectral library; only canonical splicing isoforms were included. All unique peptides, i.e. those that do not share identity with any other human protein in SwissProt database (downloaded on 07/29/2013; 39,457 entries), were initially selected. PTM-containing peptides were excluded. Given the high degree of conservation between kinases within individual families, some kinases (13%) could not be represented by more than one unique peptide. We also included 10 proteins (11 peptides) commonly detected in DDA analyses of human samples to serve as controls for non-specific carry-over during MIB enrichment (Supplementary Table 1). For each selected precursor, up to 10 most intense y and b ions (with preference for y ions) were chosen as monitored transitions. Initial scheduling method contained 944 target precursors from 182 proteins, was split into two injections with half of the targets in each, and used variable target detection windows as follows: +/- 20 min between minutes 0 and 150, +/- 10 min between

minutes 150 and 350 and +/-20 min after minute 350. The method was tested on two independent MIB enriched pools, each combining approximately 30 individual MIB samples. Raw data were imported into Skyline, and positions of auto-detected peaks were checked manually, only 15 of which were clearly erroneous (background noise in the absence of visually identifiable peaks) and were excluded from the final method. The final single-injection method contained 925 precursor peptides from 182 kinases, and used the following target detection windows: +/- 8 min between minutes 0 and 160, +/- 3.5 min between minutes 150 and 350 and +/-8 min after minute 310. The same two pooled MIB samples were used to test the single-injection method. For both two-injection and single-injection methods, precursors were considered successfully detected if Skyline auto-detected peaks satisfied the following criteria: library dot product >0. 5, peaks found ratio >0.5 (with at least 3 fragments detected), and fragment mass error <20 ppm.

4. MIB-PRM experiments in HCT116 cells

The single-injection kinase detection method was used without any modifications on the HCT116 experimental samples. Raw data were imported into Skyline v. 3.5, and auto-detected peaks in each sample were filtered according to the same specificity criteria as above (library dot product >0. 5, peaks found ratio >0.5, and fragment mass error <20 ppm). Successfully detected peaks were used to normalize data by median centering log2 peak areas in each sample to match the global dataset median. Since undetected peaks could mean either biologically relevant depletion in kinase binding or a technical failure of the method to detect the target precursors, the following pre-processing was applied to the undetected peaks. If in a given condition, a precursor was detected in one of two biological replicates, the undetected value was set to the mean of all non-zero observations for that precursor (i.e. lack of detection is likely due to a technical failure and thus its statistical significance is penalized). Log2 peak area of a precursor was set to 1 (a small number not equal 0 to allow calculation of ratios) only if it

was undetected in both biological replicates of a given condition and only if no other precursor from that kinase was detected in that condition (i.e. lack of detection is likely due to a real biological kinase depletion). This pre-processing strategy is similar to that used for imputing missing values in MSStats (34), except it is more conservative in that it is not applied to all undetected peaks and results in fewer false positives. The number of precursors quantified versus targeted as well as percent imputed measurements for each kinase are listed in Supplementary Table 1. The data were then converted to a matrix of log2 ratios of inhibitor conditions vs DMSO control and analyzed in MSStats version 2.6.0 using no further pre-processing. MSStats input file with PRM measurements listed by precursor and output file with estimated aggregate kinase abundances are available as Supplementary Files 1 and 2, respectively; Skyline report with PRM measurements by transitions is available as Supplementary File 3 (see Supplementary Data). Based on the distributions of log2 ratios and corresponding p-values calculated by MSStats for each inhibitor condition, a conservative cutoff of |log2 ratio| > 4 and p-value < 0.05 was chosen to identify the most significant observations. Heat map diagram of kinases with statistically significant inhibition or activation was constructed by clustering all kinases with a statistically significant log2 ratio in at least one of the three inhibitor conditions. Complete linkage clustering using city block distance and image generation were performed in GENE-E software (http://www.broadinstitute.org/cancer/software/GENE-E/). Skyline document with PRM data collected in MIB samples, pool injections and HCT116 experiments, is available on Panorama Web, dataset ID 2979 (https://panoramaweb.org/labkey/targetedms/UCSF- MSF/MIB-PRM%20paper/showPrecursorList.view?id=2979).

References

1. Manning G, et al. (2002) The protein kinase complement of the human genome. *Science* 298(5600):1912–34.
2. Blume-Jensen P, Hunter T (2001) Oncogenic kinase signalling. *Nature* 411(6835):355–65.

3.   Uhlen M, et al. (2010) Towards a knowledge-based Human Protein Atlas. *Nat Biotechnol* 28(12):1248–1250.
4.   Daub H (2015) Quantitative Proteomics of Kinase Inhibitor Targets and Mechanisms.
5.   Duncan JS, et al. (2012) Dynamic reprogramming of the kinome in response to targeted MEK inhibition in triple-negative breast cancer. *Cell* 149(2):307–21.
6.   Cooper MJ, et al. (2013) Application of multiplexed kinase inhibitor beads to study kinome adaptations in drug-resistant leukemia. *PLoS One* 8(6):e66755.
7.   Stuhlmiller TJ, et al. (2015) Inhibition of Lapatinib-Induced Kinome Reprogramming in ERBB2-Positive Breast Cancer by Targeting BET Family Bromodomains Article Inhibition of Lapatinib-Induced Kinome Reprogramming in ERBB2-Positive Breast Cancer by Targeting BET Family Bromodomains. *CellReports*:1–15.
8.   Sos M, et al. (2014) Oncogene Mimicry as a Mechanism of Primary Resistance to BRAF Inhibitors. *Cell Rep* 8(4):1037–1048.
9.   Wiese S, Reidegeld KA, Meyer HE, Warscheid B (2007) Protein labeling by iTRAQ: A new tool for quantitative mass spectrometry in proteome research. *Proteomics* 7(3):340–350.
10.   Ow SY, et al. (2009) iTRAQ underestimation in simple and complex mixtures: "the good, the bad and the ugly". *J Proteome Res* 8(11):5347–5355.
11.   Lange V, Picotti P, Domon B, Aebersold R (2008) Selected reaction monitoring for quantitative proteomics: a tutorial. *Mol Syst Biol* 4(222):222.
12.   Patricelli MP, et al. (2011) In situ kinase profiling reveals functionally relevant properties of native kinases. *Chem Biol* 18(6):699–710.
13.   Worboys JD, Sinclair J, Yuan Y, Jørgensen C (2014) Systematic evaluation of quantotypic peptides for targeted analysis of the human kinome. *Nat Methods* 11(10):1041–4.
14.   Peterson a. C, Russell JD, Bailey DJ, Westphall MS, Coon JJ (2012) Parallel reaction monitoring for high resolution and high mass accuracy quantitative, targeted proteomics. *Mol Cell Proteomics*:1475–1488.
15.   Gallien S, et al. (2012) Targeted Proteomic Quantification on Quadrupole-Orbitrap Mass Spectrometer. *Mol Cell Proteomics*:1709–1723.
16.   Gallien S, Kim SY, Domon B, Domon B (2015) Large-Scale Targeted Proteomics Using Internal Standard Triggered-Parallel Reaction Monitoring. *Mol Cell Proteomics*:1–37.
17.   Miyamoto K, et al. (2008) High-efficiency liquid chromatographic separation utilizing long monolithic silica capillary columns. *Anal Chem* 80(22):8741–8750.
18.   Yamana R, et al. (2013) Rapid and deep profiling of human induced pluripotent stem cell proteome by one-shot NanoLC-MS/MS analysis with meter-scale monolithic silica columns. *J Proteome Res* 12(1):214–221.
19.   Horie K, et al. (2012) Estimation and optimization of the peak capacity of one-dimensional gradient high performance liquid chromatography using a long monolithic silica capillary column. *J Chromatogr A* 1228:283–291.
20.   Lwasaki M, et al. (2010) One-dimensional capillary liquid chromatographic separation coupled with tandem mass spectrometry unveils the escherichia coli proteome on a microarray scale. *Anal Chem* 82(7):2616–2620.
21.   Wolcott RG, et al. (2000) Control of column temperature in reversed-phase liquid chromatography. *Journal of Chromatography A*, pp 211–230.
22.   Hancock WS, Chloupek RC, Kirkland JJ, Snyder LR (1994) Temperature as a variable in reversed-phase high-performance liquid chromatographic separations of peptide and protein samples. I. Optimizing the separation of a growth hormone tryptic digest. *J Chromatogr A* 686(1):31–43.
23.   Ashburner M, et al. (2000) Gene Ontology: tool for the unification of biology. *Nat Genet* 25(1):25–29.

24. MacLean B, et al. (2010) Skyline: An open source document editor for creating and analyzing targeted proteomics experiments. *Bioinformatics* 26(7):966–968.
25. Stergachis AB, MacLean B, Lee K, Stamatoyannopoulos J a, MacCoss MJ (2011) Rapid empirical discovery of optimal peptides for targeted proteomics. *Nat Methods* 8(12):1041–1043.
26. Boutros T, Chevet E, Metrakos P (2008) Mitogen-activated protein (MAP) kinase/MAP kinase phosphatase regulation: roles in cell growth, death, and cancer. *Pharmacol Rev* 60(3):261–310.
27. Dhillon AS, Hagan S, Rath O, Kolch W (2007) MAP kinase signalling pathways in cancer. *Oncogene* 26(22):3279–90.
28. Schubbert S, Shannon K, Bollag G (2007) Hyperactive Ras in developmental disorders and cancer. *Nat Rev Cancer* 7(4):295–308.
29. Downward J (2003) Targeting RAS signalling pathways in cancer therapy. *Nat Rev Cancer* 3(1):11–22.
30. Roberts PJ, Der CJ (2007) Targeting the Raf-MEK-ERK mitogen-activated protein kinase cascade for the treatment of cancer. *Oncogene* 26(22):3291–3310.
31. Hatzivassiliou G, et al. (2013) Mechanism of MEK inhibition determines efficacy in mutant KRAS- versus BRAF-driven cancers. *Nature* 501(7466):232–6.
32. Morris EJ, et al. (2013) Discovery of a novel ERK inhibitor with activity in models of acquired resistance to BRAF and MEK inhibitors. *Cancer Discov* 3(July):742–750.
33. Carlino MS, et al. (2014) Differential activity of MEK and ERK inhibitors in BRAF inhibitor resistant melanoma. *Mol Oncol* 8(3):544–554.
34. Choi M, et al. (2014) MSstats: an R package for statistical analysis of quantitative mass spectrometry-based proteomic experiments. *Bioinformatics* 30(17):1–2.
35. Heldin CH, Landstrom M, Moustakas A (2009) Mechanism of TGF-beta signaling to growth arrest, apoptosis, and epithelial-mesenchymal transition. *Curr Opin Cell Biol* 21(2):166–176.
36. Goumans MJ, et al. (2002) Balancing the activation state of the endothelium via two distinct TGF-β type I receptors. *EMBO J* 21(7):1743–1753.
37. James D, Levine AJ, Besser D, Hemmati-Brivanlou A (2005) TGFbeta/activin/nodal signaling is necessary for the maintenance of pluripotency in human embryonic stem cells. *Development* 132(6):1273–1282.
38. Calon A, et al. (2012) Dependency of Colorectal Cancer on a TGF- b -Driven Program in Stromal Cells for Metastasis Initiation. *Cancer Cell*:571–584.
39. Derynck R, Zhang YE (2003) Smad-dependent and Smad-independent pathways in TGF- . 4.
40. Javelaud D, Mauviel A (2005) Crosstalk mechanisms between the mitogen-activated protein kinase pathways and Smad signaling downstream of TGF-beta: implications for carcinogenesis. *Oncogene* 24(37):5742–5750.
41. Médard G, et al. (2015) Optimized chemical proteomics assay for kinase inhibitor profiling. *J Proteome Res*:150208132244001.
42. Ruprecht B, et al. (2015) Evaluation of Kinase Activity Profiling Using Chemical Proteomics. *ACS Chem Biol* 10(12):2743–2752.
43. Ong S-E (2002) Stable Isotope Labeling by Amino Acids in Cell Culture, SILAC, as a Simple and Accurate Approach to Expression Proteomics. *Mol Cell Proteomics* 1(5):376–386.
44. Miyata N, et al. (2012) Transforming growth factor β and Ras/MEK/ERK signaling regulate the expression level of a novel tumor suppressor Lefty. *Pancreas* 41(5):745–52.
45. Nagaraj NS, Datta PK (2010) Targeting the transforming growth factor-beta signaling pathway in human cancer. *Expert Opin Investig Drugs* 19(1):77–91.
46. Burgess MW, Keshishian H, Mani DR, Gillette M a, Carr S a (2014) Simplified and

Efficient Quantification of Low-abundance Proteins at Very High Multiplex via Targeted Mass Spectrometry. *Mol Cell Proteomics* 13(4):1137–49.

47.   Gallien S, Kim SY, Domon B (2015) Large-Scale Targeted Proteomics Using Internal Standard Triggered-Parallel Reaction Monitoring (IS-PRM). *Mol Cell Proteomics* 14(6):1630–1644.

48.   Baker PR, Chalkley RJ (2014) MS-viewer: a web-based spectral viewer for proteomics results. *Mol Cell Proteomics* 13(5):1392–6.

49.   Chalkley RJ, et al. (2005) Comprehensive Analysis of a Multidimensional Liquid Chromatography Mass Spectrometry Dataset Acquired on a Quadrupole Selecting, Quadrupole Collision Cell, Time-of-flight Mass Spectrometer. *Mol Cell Proteomics* 4:1194–1204.

50.   The UniProt Consortium (2014) UniProt: a hub for protein information. *Nucleic Acids Res* 43(Database issue):D204–12.

51.   Bairoch A, Apweiler R (2000) The SWISS-PROT protein sequence database and its supplement TrEMBL in 2000. *Nucleic Acids Res* 28(1):45–48.

52.   Sharma V, et al. (2014) Panorama: A targeted proteomics knowledge base. *J Proteome Res* 13(9):4205–4210.

53.   Guan S, Price JC, Prusiner SB, Ghaemmaghami S, Burlingame a. L (2011) A Data Processing Pipeline for Mammalian Proteome Dynamics Studies Using Stable Isotope Metabolic Labeling. *Mol Cell Proteomics* 10(12):M111.010728–M111.010728.

Appendix 1

Substrates of TAK1 identified by covalent capture

Accession	Gene	Peptide	Protein.Mods
Q86UQ4	ABCA13	MVICLTLEALWKNLKK	Phospho@2742
O95342	ABCB11	FTDYELKAYAKAGVVADEVISSMR	Phospho@286|287
Q9NYB9	ABI2	HSPYRTLEPVRPPVVPNDYVPSPTR	Phospho@200=17
Q9P2A4	ABI3	VVTLYPYTSQK	Phospho@315;Phospho@320;Phospho@321
P60709	ACTB	VAPEEHPVLLTEAPLNPK	Phospho@106
P60709	ACTB	SYELPDGQVITIGNER	Phospho@249=46
P60709	ACTB	IWHHTFYNELR	Phospho@89
P60709	ACTB	AVFPSIVGRPR	Phospho@33
P60709	ACTB	EITALAPSTMK	Phospho@318=78;Oxidation@325
P60709	ACTB	EITALAPSTMK	Oxidation@325;Phospho@323|324
P60709	ACTB	RGILTLK	Phospho@66
P63261	ACTG1	EITALAPSTMK	Phospho@318=65;Oxidation@325
P63261	ACTG1	SYELPDGQVITIGNER	Phospho@249=57
P63261	ACTG1	EITALAPSTMK	Phospho@324=6;Oxidation@325
P63261	ACTG1	GYSFTTTAER	Phospho@201|202
P63261	ACTG1	IWHHTFYNELR	Phospho@89
P63261	ACTG1	RGILTLK	Phospho@66
P63261	ACTG1	VAPEEHPVLLTEAPLNPK	Phospho@106
P63261	ACTG1	EITALAPSTMK	Oxidation@325;Phospho@323|324
P58397	ADAMTS12	LSASFCQTLKAMKK	Phospho@1545|1547
P35611	ADD1	EYQPHVIVSTTGPNPFTTLTDRELEEYRR	Phospho@565|566|568
Q8WYP5	AHCTF1	EISEASENIYSDVR	Phospho@1791=63
Q9P2R3	ANKFY1	IKVGDRHISAHK	Phospho@80
Q9BXS5	AP1M1	ILQEYITQEGHK	Phospho@136
P63010	AP2B1	YFTTNKKGEIFELK	Phospho@8|9
P63010	AP2B1	YFTTNKK	Phospho@8=8
O00203	AP3B1	MHVFNPIDSLEPEGSITVSMGIDFCDSTQTASFQLCTK	Oxidation@949=19;Phospho@938&944&956|
O14497	ARID1A	QSTGSAPQGPAYHGVNRTDEMLHTDQR	Oxidation@1532;Phospho@1529|1535
Q5H9R4	ARMCX4	AETHILAEKETEINRVMVTQSETLAVPR	Phospho@296=14;Oxidation@310;Phospho@312&314|312&316|314&316
O75129	ASTN2	AAAEATQETVESLMQKFKESFR	Oxidation@352;Phospho@358=43
P15336	ATF2	NDSVIVADQTPTPTR	Phospho@69=11
Q8WXX7	AUTS2	ALSLASSSGSDK	Phospho@50|51|52|54
P46379	BAG6	LINLVGESLR	Phospho@329
Q9NYF8	BCLAF1	NSERITVK	Phospho@489=61
O14503	BHLHE40	VVSELLQGGTSR	Phospho@180=60;Phospho@187|188
Q14137	BOP1	MAGSRGAGRTAAPSVRPEK	Phospho@4=7
Q8TDL5	BPIFB1	ALGFEAAESSLTK	Phospho@461|462|464
O95696	BRD1	ELTGGGTTFSVR	Phospho@375=17;Phospho@376=19;Phospho@378=19
Q9HCM1	C12orf35	ATAALKVDVSGPVASTATSTK	Phospho@811=70;Phospho@819=70;Phospho@824=20;Phospho@825|827|828|829
Q96C57	C12orf43	VASVDSAVAATTPTSMATVQK	Phospho@210=6;Oxidation@215;Phospho@211&213|211&214|211&217|213&214|213&217
Q96GQ5	C16orf58	MADDAGLETPLCSEQFGSGEAR	Met-loss@1;Phospho@13|18
Q5T0J7	C1orf49	AVKQEGRFTK	Phospho@44
Q6P1W5	C1orf94	QKVAMPVISSR	Gln->pyro-Glu@187;Oxidation@191;Phospho@195=10

P01024	C3	FVTVQATFGTQVVEK	Phospho@111=18;Phospho@114=37
Q6ZUJ4	C3orf62	TWSLLGEMSEKLR	Oxidation@13;Phospho@6|8
Q5TF21	C6orf174	QTIAATRSPVGAGTKLNSVR	Gln->pyro-Glu@52;Phospho@65=14
Q9HB71	CACYBP	EKPSYDTETDPSEGLMNVLKK	Oxidation@192;Phospho@180|183|185
Q01518	CAP1	HVSDDMKTHKNPALK	Oxidation@278;Phospho@280=24
P78371	CCT2	DASLMVTNDGATILK	Oxidation@62;Phospho@64=16
P49368	CCT3	KGESQTDIEITREEDFTR	Phospho@259=26
P49368	CCT3	KGESQTDIEITR	Phospho@254=11
P50991	CCT4	DKPAQIRFSNISAAK	Phospho@36=10
P50991	CCT4	MIQDGKGDVTITNDGATILK	Oxidation@60;Phospho@71=10
P50991	CCT4	AVADAIRTSLGPK	Phospho@50=12
P50991	CCT4	AVADAIRTSLGPK	Phospho@50|51
P50991	CCT4	HAQGEKTAGINVR	Phospho@490
P50991	CCT4	MIQDGKGDVTITNDGATILK	Oxidation@60;Phospho@69|71
P40227	CCT6A	GLQDVLRTNLGPK	Phospho@36
P40227	CCT6A	MAAVKTLNPK	Met-loss+Acetyl@1;Phospho@6
Q96FF9	CDCA5	LETLGSASTSTPGRR	Phospho@151=33
Q00534	CDK6	SAQPIEKFVTDIDELGK	Phospho@267=17
Q5SW79	CEP170	SGDPRPQAAEPPDHLTITR	Phospho@1399=9
Q5SW79	CEP170	SGDPRPQAAEPPDHLTITR	Phospho@1399|1401
Q6P2H3	CEP85	SHVTIPTAHVMPSTLGTSPAKPNSTPVGPSSSK	Phospho@102&114&115|102&114&116|102&115&116|114&115&116
P23528	CFL1	EILVGDVGQTVDDPYATFVK	Phospho@70=72
P23528	CFL1	YALYDATYETKESK	Phospho@91=12
P23528	CFL1	NIILEEGKEILVGDVGQTVDDPYATFVK	Phospho@63=21
Q8WUX9	CHMP7	HFTNSVPNPR	Phospho@408=27
Q9Y3Y2	CHTOP	ATRTLLRGGMSLR	Phospho@132=30
Q14011	CIRBP	DSYDSYATHNE	Phospho@169=36
P51800	CLCNKA	NFGAKVVGLSCTLATGSTLFLGK	Phospho@152|154
P53618	COPB1	LVTEMGTYATQSALSSSRPTK	Oxidation@518;Phospho@523=17
P53618	COPB1	LVTEMGTYATQSALSSSRPTK	Oxidation@518;Phospho@523|525|528|529
P67870	CSNK2B	SPVKTIR	Phospho@209|213
P67870	CSNK2B	SPVKTIR	Phospho@213=18
P35221	CTNNA1	SRTSVQTEDDQLIAGQSAR	Phospho@654|655
P35221	CTNNA1	SRTSVQTEDDQLIAGQSAR	Phospho@652|654|655
P26232	CTNNA2	SRTSVQTEDDQLIAGQSAR	Phospho@651|653
P26232	CTNNA2	SRTSVQTEDDQLIAGQSAR	Phospho@651|653|654
P26232	CTNNA2	QVRVLTEAVDDITSVDDFLSVSENHILEDVNK	Gln->pyro-Glu@492;Phospho@505=12;Phospho@497&511|497&513|504&511|504&513
Q14247	CTTN	ENVFQEHQTLKEK	Phospho@68
Q5QP82	DCAF10	LNTKVCTLHGHTSWVK	Phospho@244|248
Q92841	DDX17	ESAAPAAAPTAEAPPPSVVTRPEPQALPSPAIR	Phospho@52|55
Q92841	DDX17	ESAAPAAAPTAEAPPPSVVTRPEPQALPSPAIR	Phospho@52=8
P17844	DDX5	TQNGVYSAANYTNGSFGSNFVSAGIQTSFR	Phospho@536|541|544|547
P17844	DDX5	TQNGVYSAANYTNGSFGSNFVSAGIQTSFR	Phospho@536|541|544
P80370	DLK1	ILKVSMKELNK	Phospho@288
Q6XZF7	DNMBP	HLTGFAPQIKDEVFEETEK	Phospho@1012=85
Q14185	DOCK1	MKTTSPPGDDIK	Phospho@1386=16;Phospho@1388=23
P15924	DSP	YEVTSGGGGTSR	Phospho@31=7
Q14204	DYNC1H1	MQMLEDEDDLAYAETEKK	Phospho@4360;Oxidation@4346|4348

P68104	EEF1A1	IGGIGTVPVGR	Phospho@261
P68104	EEF1A1	VETGVLKPGMVVTFAPVNVTTEVK	Oxidation@276;Phospho@286|287
P68104	EEF1A1	TIEKFEK	Phospho@38
P68104	EEF1A1	VETGVLKPGMVVTFAPVNVTTEVK	Phospho@269=64;Oxidation@276
P68104	EEF1A1	VETGVLKPGMVVTFAPVNVTTEVK	Oxidation@276;Phospho@279|286
P68104	EEF1A1	VETGVLKPGMVVTFAPVNVTTEVK	Oxidation@276;Phospho@286=10
P68104	EEF1A1	VETGVLKPGMVVTFAPVNVTTEVK	Oxidation@276;Phospho@279=8
P29692	EEF1D	QVEPPAKKPATPAEDDEDDDIDLFGSDNEEEDKEAAQLR	Phospho@162=54
P13639	EEF2	STLTDSLVCK	Phospho@36=10
P13639	EEF2	FTDTRKDEQER	Phospho@57|59
P13639	EEF2	FTDTRKDEQER	Phospho@59=25
P13639	EEF2	TGTITTFEHAHNMR	Oxidation@494;Phospho@484|486|487
P13639	EEF2	TGTITTFEHAHNMR	Oxidation@494;Phospho@482|484
P13639	EEF2	TGTITTFEHAHNMR	Phospho@484=18;Oxidation@494
P13639	EEF2	TGTITTFEHAHNMR	Oxidation@494;Phospho@482|484|486|487
Q9H223	EHD4	AGGADAVQTVTGGLR	Phospho@23|25
Q14152	EIF3A	TKNETDEDGWTTVRR	Phospho@1378|1379
Q14152	EIF3A	TKNETDEDGWTTVRR	Phospho@1379=6
Q13347	EIF3I	TERPVNSAALSPNYDHVVLGGGQEAMDVTTTSTR	Oxidation@253;Phospho@256|257|258
Q13347	EIF3I	TERPVNSAALSPNYDHVVLGGGQEAMDVTTTSTR	Oxidation@253;Phospho@257|258
Q9Y262	EIF3L	FEELNRTLKK	Phospho@556
P23588	EIF4B	DRYDSDRYR	Phospho@230
Q04637	EIF4G1	GSRPIDTSRLTK	Phospho@1070=9
P29317	EPHA2	VLEDDPEATYTTSGGKIPIR	Phospho@773|774
P29317	EPHA2	VLEDDPEATYTTSGGKIPIR	Phospho@771|773|774
O43414	ERI3	SIFVTCGDWDLKVMLPGQCQYLGLPVADYFK	Phospho@240|244
Q9BSJ8	ESYT1	HLSPYATLTVGDSSHK	Phospho@824=22
Q9BSJ8	ESYT1	QRLTHVDSPLEAPAGPLGQVK	Phospho@959=11
Q9BSJ8	ESYT1	QRLTHVDSPLEAPAGPLGQVK	Phospho@959|963
Q9UNN5	FAF1	SSPAQTREQSEEQITDVHMVSDSDGDDFEDATEFGVDDGEVFGMASSALR	Phospho@300&314|300&315|314&315
Q96E09	FAM122A	MHSSRLHQIKQEEGMDLINR	Oxidation@80=34;Phospho@82|83
Q7Z309	FAM122B	RIDFTPVSPAPSPTR	Phospho@112&119|112&121|115&119|115&121
P78312	FAM193A	RFIEEQLTNK	Phospho@174
A6NMK8	FAM196B	VPKVQSNGPVSICLEAGTWR	Phospho@179;Phospho@184;Phospho@191
Q9H019	FAM54B	NASVPNLR	Phospho@103
P35556	FBN2	LSSTGLICIDSLK	Phospho@884|885|886
P02679	FGG	YEASILTHDSSIR	Phospho@125|128
P02679	FGG	YEASILTHDSSIR	Phospho@128=23
P07954	FH	THTQDAVPLTLGQEFSGYVQQVK	Phospho@234|236
P07954	FH	THTQDAVPLTLGQEFSGYVQQVK	Phospho@236=7
Q9C0D6	FHDC1	QKPEENKTCR	Phospho@1002
P21333	FLNA	ALTQTGGPHVK	Phospho@1286=23
P21333	FLNA	ALTQTGGPHVK	Phospho@1286|1288
Q14315	FLNC	VEESTQVGGDPFPAVFGDFLGR	Phospho@2210|2211
Q5CZC0	FSIP2	ISATETILSQELTDFTFVGR	Phospho@2329=17;Phospho@2315&2317|2315&2319|
Q8IY81	FTSJ3	KKAEAVVNTVDISER	Phospho@770=25
Q14C86	GAPVD1	DKDDLGPDRFSTLTDDPSPR	Phospho@1012|1013
Q14C86	GAPVD1	DKDDLGPDRFSTLTDDPSPR	Phospho@1012=6
P48060	GLIPR1	GATCSACPNNDK	Phospho@191=13

Q13439	GOLGA4	NVYATTVGTPYK	Phospho@2150|2151
Q13439	GOLGA4	NVYATTVGTPYK	Phospho@2150=9
P51654	GPC3	VAHVEHEETLSSR	Phospho@383|385|386
Q9NQX3	GPHN	MATEGMILTNHDHQIR	Met-loss+Acetyl@1;Oxidation@6;Phospho@9=32
Q8IZF6	GPR112	VTASVTVSSFPDIEKLSTPLDNKTATTEVR	Phospho@894=12;Phospho@895=10;Phospho@901|903|904
P78347	GTF2I	TPTQTNGSNVPFKPR	Phospho@703|705|707
Q7Z4H3	HDDC2	MASVSSATFSGHGAR	Met-loss+Acetyl@1;Phospho@8=6
Q7Z4H3	HDDC2	MASVSSATFSGHGAR	Met-loss+Acetyl@1;Phospho@6|8
P51858	HDGF	GNAEGSSDEEGKLVIDEPAKEK	Phospho@132;Phospho@133
P41235	HNF4A	LLPGAVATIVKPLSAIPQPTITK	Phospho@455=30
P09651	HNRNPA1	EDSQRPGAHLTVK	Phospho@95=57
P22626	HNRNPA2B1	YHTINGHNAEVR	Phospho@176
P07910	HNRNPC	MASNVTNKTDPR	Met-loss+Acetyl@1;Phospho@6=15
P52597	HNRNPF	MRPGAYSTGYGGYEEYSGLSDGYGFTTDLFGR	Oxidation@231;Phospho@256|257
P52597	HNRNPF	FMSVQRPGPYDRPGTAR	Oxidation@202;Phospho@203=48
P07900	HSP90AA1	AQALRDNSTMGYMAAK	Phospho@623=19;Oxidation@625;Oxidation@628
P08238	HSP90AB1	TLTLVDTGIGMTK	Phospho@85=19;Oxidation@93
P08238	HSP90AB1	TLTLVDTGIGMTK	Oxidation@93;Phospho@83|85
P08238	HSP90AB1	EKEISDDEAEEEKGEK	Phospho@226
P14625	HSP90B1	DISTNYYASQKK	Phospho@674|675
P14625	HSP90B1	AQAYQTGKDISTNYYASQK	Phospho@669=42
P14625	HSP90B1	DISTNYYASQKK	Phospho@675=8
P38646	HSPA9	KDSETGENIRQAASSLQQASLK	Phospho@638|639
P04792	HSPB1	QLSSGVSEIR	Phospho@82|83
P04792	HSPB1	QLSSGVSEIR	Phospho@82=12
P10809	HSPD1	DRVTDALNATR	Phospho@422=67
P10809	HSPD1	LVQDVANNTNEEAGDGTTTATVLAR	Phospho@105|113|114|115
P10809	HSPD1	LVQDVANNTNEEAGDGTTTATVLAR	Phospho@105=42
P10809	HSPD1	TVIIEQSWGSPKVTKDGVTVAK	Phospho@74=10
Q7Z6Z7	HUWE1	SDDELLDDFFHDQSTATSQAGTLSSIPTALTR	Phospho@2632|2633|2635|2636
Q7Z6Z7	HUWE1	GLLPLVTILGLPNLPIDFPTSAACQAVAGVCKSILTLSHEPK	Phospho@804=28;Phospho@817=28;Phospho@818=28
Q7Z6Z7	HUWE1	HADHSSLTLGSGSSTTR	Phospho@2529=6
Q9Y4L1	HYOU1	FPEHELTFDPQR	Phospho@126
Q12906	ILF3	KQPHGGQQKPSYGSGYQSHQGQQQSYNQSPYSNYGPPQGK	Phospho@744|747|751|758
Q8NFU5	IPMK	LNDRTLAEKFLSK	Phospho@279=30
P05556	ITGB1	SAVTTVVNPK	Phospho@788|789
P05556	ITGB1	NVLSLTNKGEVFNELVGK	Phospho@224|226
Q14571	ITPR2	LTVEKSELWVEK	Phospho@1122|1126
Q92831	KAT2B	LRSPNDDISGYKENYTR	Phospho@270=10
O75449	KATNA1	MSLLMISENVK	Oxidation@1;Oxidation@5;Phospho@7=74
Q2KHM9	KIAA0753	DATKEPLQQEDPQEESHLTGAVEHEAAR	Phospho@601=11
Q0VF49	KIAA2012	YDAQESQVSLDGR	Phospho@312;Phospho@315
P33176	KIF5B	ANLEAFTVDKDITLTNDKPATAIGVIGNFTDAER	Phospho@397|399|405
Q8IXQ5	KLHL7	MVISGMRYHLLSPEDR	Oxidation@262=12;Phospho@273=33
P04264	KRT1	TTSSSTRRSGGGGGR	Phospho@31|32|33
P05783	KRT18	STFSTNYR	Phospho@11=7
P05783	KRT18	STFSTNYR	Phospho@10|11
P08727	KRT19	QSSATSSFGGLGGGSVR	Phospho@10|12|13
P08727	KRT19	QSSATSSFGGLGGGSVR	Phospho@12|13

P08727	KRT19	FVSSSSSGAYGGGYGGVLTASDGLLAGNEK	Phospho@70|72
P08727	KRT19	QSSATSSFGGLGGGSVR	Phospho@9|10|12|13
P08727	KRT19	QSSATSSFGGLGGGSVR	Phospho@13|14
P08727	KRT19	QSSATSSFGGLGGGSVR	Phospho@12=8
P08727	KRT19	QSSATSSFGGLGGGSVR	Phospho@14=8
P13647	KRT5	SFSTASAITPSVSRTSFTSVSRSGGGGGGGGGFGR	Phospho@36|38
P13647	KRT5	ISISTSGGSFRNR	Phospho@75=15;Phospho@78|79|82
P08729	KRT7	VRQEESEQIKTLNNK	Phospho@97=47
P08729	KRT7	EVTINQSLLAPLRLDADPSLQR	Phospho@67=60
P08729	KRT7	MSIHFSSPVFTSR	Met-loss+Acetyl@1;Phospho@11=9
P08729	KRT7	MSIHFSSPVFTSR	Met-loss+Acetyl@1;Phospho@11|12
P05787	KRT8	TTSGYAGGLSSAYGGLTSPGLSYSLGSSFGSGAGSSSFSR	Phospho@415|416|417|431|432
P05787	KRT8	ISSSSFSR	Phospho@34|35|36
P05787	KRT8	TTSGYAGGLSSAYGGLTSPGLSYSLGSSFGSGAGSSSFSR	Phospho@415|416|417|424|425
P05787	KRT8	GGLGGGYGGASGMGGITAVTVNQSLLSPLVLEVDPNIQAVRTQEK	Oxidation@60;Phospho@89=55
P05787	KRT8	TQEKEQIKTLNNK	Phospho@97=22
P05787	KRT8	ISSSSFSR	Phospho@35|36|37
P05787	KRT8	TTSGYAGGLSSAYGGLTSPGLSYSLGSSFGSGAGSSSFSR	Phospho@431|432|436
P05787	KRT8	TTSGYAGGLSSAYGGLTSPGLSYSLGSSFGSGAGSSSFSR	Phospho@415|416|417
P05787	KRT8	ISSSSFSR	Phospho@34|35
P05787	KRT8	MSIRVTQK	Met-loss+Acetyl@1;Phospho@6=15
P05787	KRT8	ISSSSFSR	Phospho@35|36|37|39
Q6JVE6	LCN10	QNVSSFQSLKEFMDACDILGLSK	Gln->pyro-Glu@148;Phospho@152=6
P00338	LDHA	MATLKDQLIYNLLK	Met-loss+Acetyl@1;Phospho@3
Q2VYF4	LETM2	GPITSSEEPTLQAKSQMTAQNSKASSK	Oxidation@479;Phospho@468|472|477|480|484|487|488
Q12907	LMAN2	GRLTVMTDLEDKNEWK	Phospho@225=11;Oxidation@227
P02545	LMNA	SGAQASSTPLSPTRITR	Phospho@24|27
P02545	LMNA	SGAQASSTPLSPTRITR	Phospho@27=20
Q9Y2L9	LRCH1	DSDSGVGSDNGDKR	Phospho@321;Phospho@323;Phospho@327
P46821	MAP1B	ITSFPESEGYSYETSTKTTR	Phospho@2031=7
P46821	MAP1B	ITSFPESEGYSYETSTKTTR	Phospho@2028|2029|2031
P46821	MAP1B	ITSFPESEGYSYETSTKTTR	Phospho@2031|2032
O43318	MAP3K7	CWSKDPSQRPSMEEIVK	Phospho@268=45;Oxidation@277
Q15691	MAPRE1	KPLTSSSAAPQRPISTQR	Phospho@155|156|157|165|166
Q15691	MAPRE1	KPLTSSSAAPQRPISTQR	Phospho@154|155|156|157|165|166
Q15691	MAPRE1	KPLTSSSAAPQRPISTQR	Phospho@165|166
P29966	MARCKS	LSGFSFKK	Phospho@170=15
O15021	MAST4	SFSCLNRSLSSGESLPGSPTHSLSPR	Phospho@1309=11;Phospho@1286|1288|1293|1295|1296
P43243	MATR3	SATREPPYRVPR	Phospho@164|166
Q9P267	MBD5	QSRGFGELLSTAKQDLVLEEQSPSSSNSLENSLVK	Phospho@1318&1320|1318&1321|1318&1322|1318&1324|
Q00987	MDM2	RAISETEENSDELSGERQR	Phospho@166=27;Phospho@168=18;Phospho@172=10
Q03164	MLL	KGLVFEISSDDGFQICAESIEDAWKSLTDK	Phospho@3674&3692|3674&3694|3675&3692|
Q99547	MPHOSPH6	RYETLVGTIGKK	Phospho@120=47
Q9NRX2	MRPL17	RDSHLTLLNQLLQGLR	Phospho@140=11
O94776	MTA2	GHLSRPEAQSLSPYTTSANR	Phospho@439|440
O94776	MTA2	GHLSRPEAQSLSPYTTSANR	Phospho@439=7
O94776	MTA2	GHLSRPEAQSLSPYTTSANR	Phospho@438|439

P11586	MTHFD1	KITIGQAPTEK	Phospho@545=76
Q9BQG0	MYBBP1A	DPAQPMSPGEATQSGARPADR	Oxidation@10;Phospho@16|18
P35749	MYH11	LQDFASTVEALEEGK	Phospho@1385|1386
Q9NPC6	MYOZ2	VSIPRDIMLEELSHLSNRGAR	Phospho@51=14
Q8IVL1	NAV2	LREPSKTALGSSLPGLVNQTDK	Phospho@1257|1259|1263|1264
Q15021	NCAPD2	ESTGNMVTGQTVCK	Oxidation@589;Phospho@591=25;Phospho@594=25
Q9Y618	NCOR2	EGSITQGTPLKYDTGASTTGSK	Phospho@1469=21
Q9Y618	NCOR2	DLTEAYKTQALGPLK	Phospho@1407=43
Q92597	NDRG1	SHTSEGAHLDITPNSGAAGNSAGPK	Phospho@366|367
Q92597	NDRG1	SRTASGSSVTSLDGTR	Phospho@326|328|330|332
Q92597	NDRG1	SHTSEGAHLDITPNSGAAGNSAGPK	Phospho@364|366
Q96PY6	NEK1	NSLLIGLSTGLFDANNPK	Phospho@1036|1037
Q96PY6	NEK1	EVGVDSSLTDTR	Phospho@690|692
Q9H841	NIPAL2	AVSGMITFSVMDK	Phospho@236=25
P15559	NQO1	MVGRRALIVLAHSER	Met-loss@1;Phospho@13
O14786	NRP1	IESPGYLTSPGYPHSYHPSEK	Phospho@40|41
O14786	NRP1	IESPGYLTSPGYPHSYHPSEK	Phospho@40=13
Q8N1F7	NUP93	TLTRTSQETADVK	Phospho@49|51|52
Q9ULJ1	ODF2L	ELERVCDSLTAAER	Phospho@471|473
Q9UKZ4	ODZ1	ILENGVNVTVSQMTSVLNGRTRR	Phospho@2610=7;Phospho@2609|2616
Q01804	OTUD4	RPEPSTLENITDDKYATVSSPSK	Phospho@542|544
Q01804	OTUD4	RPEPSTLENITDDKYATVSSPSK	Phospho@542|544|545
P13674	P4HA1	GEGIKMTPR	Oxidation@300;Phospho@301
Q8N7H5	PAF1	EDGHRPNSHRTLPER	Phospho@22=26
Q15365	PCBP1	LEEDINSSMTNSTAASRPPVTLR	Oxidation@87;Phospho@86|88
Q15365	PCBP1	LEEDINSSMTNSTAASRPPVTLR	Oxidation@87;Phospho@88=9
Q15366	PCBP2	LHQLAMQQSHFPMTHGNTGFSGIESSSPEVK	Oxidation@251;Oxidation@258;Phospho@254|259|263
Q15366	PCBP2	LEEDISSSMTNSTAASRPPVTLR	Oxidation@87;Phospho@86|88
Q15366	PCBP2	LHQLAMQQSHFPMTHGNTGFSGIESSSPEVK	Oxidation@251;Oxidation@258;Phospho@259|263|266|270
Q15366	PCBP2	AFAMIIDKLEEDISSSMTNSTAASRPPVTLR	Oxidation@74;Oxidation@87;Phospho@88=9
Q15366	PCBP2	LEEDISSSMTNSTAASRPPVTLR	Oxidation@87;Phospho@85|86|88|90|91
Q15366	PCBP2	LEEDISSSMTNSTAASRPPVTLR	Oxidation@87;Phospho@85|86|88
O76083	PDE9A	DKVTKATAQIGFIK	Phospho@508;Phospho@511
P08559	PDHA1	VLSGASQKPASR	Phospho@13=63;Phospho@16|21
Q9NTI5	PDS5B	TRTNDGKITYPPGVK	Phospho@6|8
Q9BUL5	PHF23	VASPLSPTSLTHTSRPPAALTPVPLSQGDLSHPPR	Phospho@150|152|153|155
Q86UU1	PHLDB1	SALLTQNGTGSLPR	Phospho@1011=13
Q86UU1	PHLDB1	MREKQFSQARPLTR	Phospho@1217|1223
Q86UU1	PHLDB1	SALLTQNGTGSLPR	Phospho@1007|1011
P14618	PKM2	LNFSHGTHEYHAETIKNVR	Phospho@87=23
Q6IQ23	PLEKHA7	YQTLPGR	Phospho@1013
P49005	POLD2	VPVATYTNSSQPFR	Phospho@31|33
P49005	POLD2	VPVATYTNSSQPFR	Phospho@31=9
P49005	POLD2	VPVATYTNSSQPFR	Phospho@33=9
Q9NP87	POLM	ARVGSPSGDAASSTPPSTRFPGVAIYLVEPR	Phospho@19=9;Phospho@20=9;Phospho@21=9;Phospho@24|25
P05423	POLR3D	DLTLGGVK	Phospho@49
O00411	POLRMT	QIGGGIQSITYTHNGDISR	Phospho@1097|1099|1101
O00411	POLRMT	QIGGGIQSITYTHNGDISR	Phospho@1101=12
Q9H237	PORCN	GAQMIVAMKAVSLGFDLDR	Oxidation@128;Oxidation@132;Phospho@136

O14974	PPP1R12A	ETLIIEPEKNASR	Phospho@332=61
P62714	PPP2CB	RGEPHVTRR	Phospho@301
Q16537	PPP2R5E	VLIPLHTVR	Phospho@273
P14314	PRKCSH	SLKDMEESIR	Phospho@383;Oxidation@387;Phospho@390
P78527	PRKDC	ATQQHDFTLTQTADGR	Phospho@2647=11
P78527	PRKDC	ATQQHDFTLTQTADGR	Phospho@2645|2647
Q9P1D8	PRO2289	ITPNFPNTLDPAISRSSS	Phospho@48=31
P62191	PSMC1	IETLDPALIRPGR	Phospho@336
P62191	PSMC1	DDLSGADIKAICTEAGLMALR	Phospho@400=39
P43686	PSMC4	ADTLDPALLRPGR	Phospho@316
P06454	PTMA	MSDAAVDTSSEITTK	Met-loss+Acetyl@1;Phospho@13=11
P06454	PTMA	MSDAAVDTSSEITTK	Met-loss+Acetyl@1;Phospho@13|14
P06454	PTMA	MSDAAVDTSSEITTK	Met-loss+Acetyl@1;Phospho@10|13|14
P23470	PTPRG	NRNSSVVPSER	Phospho@1187=25
P06737	PYGL	HLHFTLVK	Phospho@39
P62820	RAB1A	FRTITSSYYR	Phospho@77=6
P62820	RAB1A	FRTITSSYYR	Phospho@75=28
P62820	RAB1A	FRTITSSYYR	Phospho@75|77|78|79
Q9H082	RAB33B	MAEEMESSLEASFSSSGAVSGASGFLPPARSRIFK	Met-loss+Acetyl@1;Phospho@12=7;Phospho@14|15|16|20
O95716	RAB3D	YRTITTAYYR	Phospho@86=21
Q96JH8	RADIL	MFYGTHFIMSPPTKSKLK	Met-loss+Acetyl@1;Phospho@10|13
Q9UKM9	RALY	LQASNVTNKNDPK	Phospho@8|11
Q9UKM9	RALY	LQASNVTNKNDPK	Phospho@11=7
P50749	RASSF2	MDYSHQTSLVPCGQDKYISKNELLLHLK	Oxidation@1;Phospho@19=13
P98175	RBM10	ENFKNSFQPISSLR	Phospho@672=25
Q96PK6	RBM14	AQPSASLGVGYRTQPMTAQAASYR	Phospho@263=12;Oxidation@266
P38159	RBMX	DSYSSSRSDLYSSGR	Phospho@328|329|330
P38159	RBMX	DYTYRDYGHSSSR	Phospho@242=95
P38159	RBMX	DSYSSSRSDLYSSGR	Phospho@326|328|329|330
P38159	RBMX	DDGYSTKDSYSSR	Phospho@215|216
P38159	RBMX	DYPSSRDTRDYAPPPR	Phospho@227|228|231
P38159	RBMX	DSYSSSRSDLYSSGR	Phospho@326|329|330
P38159	RBMX	DSYSSSRSDLYSSGR	Phospho@326|328|329|330|332
P38159	RBMX	DYPSSRDTRDYAPPPR	Phospho@227|228
P38159	RBMX	DSYSSSRSDLYSSGR	Phospho@332=12
P38159	RBMX	DYPSSRDTRDYAPPPR	Phospho@231=20
P38159	RBMX	DDGYSTKDSYSSR	Phospho@216=10
Q96NR8	RDH12	LWNVSCELLGIR	Phospho@307
Q5UIP0	RIF1	GQSPLAPLLETLEDPSASHGGQTDAYLTLTSR	Phospho@32=19
Q8NCN4	RNF169	GSVDQYLLRSSNMAGAK	Phospho@693=27;Oxidation@704
P78317	RNF4	DVYVTTHTPR	Phospho@109=14
P78317	RNF4	DRDVYVTTHTPR	Phospho@109|110
P27694	RPA1	AAGPSLSHTSGGTQSK	Phospho@176=12
P27694	RPA1	AAGPSLSHTSGGTQSK	Phospho@174|176
P62750	RPL23A	TSPTFR	Phospho@42|43|45
P62750	RPL23A	TSPTFR	Phospho@42|43
Q9NQG5	RPRD1B	TFQQIQEEEDDDYPGSYSPQDPSAGPLLTEELIK	Phospho@164|166
P46783	RPS10	GLEGERPARLTR	Phospho@118
P62847	RPS24	MNDTVTIRTRK	Met-loss@1;Phospho@6|9

P62081	RPS7	IVKPNGEKPDEFESGISQALLELEMNSDLK	Phospho@24=18;Phospho@34=35
Q99590	SCAF11	TKSKSSSFGR	Phospho@947|949|951|952
Q99590	SCAF11	SPKRDTTR	Phospho@872=11
Q99590	SCAF11	QTSGTSNTRGSR	Gln->pyro-Glu@300;Phospho@305|307
Q99590	SCAF11	QEEETSGQDSSLK	Phospho@1189=12;Phospho@1183&1184|1183&1188|1184&1188
O14828	SCAMP3	NYGSYSTQASAAAATAELLKK	Phospho@85|87|88
Q9Y6Y8	SEC23IP	VIVQFQPSSVPDEWGTTQDGQTRPR	Phospho@413|414
Q9P0U3	SENP1	RHVSTAEETVQEEER	Phospho@185=38
Q9P0U3	SENP1	HVSTAEETVQEEER	Phospho@180|181|185
P05155	SERPING1	TTFDPKKTR	Phospho@301;Phospho@302;Phospho@308
O95470	SGPL1	YGYAPKGSSLVLYSDK	Phospho@361|367
P34897	SHMT2	IMGLDLPDGGHLTHGYMSDVK	Oxidation@162;Phospho@173=30;Oxidation@177
Q00325	SLC25A3	IQTQPGYANTLR	Phospho@199=47
Q00325	SLC25A3	IQTQPGYANTLR	Phospho@192=70
Q14BN4	SLMAP	LIVEGHLTKAVEETK	Phospho@426=24
Q9NWH9	SLTM	MAAATGAVAASAASGQAEGKK	Met-loss@1;Phospho@11|14
Q9NY59	SMPD3	IGGEEGGRRPPEADDPVPGGQARNGAGGGPRGQTPNHNQQDGDSGSLGSPSASR	Phospho@279=13;Phospho@294=7;Phospho@289|291
O60504	SORBS3	DFVYPSSTRDPSASNGGGSPAR	Phospho@361|362|366
O60504	SORBS3	DFVYPSSTRDPSASNGGGSPAR	Phospho@360|361|362
O60504	SORBS3	DFVYPSSTRDPSASNGGGSPAR	Phospho@362|366
P48431	SOX2	MYNMMETELKPPGPQQTSGGGGGNSTAAAAGGNQKNSPDR	Oxidation@1&Phospho@7&17&18|Oxidation@1&Phospho@7&17&25|
O60271	SPAG9	ERPISLGIFPLPAGDGLLTPDAQK	Phospho@217=88
Q96T58	SPEN	QISEDSERTGGSPSVR	Gln->pyro-Glu@1250;Phospho@1255|1258|1261|1263
Q96T58	SPEN	WDSQMKQDAGR	Phospho@1342;Oxidation@1344
Q9NRC6	SPTBN5	DLEAFSPRIER	Phospho@3052
O15270	SPTLC2	SSAAAAAAAAAGQIHHVTQNGGLYK	Phospho@49=53
Q9UQ35	SRRM2	IPDHQRTSVPENHAQSR	Phospho@2170|2171
Q9UQ35	SRRM2	RSRSNSSPEMK	Oxidation@749;Phospho@741|743|745|746
Q9UQ35	SRRM2	IPDHQRTSVPENHAQSR	Phospho@2170=9
Q9UQ35	SRRM2	MTSERAPSPSSR	Oxidation@2419;Phospho@2426|2428
P61647	ST8SIA6	AKLASCCDAVQNFVVSQNNTPVGTNMSYEVESK	Phospho@131=18;Oxidation@152;Phospho@158=11;Phospho@142|146|150
P61956	SUMO2	EGVKTENNDHINLK	Phospho@12
O60343	TBC1D4	SLTSSLENIFSR	Phospho@568=7
Q8IYF1	TCEB3B	EGGQAGSGQR	Phospho@290
P17987	TCP1	DDKHGSYEDAVHSGALND	Phospho@551=21
P17987	TCP1	MLVDDIGDVTITNDGATILK	Oxidation@44;Phospho@55=11
P17987	TCP1	MLVDDIGDVTITNDGATILK	Oxidation@44;Phospho@53|55
O75443	TECTA	TFLSITVPRSMQNSTYGLCGRYNGNPDDDLEMPMGLLASSVNEFGQSWVK	Phospho@1223=9;Phospho@1226=9;Oxidation@1233&Phospho@1261|
P21980	TGM2	EDITHTYKYPEGSSEER	Phospho@440|442
Q9BU02	THTPA	LQELGGTLEYRVTFR	Phospho@34=8
Q9NXG2	THUMPD1	FTDKDQQPSGSEGEDDDAEAALKK	Phospho@86=12;Phospho@88=12
Q9BV44	THUMPD3	NITHFGPTTLR	Phospho@296=57
Q07157	TJP1	YESSSYTDQFSR	Phospho@1067=11
Q9NV96	TMEM30A	MILSTISWMGGK	Oxidation@310;Phospho@314=12;Oxidation@318
Q8NDV7	TNRC6A	LEEKGTGESQSRDR	Phospho@690|692
Q68CZ2	TNS3	ERTFGSREPK	Phospho@554=13
P55327	TPD52	TDPVPEEGEDVAATISATETLSEEEQEELRR	Phospho@66|68|70
P12270	TPR	TVPSTPTLVVPHRTDGFAEAIHSPQVAGVPR	Phospho@2133|2136|2137|2139|2146

O60704	TPST2	VLAMRQAWSKSGR	Oxidation@109;Phospho@114=9
P62995	TRA2B	RRSPSPYYSR	Phospho@264=60;Phospho@266=33
Q8TDR0	TRAF3IP1	LQQSPKPGEK	Phospho@557
Q7Z4K8	TRIM46	ILLGSGASSNAGLTGR	Phospho@665|668|669
Q99816	TSG101	DGTISEDTIR	Phospho@220=24
Q8N0Z6	TTC5	VSLQNLSMVLRQLRTDTEDEHSHHVMDSVR	Oxidation@144;Oxidation@162;Phospho@164=8
Q8WZ42	TTN	ETDRVSITTTKDR	Phospho@29624=8;Phospho@29625=8
P68363	TUBA1B	TIGGGDDSFNTFFSETGAGK	Phospho@48|51
P68363	TUBA1B	AYHEQLSVAEITNACFEPANQMVK	Phospho@292=13;Oxidation@302
P68363	TUBA1B	DVNAAIATIK	Phospho@334
P68363	TUBA1B	TIGGGDDSFNTFFSETGAGK	Phospho@56=10
P68363	TUBA1B	TIGGGDDSFNTFFSETGAGKHVPR	Phospho@54|56
P68363	TUBA1B	QLFHPEQLITGKEDAANNYAR	Phospho@94
P68363	TUBA1B	TIGGGDDSFNTFFSETGAGK	Phospho@51=14
P68363	TUBA1B	AVFVDLEPTVIDEVRTGTYR	Phospho@80=9
P07437	TUBB	GHYTEGAELVDSVLDVVR	Phospho@107=95
P07437	TUBB	IMNTFSVVPSPK	Oxidation@164;Phospho@166=30
P07437	TUBB	LHFFMPGFAPLTSR	Oxidation@267;Phospho@274=10
P07437	TUBB	ALTVPELTQQVFDAK	Phospho@285=23
Q12792	TWF1	HQTLQGVAFPISR	Phospho@174=103
Q6IBS0	TWF2	HQTLQGLAFPLQPEAQR	Phospho@174
Q14157	UBAP2L	IFTASNVSSVPLPAENVTITAGQR	Phospho@275=14
Q13404	UBE2V1	MAATTGSGVKVPR	Met-loss+Acetyl@1;Phospho@5=12
Q8WVY7	UBLCP1	ITFMLDSAAMITVHTPR	Oxidation@210=44;Phospho@218|221
Q8WUN7	UBTD2	LVVRSTDTVFHMKR	Phospho@170=11;Phospho@173=21
Q8WUN7	UBTD2	LVVRSTDTVFHMKR	Phospho@173=22;Phospho@170|171
O14795	UNC13B	AGITSAMATRTSLKDEELK	Oxidation@445;Phospho@442|443
Q96K76	USP47	IYLDGAPNKDLTQD	Phospho@1373
P08670	VIM	SLYASSPGGVYATR	Phospho@63=40
Q4G0F5	VPS26B	TPSQLSDNNCR	Phospho@330=31
Q96N03	VSTM2L	VVGSNISHK	Phospho@121|124
Q9Y6W5	WASF2	EEEVSLQGINTRK	Phospho@96=17
Q9C0J8	WDR33	RPDFAQQQAMQQLTFDGKR	Oxidation@38;Phospho@42
Q9H3P2	WHSC2	MASMRESDTGLWLHNK	Phospho@3=14
A4UGR9	XIRP2	ILYSDKEMTTPAK	Oxidation@209;Phospho@210|211
P13010	XRCC5	TEQGGAHFSVSSLAEGSVTSVGSVNPAENFR	Phospho@580|585|587
Q5TC79	ZBTB37	TENLEEWLGPENQPSGEDGSSAEEVTAMVIDTTGHG SVGQENYTLGSSGAK	Phospho@290|293|294
Q9Y2X9	ZNF281	MKIGSGFLSGGGGTGSSGGSGSGGGGSGGGGGGG SSGRR	Phospho@9|14|16|17|20|22
Q8N8H1	ZNF321P	MMKEFSSTAQGNTEVIHTGTLQRHESHHIR	Met-loss@1;Oxidation@2;Phospho@26=15;Phospho@13|18|20
Q92618	ZNF516	FSMDLKMPAFHPKQEVPVPGDGVEFPSSTGAEGQTG HPAEK	Oxidation@671&Phospho@695|Oxidation@671&Phospho@696|
Q32M78	ZNF699	AFSCSSSLSKHKR	Phospho@319|320|321|323
Q0D2J5	ZNF763	ALSYKFSNTPK	Phospho@382|384

Appendix 2

Supplemental figures in reference to Chapter 5
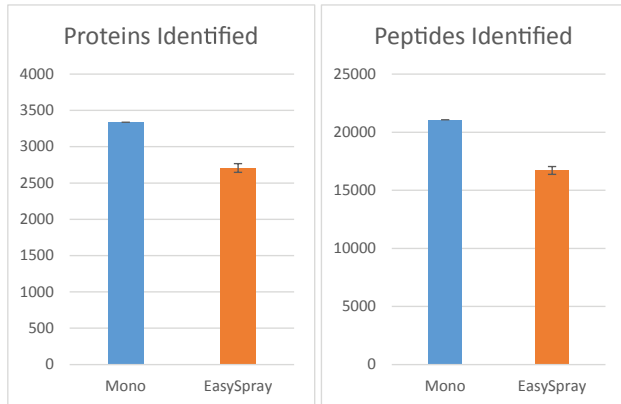
Figure S1

Figure S1: Peptide and protein detection with 200 cm monolithic silica-C18 column and 50 cm C18 silica particle-packed EasySpray column (Thermo). Tryptic digest of a mouse bone marrow lysate (100 ng) was loaded on either monolithic or particle-packed column and resolved using a 6-hr reverse phase gradient with subsequent peptide detection by DDA MS.
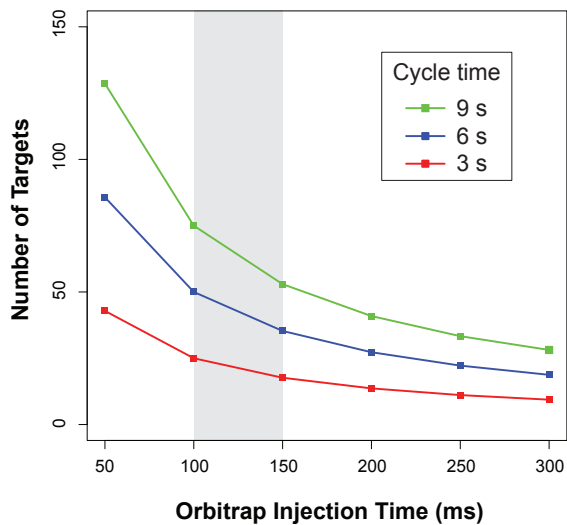
Figure S2

Figure S2: PRM multiplexing limits. PRM cycle times were measured in a set of runs on a Q Exactive Plus instrument (Thermo) with different Orbitrap injection times to estimate the limits of multiplexing. Estimated numbers of targets are plotted as a function of injection time assuming constant cycle times of 3, 6 or 9 seconds.

Fraction of Peptides per Protein Identified
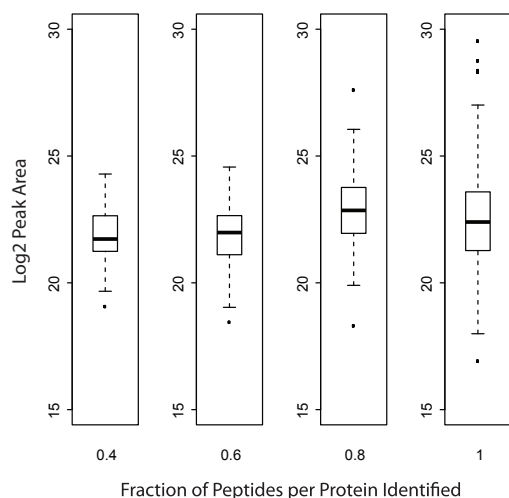
Figure S3: PRM detection of multiple peptides per protein as a function of protein abundance. Distributions of log2 peak areas, as estimates of protein abundance, are displayed as box plots in bins of increasing ratio of detected vs total scheduled precursors per protein. Bins: 0-0.4; 0.4-0.6; 0.6-0.8; 0.8-1. Solid line = median, box = interquartile range, whiskers = 1.5 x interquartile distance, dots = individual observations outside whiskers.
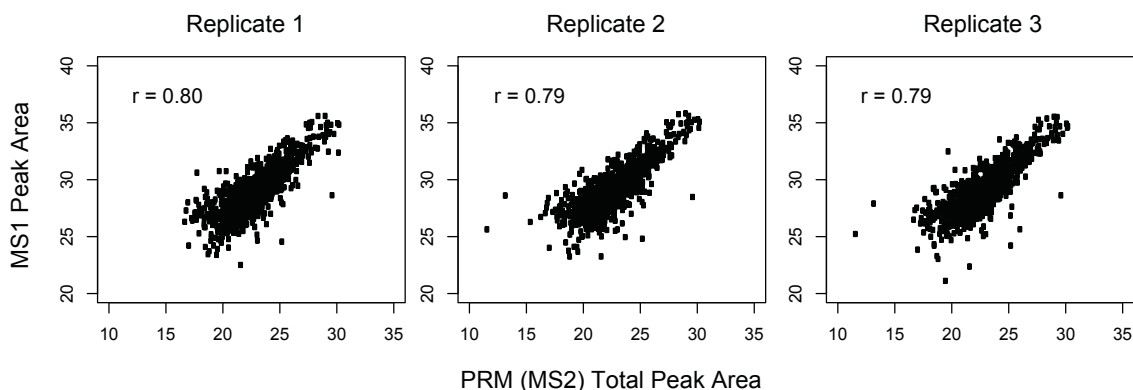
Figure S4

Figure S4: Comparison of MS1-level and MS2-level quantitation. Bone marrow lysate was analyzed in triplicate by DDA and by high-multiplexing PRM on the 200 cm monolithic silica-C18 column using the same chromatographic gradient. A comparison of log2 transformed MS1 peak areas derived from the DDA runs and MS2 total peak areas (i.e. summed areas of all fragments) measured by PRM is shown.

a RT agreement between two pools

b RT agreement

c Intensity agreement
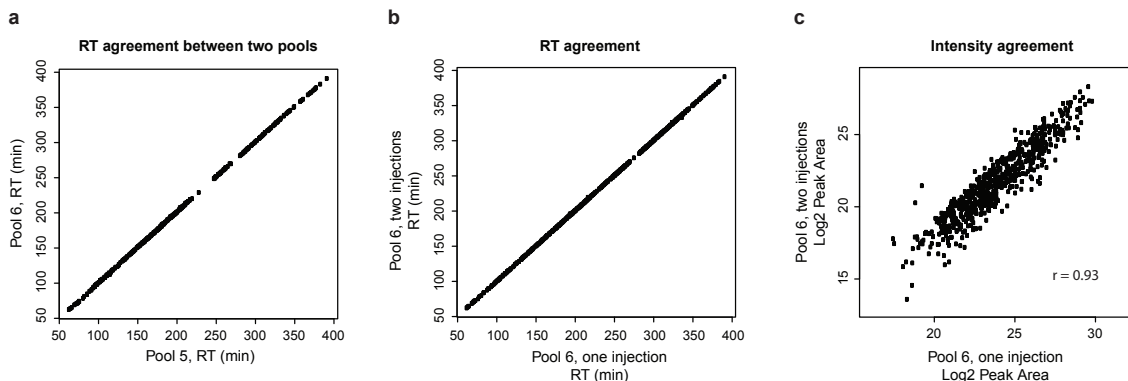
Figure S5: Reproducibility of PRM detection in MIB samples.

Kinases were detected by PRM in two independent pools of MIB enriched samples (~30 samples in each pool), first using a two-injection method with ~465 target precursors per injection and +/-10 min target detection windows, followed by a single- injection method using +/-3.5 min windows and targeting 929 precursor peptides from 182 kinases. (**a**) Retention times observed in the two MIB pools (#5 and #6) by the two-injection method are compared using all peaks auto-detected by Skyline and meeting the specificity criteria in both samples. (**b**) Retention times observed in the same MIB pool (#6) by the two- injection method and single-injection method are compared using all peaks auto-detected by Skyline and meeting the specific- ity criteria. (**c**) Peak intensities (log2 peak areas) observed in the same MIB pool (#6) by the two-injection method and single- injection method are compared using all peaks auto-detected by Skyline and meeting the specificity criteria.
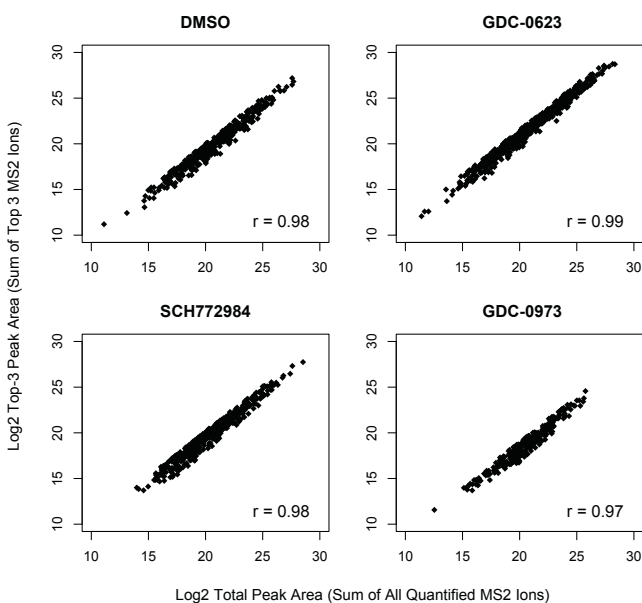
Figure S6: Comparison of PRM quantitation using the total area of all detected fragment ions and that of only top 3 most intense fragment ions. For each precursor, total and top-3

peak areas were calculated in Skyline and plotted for each biological condition. Log2 transformed values are compared.
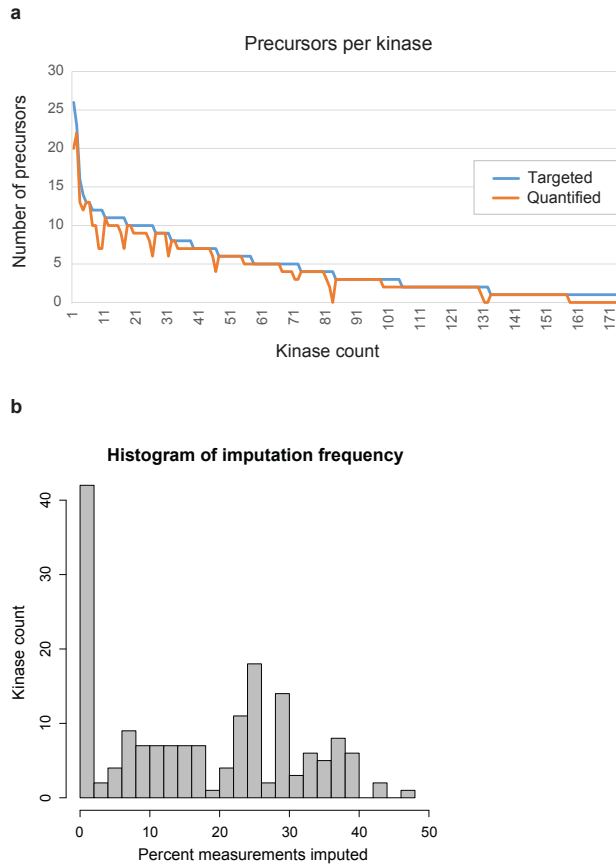
Figure S7

a

b

Figure S7: Kinase detection by PRM.

A total of 814 precursors among 929 targeted were quantified. A conservative preprocessing strategy to impute missing values was used. (**a**) Distribution of targeted and quantified precursors among individual kinases. (**b**) Histogram of the frequency of imputed measurements among quantified kinases.
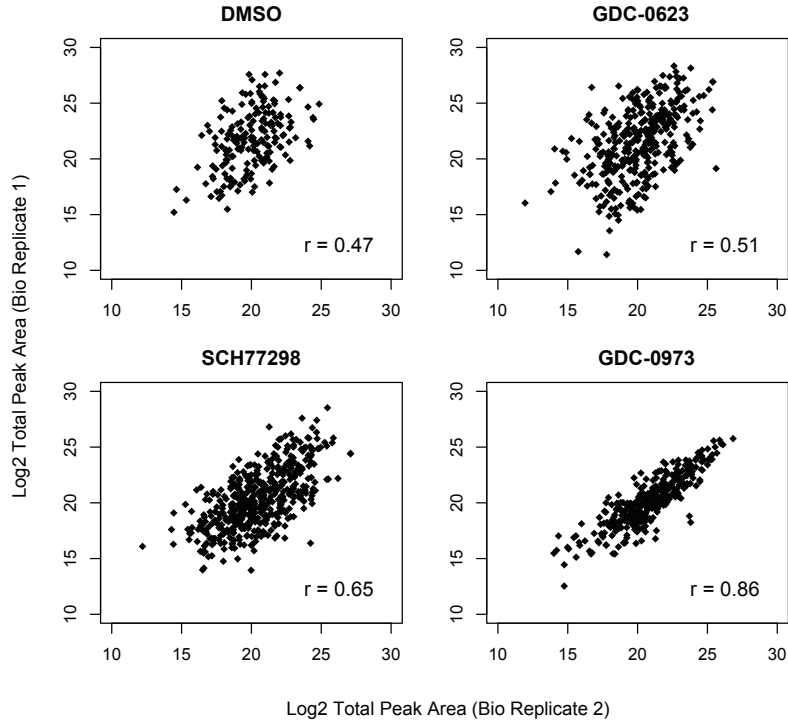
Figure S8: Reproducibility of PRM kinase abundance measurements in biological replicates in HCT116 cells treated with MAPK inhibitors or DMSO control. Agreement between log2 total peak areas of individual precursors measured in two biological replicates is shown for each condition.
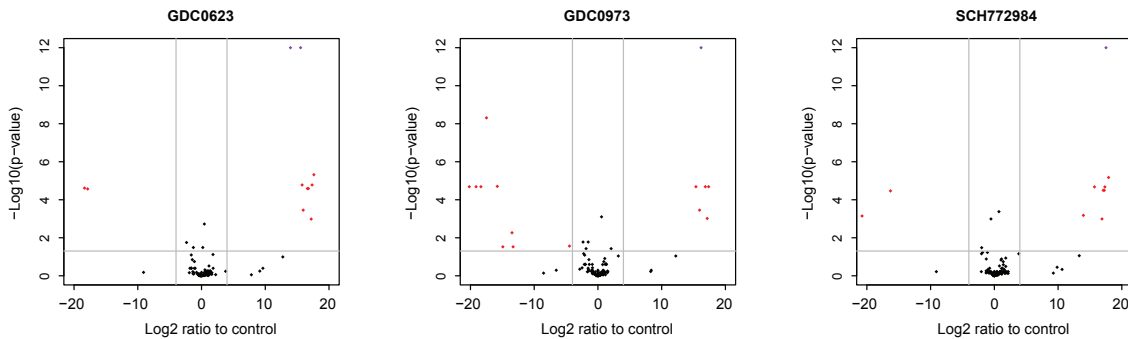
Figure S9: Volcano plots of PRM measured changes in kinase abundance in MIB eluates in HCT116 cells treated with MAPK inhibitors. Aggregated by kinase normalized log2 ratios for each inhibitor relative to DMSO control and their corresponding p-values were calculated in MSStats. Threshold of significance was defined as |log2 ratio| > 4 (vertical lines) and p-value <0.05 (horizontal line); significant observations are in red.
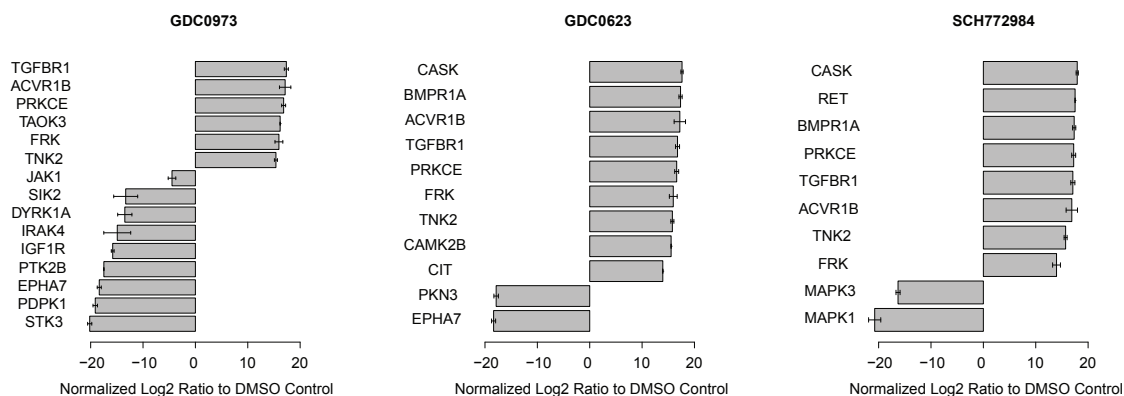
Figure S10: Statistically significant changes in kinase abundance in MIB eluates in HCT116 cells treated with MAPK inhibitors. All kinases with log2 ratios meeting the significance criteria (red dots in Figure S5) for a given inhibitor are plotted. Bars represent log2 ratios to DMSO control estimated by MSStats, and error bars represent standard deviations of the measured log2 ratios when all precursors in a given kinase and all biological replicates are considered.

Publishing Agreement

It is the policy of the University to encourage the distribution of all theses, dissertations, and manuscripts. Copies of all UCSF theses, dissertations, and manuscripts will be routed to the library via the Graduate Division. The library will make all theses, dissertations, and manuscripts accessible to the public and will preserve these to the best of their abilities, in perpetuity.

Please sign the following statement:

I hereby grant permission to the Graduate Division of the University of California, San Francisco to release copies of my thesis, dissertation, or manuscript to the Campus Library to provide access and preservation, in whole or in part, in perpetuity.

Author Signature   6/28/16

Date